SERI/STR--211-3582

DE89 009495

Research on High-Efficiency, Single-Junction, Monolithic, Thin-Film Amorphous Silicon Solar Cells

Phase I Annual Subcontract Report
1 February 1987 - 31 January 1988

A. W. Catalano, D. E. Carlson, R. R. Ayra,
M. S. Bennett, R. V. D'Aiello, C. R. Dickson,
C. M. Fortmann, B. Goldstein, J. McVeigh,
J. Morris, J. L. Newton, S. Wiedeman
Solarex Thin Film Division
Newtown, Pennsylvania

October 1989

SERI Technical Monitor: B. Stafford

Prepared under Subcontract No. ZB-7-06003-2

Solar Energy Research Institute
A Division of Midwest Research Institute

1617 Cole Boulevard
Golden, Colorado 80401-3393

Prepared for the
U.S. Department of Energy
Contract No. DE-AC02-83CH10093

MASTER

DISTRIBUTION OF THIS DOCUMENT IS UNLIMITED

NOTICE

This report was prepared as an account of work sponsored by an agency of the United States government. Neither the United States government nor any agency thereof, nor any of their employees, makes any warranty, express or implied, or assumes any legal liability or responsibility for the accuracy, completeness, or usefulness of any information, apparatus, product, or process disclosed, or represents that its use would not infringe privately owned rights. Reference herein to any specific commercial product, process, or service by trade name, trademark, manufacturer, or otherwise does not necessarily constitute or imply its endorsement, recommendation, or favoring by the United States government or any agency thereof. The views and opinions of authors expressed herein do not necessarily state or reflect those of the United States government or any agency thereof.

Printed in the United States of America
Available from:
National Technical Information Service
U.S. Department of Commerce
5285 Port Royal Road
Springfield, VA 22161

Price: Microfiche A01
Printed Copy A08

Codes are used for pricing all publications. The code is determined by the number of pages in the publication. Information pertaining to the pricing codes can be found in the current issue of the following publications which are generally available in most libraries: *Energy Research Abstracts (ERA)*; *Government Reports Announcements* and Index (*GRA* and I); *Scientific and Technical Abstract Reports (STAR)*; and publication NTIS-PR-360 available from NTIS at the above address.

SUMMARY

Task B: Research on Stable High-Efficiency, Large-Area, Amorphous Silicon Based Submodules

Conversion efficiencies up to 11.95% have been obtained in small-area, single-junction amorphous silicon (a-Si) solar cells. These high conversion efficiencies were attained by using textured tin oxide, superlattice p layers, graded carbon concentrations near the p/i interface and highly reflective ITo/silver back contacts. We have also fabricated single-junction amorphous silicon-carbon (a-SiC) and amorphous silicon-germanium (a-SiGe) p-i-n cells with conversion efficiencies in the 9 to 11% range. We have recently started fabricating stacked-junction cells of a-SiC/a-Si, a-Si/a-Si, a-SiC/a-SiGe and a-SiC/a-Si/a-SiGe, and have obtained conversion efficiencies of ~10% for some of these structurs.

The materials research program is focussed on the optimization of the electronic and optical properties of a-SiC, a-SiGe and microcrystalline SiC films. We have recently developed boron-doped microcrystalline SiC films that contain up to 6 at.% carbon with conductivities of $3\times10^{-3}\Omega^{-1}cm^{-1}$ at room temperature and activation energies of 0.11eV. Recently we have shown that the growth of microcrystalline films is strongly influenced by the nature of the substrate with nucleation occurring more readily on a-Si substrates than on tin oxide.

Stability studies show that light-induced degradation is usually enhanced by the presence of carbon grading near the p/i interface. In general; the addition of either germanium (from GeH_4) or carbon (from CH_4) to the i-layer of a p-i-n cell leads to enhanced light-induced degradation. We have also observed that light-induced degradation of the fill factor of p-i-n cells strongly correlates with the optical absorption at 1.2eV as measured by photothermal deflection spectroscopy. We observe no significant difference in the rate of degradation for a-Si solar cells exposed to continuous illumination and for cells exposed to cyclic illumination (8 hours, AM1.5, 50°C and 16 hours, dark 24°C).

Multi-junction cells exhibit less degradation then that expected from an analysis of single-junction cells.

TABLE OF CONTENTS

Section Page

FIGURE CAPTIONS

Figure Page

LIST OF TABLES

SECTION 1.0

INTRODUCTION

The principle objective of this three year research program is to develop multi-junction submodules of amorphous silicon based alloys having a conversion efficiency of at least 13% over an area greater than 900cm^2.

The research program consists of three subtasks. The purpose of Subtask B1: Semiconductor Materials Research is to prepare, characterize and optimize the chemical, structural, optical and electronic properties of the amorphous silicon (a-Si) based alloys that will be used in submodule research. Subtask B2: Non-Semiconductor Materials Research involves the production, characterization and optimization of non-semiconductor materials that are required to make high performance multi-junction submodules. In Subtask B3: Submodule Research, we will develop an a-Si based submodule with a 13% conversion efficiency over a total area of at least 900cm^2 in a multi-junction configuration.

SECTION 2.0

SUBTASK B1: MATERIALS RESEARCH

2.1 PURITY OF FEEDSTOCK MATERIALS

The Solarex Thin Film Division continues to update its information on feedstock materials used in amorphous silicon depositions. Efforts have centered on analyses of silane and germane.

Presently, the vendors supplying the best silane with consistency are Air Products (Mitsui Toatsu) and AlphaGaz (Tiesan). The very best silane analyses seen thus far involve silane made by Ethyl Corporation and distributed by Voltaix in aluminum cylinders. MG and Air Products also distribute silane from Ethyl, but in steel cylinders. Airco also makes excellent silane but supplies it only in aluminum cylinders. One cylinder from Liquid Carbonic was analyzed, and it was qualified by Solarex specifications.

While the silane from Ethyl Corp. is one of the best products we've seen so far, the distributors are in the process of learning cylinder preparation and the resulting silane quality varies. This is illustrated in Table 2-1. Ethyl's success at silane purity is that they use no chlorosilanes in their process. A 1 MT plant is in operation in Baton Rouge and a 100 MT plant is under construction in Houston. Prices for this silane is \$0.25 to \$0.35 per gram.

The best germane is supplied by Voltaix and Eagle Picher. The progressive improvement shown in Table 2-2 is a result of our work with these vendors. The removal of digermane, methyl germane, and oxy-germane compounds have led to excellent germane feedstock materials.

The purity of silane currently specified by the Solarex Thin Film Division is shown in Table 2-3. A comparison of Tables 2-1 and 2-3 shows that Ethyl silane easily meets our specifications and the same is generally true for silane from Mitsui Toatsu and Tiesan.

TABLE 2-1
ANALYSES OF SILANE FROM ETHYL CORPORATION DISTRIBUTED BY MG AND VOLTAIX

Vendor	Date	SiH_4	Si_2H_6O	Si_2H_6	Si_3H_8	$Si_2H_6O_2$	H_2	Inert
Voltaix (Ethyl) (alum cyl)	5/15/87	99.999%	ND	ND	ND	ND	ND	ND
MG (Ethyl) (alum cyl)	10/31/86	99.996	ND	36	ND	ND	ND	ND
MG (Ethyl)	9/25/87	99.998	ND	7	ND	ND	ND	10
MG (Ethyl)	4/6/87	99.98	66	107	ND	ND	NA	NA
MG (Ethyl)	4/6/87	99.99	6	84	ND	ND	NA	NA
MG (Ethyl)	4/6/87	99.99	10	105	ND	ND	NA	NA
MG (Ethyl)	6/24/87	99.99	ND	70	ND	ND	present	6
MG (Ethyl)	6/26/87	99.99	ND	71	ND	ND	present	6
MG (Ethyl)	6/26/87	99.99	ND	79	ND	ND	present	20

All concentrations are ppmw (except for SiH_4).

TABLE 2-2

GERMANE ANALYSES

Vendor	GeH_4	Ge_2H_6	Ge_2H_6O	CH_3GeH_3	inerts	$(CH_3\text{-}O\text{-}GeH_3)$ Unk #1	Unk #2	H_2
Matheson	97.2%	2.8%	ND	113	500	ND	ND	present
Airco	96.7%	3.2%	ND	236	trace	ND	ND	present
Synthatron (now Solkatronics)	99.9	768	ND	436	trace	ND	ND	present
Mitsui Toatsu	99.999	132	ND	ND	ND	ND	ND	present
Mitsui Toatsu	99.98	108	55	ND	trace	4	ND	present
Mitsui Toatsu	99.96	433	8	ND	trace	3	ND	present
Mitsui Toatsu	99.95	516	22	ND	13	ND	ND	present
Eagle Picher	96.4	3.6%	10	16	130	ND	70	present
Eagle Picher	99.9	1100	3	11	3	ND	ND	present
Eagle Picher	99.8	ND	ND	2150	3	ND	ND	present
Eagle Picher	99.998	23	ND	ND	trace	ND	ND	ND
Eagle Picher	99.995	15	ND	ND	37	ND	ND	present
Voltaix	99.94	516	22	ND	13	ND	ND	present
Voltaix	99.98	141	ND	ND	45	ND	ND	present
Voltaix	99.996	36	ND	ND	30	ND	ND	present
Voltaix	99.994	22	ND	ND	22	ND	ND	present

All concentrations are ppmw (except for GeH_4 and Ge_2H_6).

TABLE 2-3

RECOMMENDED PURE SILANE SPECIFICATIONS REQUESTED BY SOLAREX THIN FILM DIVISION - JUNE 1987

Impurity	Concentration (ppmw)
Si_2H_6	1000
Si_3H_8	1000
H_2	100 - 500
N_2	1
O_2	1
Ar	1
CH_4	5
CO	1
CO_2	1
Total chlorides	1
Total siloxanes	1
Total hydrocarbons	2

2.2 HIGH EFFICIENCY RESEARCH

Device-quality amorphous silicon-hydrogen alloy (a-Si:H) has an optical bandgap of about 1.7eV which, for a single-junction solar cell, is not optimum for terrestrial solar energy conversion. In order to better utilize the solar spectrum it is necessary to develop materials with both wider and narrower optical bandgaps than a-Si:H and to use them in a multi-junction (stacked cell) configuration. This allows one to split the spectrum as the two or three individual cells of a stacked cell respond to different parts of the spectrum. Hence, the overall response of a stacked cell is over a wider range of the spectrum than a single-junction cell of a-Si:H. We have chosen to develop amorphous silicon-carbon (a-SiC:H) and amorphous silicon-germanium (a-SiGe:H) as the wider and the narrower bandgap materials respectively. The high efficiency research program constitutes of developing amorphous silicon based alloys for i-layers in single-junction and multi-junction solar cells. In the single-junction solar cell effort we have developed amorphous silicon, amorphous silicon-carbide, and amorphous silicon-germanium p-i-n solar cells. We have explored a-SiC:H single-junction solar cells in which the optical bandgap of the i-layer is between 1.7 and 2.0eV and a-SiGe:H single-junction cells in which the optical bandgap is in the range of 1.7 to 1.55eV. Multi-junction cells with the combination of a-SiC, a-Si:H, a-SiGe as double-stacked and triple-stacked cells have also been explored.

2.2.1 Amorphous Silicon Single-Junction Cells

During this period we concentrated our efforts towards optimization of all aspects of high efficiency single-junction cells. From the device standpoint we have optimized a) the conventional a-SiC:H and the superlattice p-layers, and b) the p/i graded interface layer. From the optical enhancement standpoint we have optimized the texturing of the CTO and the ITO/Ag rear contact.

As mentioned in our previous report [1], the p/i graded interface consists of an undoped a-SiC:H layer which has a total thickness between 100-200Å. This layer is compositionally graded from about 1.9eV to 1.7eV and is deposited between the p- and the i-layer. The compositional grading can either be linear or in steps. This is accomplished by changing the ratio of silane and methane in the gas mixture from which it is deposited. There are two advantages of a graded interface layer: the V_{oc} is enhanced by about 10% and the fill-factor improves by about 5 to 7% [2]. We have measured open-circuit voltages as high as 0.95V and fill-factor values as high as 0.77 on cells with p/i graded interface. The insertion of a graded interface layer results in reduced carrier recombination at the metallurgical junction which manifests itself as bias independent collection of carriers at short wavelengths (400nm). We have studied the effect of varying the gradient of the graded interface (GI) layer. For a fixed thickness of the GI layer (100Å), the bandgap of the initial GI layer (the layer adjacent to the p-layer) was varied. As the bandgap of the initial layer was increased, the open-circuit voltage increased from 830mV to 950mV, the short-circuit current density remained almost constant, but the fill-factor and hence the conversion efficiency went through a broad maxima. An examination of the dark diode characteristics of these cells revealed that the reverse saturation current density, J_o remains within a factor of 2 whereas the diode quality factor, A, increases from 1.67 to 2.28 as the bandgap of the initial layer is increased. Figure 2-1 shows a plot of the photovoltaic and dark diode parameters of these cells as a function of the gas composition of the initial graded interface layer [3].

We have optimized the indium-tin-oxide (ITO)/silver rear contact. In general, an ITO/Ag rear contact results in 5 to 7% improvement in the short-circuit current density of single-junction a-Si:H cells. The development of this rear contact has resulted in short-circuit current densities as high as $18.8mA/cm^2$ with a quantum efficiency response at 700nm as high as 0.64. A comparison of various rear contacts on the long-wavelength response of cells is summarized Section 3.1.

Optimization of the above mentioned features has resulted in single-junction solar cells with conversion efficiencies in excess of 11.5% on a large number of cells deposited in three different a-Si:H deposition systems, each having a slightly different p/i graded interface layer. Table 2-4 shows the photovoltaic

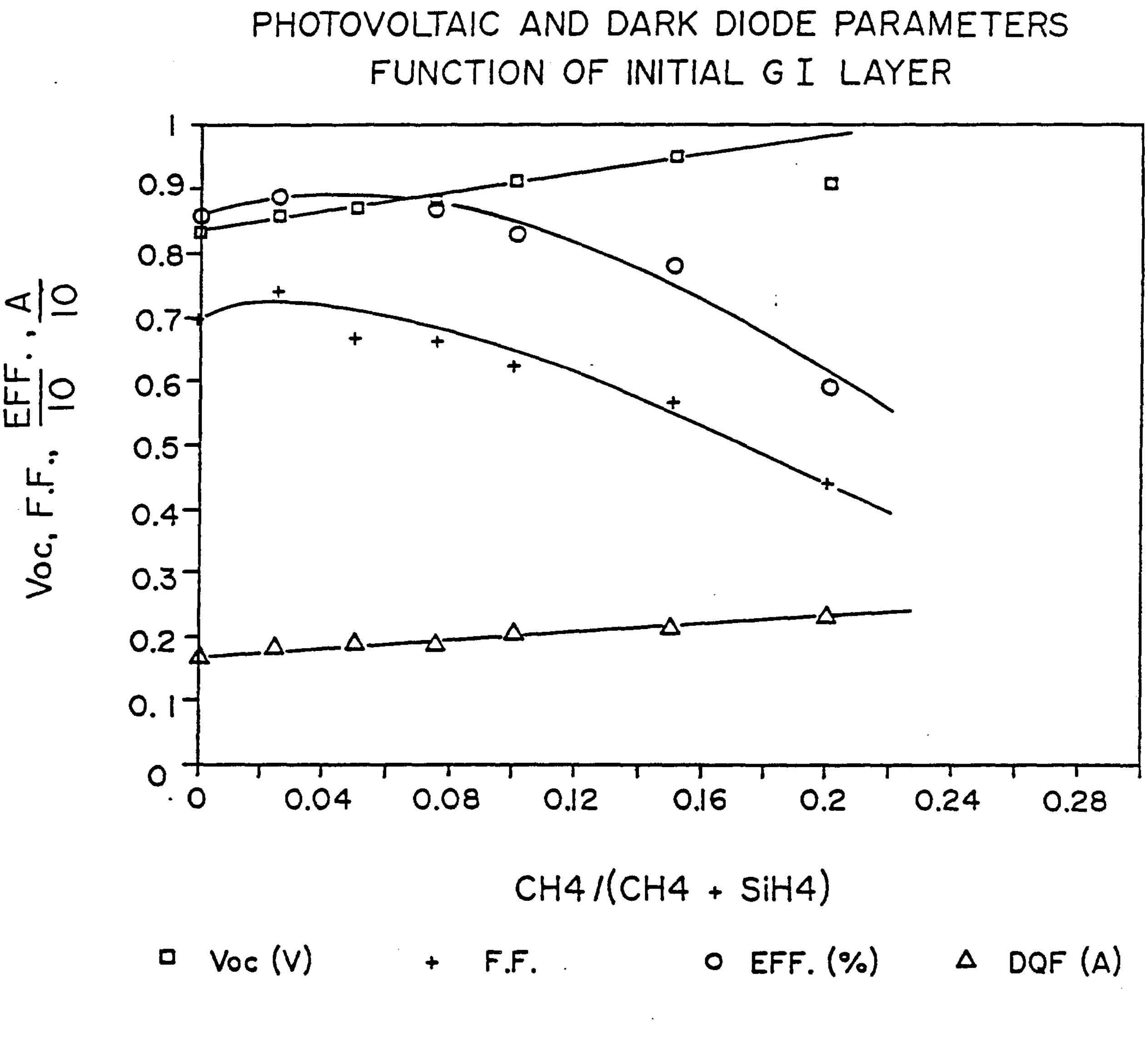

FIGURE 2-1. PHOTOVOLTAIC AND DARK DIODE PARAMETERS AS A FUNCTION OF INITIAL GI LAYER.

TABLE 2-4
PHOTOVOLTAIC PERFORMANCE PARAMETERS

Cell #	V_{oc} (mV)	J_{sc} (mA/cm^2)	FF	η (%)	Area (cm^2)	J_{sc} from QE (mA/cm^2)	η (%) with QE (J_{sc})
L7084-3E-Se	891	19.13	0.701	11.95	0.255		
L7078-3E-S6	871	19.09	0.692	11.5	0.255		
L7078-6F-S1	861	17.89	0.715	11.0	0.262		
L7070-4-4S1	870	18.63	0.703	11.4	0.635		
L7070-4-4L2	873	18.97	0.703	11.6	1.07		
LL707044B-L2	889	18.89	0.708	11.88	1.07	18.8	11.83
LL707044B-M1	8901	19.01	0.696	11.78	0.635	18.8	11.64
LL707044B-S3	891	19.09	0.706	12.01	0.259	18.6	11.70
LL707043B-S3	898	18.67	0.709	11.89	0.257	18.4	11.71
LL707043B-L2	894	19.00	0.709	12.05	1.056	18.4	11.66
LL707043A-S1	871	18.70	0.711	11.58	0.256	18.2	11.27
LL707043A-L1	872	18.64	0.712	11.57	1.060	18.2	11.29
LL707043A-L2	874	18.78	0.716	11.76	1.052	18.2	11.38
LL707043A-L2	861	18.34	0.71	11.2	1.05	----	11.2
LL707044A-M1	891	19.43	0.681	11.78	0.626	19.0	11.52
LL707064-S3	893	17.54	0.73	11.43	0.259	17.4	11.34
LL7049-3-2W1	895	17.97	0.695	11.18	1.120	17.8	11.07
CF587-S4	900	18.93	0.695	11.85	0.26	18.8	11.76
CF597-S4	900	19.78	0.658	11.70	0.26	18.8	11.12
CF613-S2	892	18.85	0.690	11.61	0.26	18.3	11.27
CF618-S2	852	19.87	0.683	11.58	0.26	18.9	11.01
CF624-S1	874	19.26	0.701	11.79	0.26	18.1	11.07

parameters of a large number of cells with conversion efficiencies in excess of 11%. The highest conversion efficiency achieved on an area of $0.255cm^2$ was 11.95% and that on an area of $1.07cm^2$ was 11.9%. Figure 2-2 and 2-3 show the J-V characteristics of these cells measured under AM1.5 Global conditions [4]. Figure 2-4 shows the quantum efficiency vs. wavelength of the cell shown in Figure 2-2. These measurements have been verified at SERI in their indoor facility. Table 2-5 shows a comparison of measurements made at Solarex vs. those made at SERI. As can be seen, the measurements, particularly the short-circuit current densities, are in very good agreement. The variations in other parameters are well within the accuracy of the measurement equipment.

2.2.2 Amorphous Silicon-Carbide Single-Junction Cells

We have explored wide bandgap a-SiC:H single-junction cells [5,6] in which the bandgap of the intrinsic layer is between 1.7eV to 2.0eV. In these p-i-n solar cells the entire i-layer is deposited from a mixture of silane and methane. Figure 2-5 shows the variation of open-circuit voltage and fill-factor of some cells as a function of methane in the gas mixture. We have fabricated single-junction cells with V_{oc}'s higher than 1 volt under AM1.5 global conditions. The photovoltaic parameters of some a-SiC:H cells are tabulated in Table 2-6.

2.2.3 Amorphous Silicon-Germanium Single-Junction Cells

It is well known that the optical bandgap of a-Si:H can be decreased by alloying it with germanium. Amorphous silicon-germanium alloys can be prepared by glow-discharge deposition in a variety of gas mixtures. We have concentrated our efforts to deposit a-SiGe:H i-layers by d.c. proximity glow-discharge from a mixture of silane (SiH_4) and germane (GeH_4), with and without hydrogen dilution. The opto-electronic properties of these alloys are discussed in a Section 2.3. As the percentage of germane in the gas mixture of germane and silane is increased from 0 to 15% the optical bandgap decreases from 1.7eV to 1.43eV. Most of the high efficiency work reported here has been done with a-SiGe:H i-layers which have optical bandgaps of either 1.55eV or 1.61eV [3].

FIGURE 2-2. J-V CHARACTERISTICS UNDER AM1.5 ILLUMINATION OF THE a-Si:H CELL WITH CONVERSION EFFICIENCY OF 11.95%.

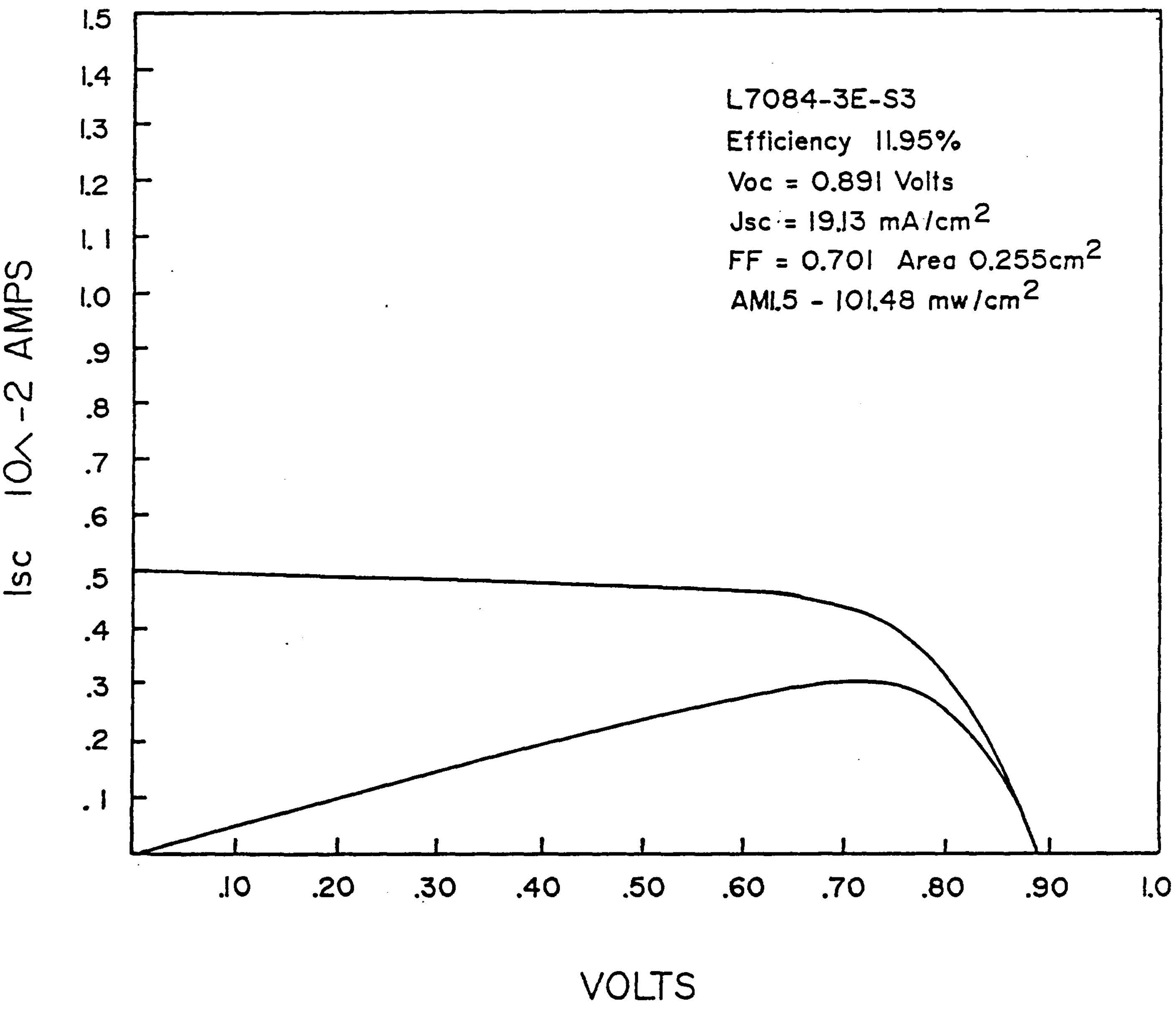

FIGURE 2-3. J-V CHARACTERISTICS UNDER AM1.5 ILLUMINATION OF THE a-Si:H CELL WITH CONVERSION EFFICIENCY OF 11.9%.

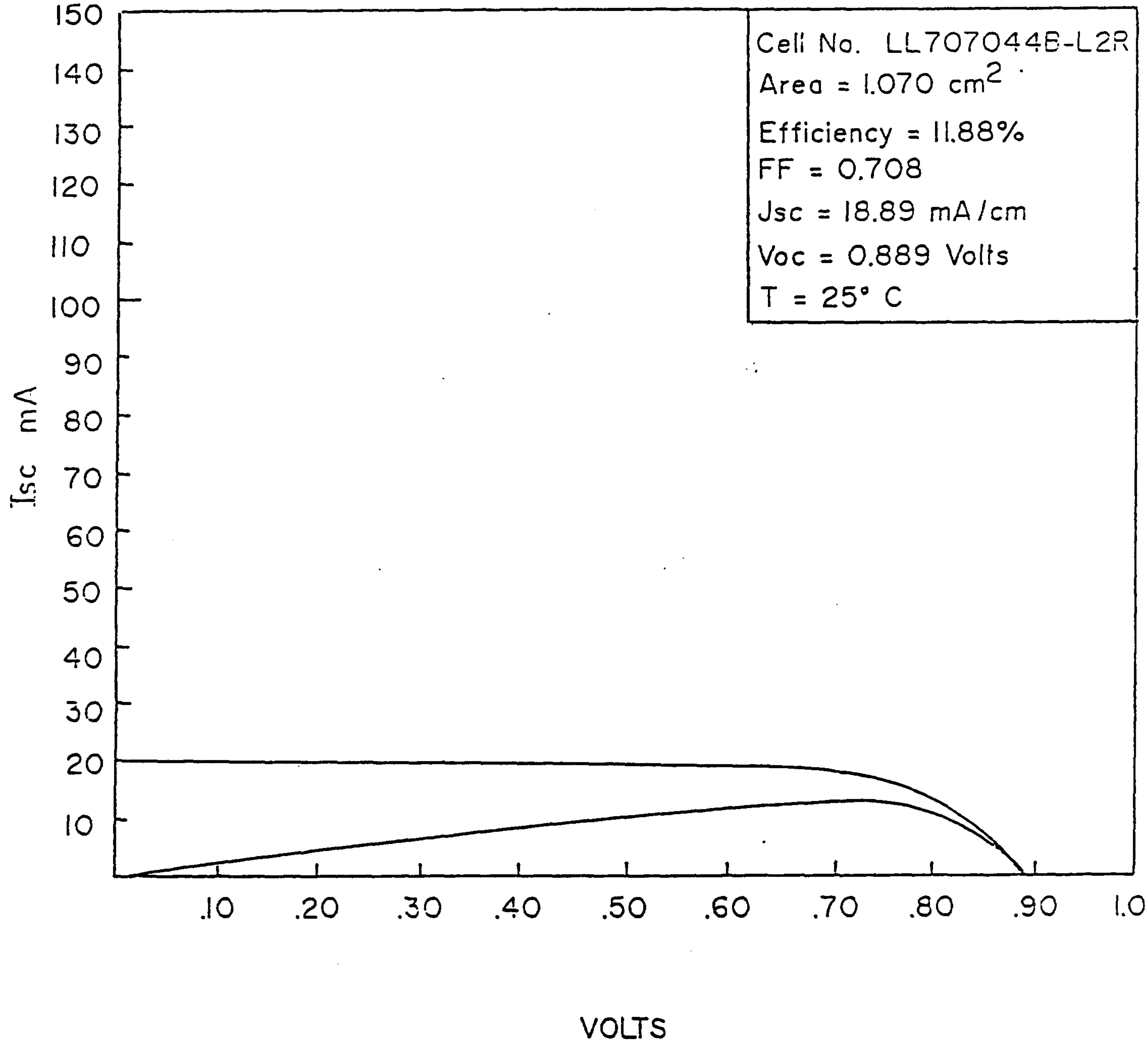

FIGURE 2-4. QUANTUM EFFICIENCY AS A FUNCTION OF WAVELENGTH OF THE CELL SHOWN IN FIGURE 2-3.

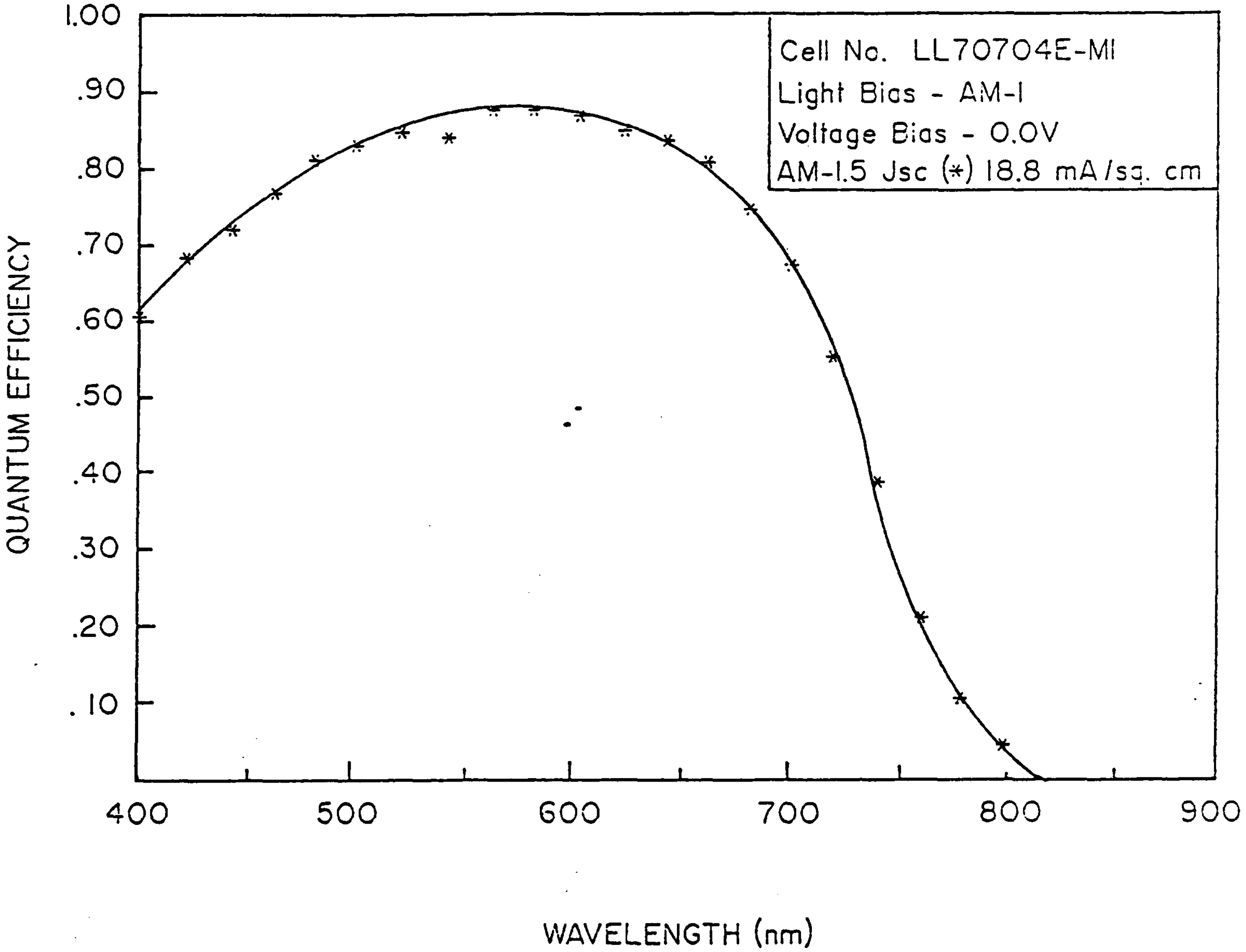

TABLE 2-5

PHOTOVOLTAIC PARAMETERS MEASURED AT SOLAREX AND AT SERI

Sample No.	Meas. Performed at	η (%)	V_{oc} (mV)	FF	J_{sc}, mA/cm²	Area (cm²)
L7084-3E-S3	Solarex	11.95	891	70.1	19.13	0.255
L7084-3E-S3	SERI	11.9	889	69.7	19.24	---
L7084-3E-S3, masked	SERI	11.7	871	70.4	18.94	---
LL707044-L2	Solarex	11.88	889	70.8	18.89	1.070
LL707044-L2	SERI	11.8	872	71.2	18.98	---
LL707044-L2, masked	SERI	11.5	846	71.8	18.88	---
L7078-3E-S6	Solarex	11.5	871	69.2	19.09	0.255
L7078-3E-S6, masked	SERI	11.3	866	69.0	18.85	---
CF613-S3	Solarex	11.39	900	68.4	18.5	0.255
CF613-Se	SERI	11.2	896	67.5	18.5	---

FIGURE 2-5. PHOTOVOLTAIC PARAMETERS OF a-SiC:H SINGLE-JUNCTION CELLS AS A FUNCTION OF METHANE CONCENTRATION.

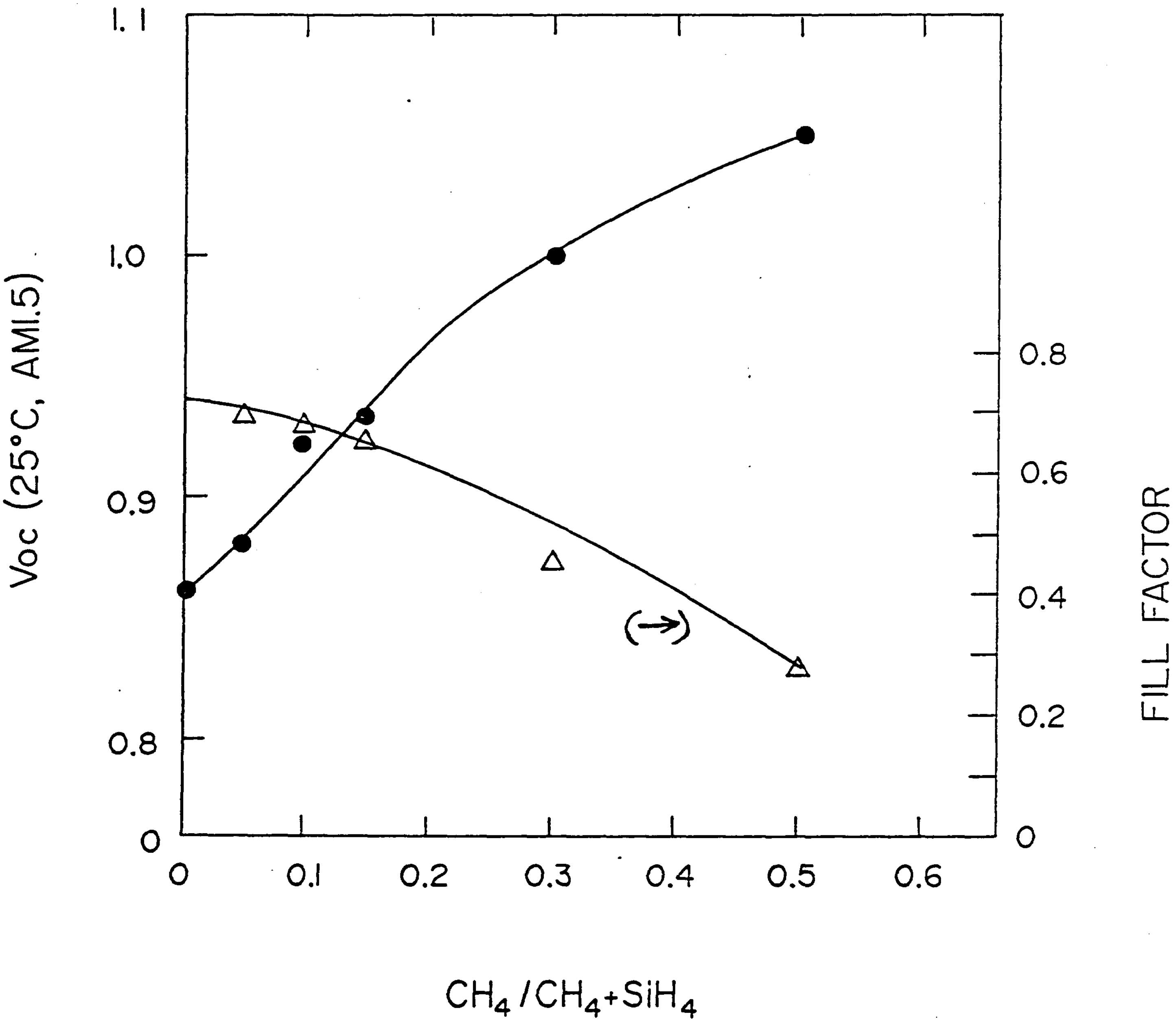

TABLE 2-6

PHOTOVOLTAIC PARAMETERS OF SOME a-SiC:H CELLS

Cell #	E_g (eV)	R (A/s)	V_{oc} (mV)	J_{sc} (mA/cm^2)	FF	(%)
CF233	1.8	10.0	890	10.66	0.723	6.72
CF328	1.72	0.6	820	8.63	0.606	4.31
CF732	1.8	10.0	881	10.89	0.610	5.86
CF731	1.8	10.0	892	9.30	0.564	4.68
CF716	1.75	0.6	872	11.46	0.651	6.51
CF715	1.80	0.6	901	8.85	0.567	4.52

In single-junction a-SiGe:H cells the concept of a p/i graded interface has been extended to the i(a-Si:H)/i(a-SiGe:H) interface. These cells have the same p-layer and the same p/i graded interfaces as those employed in our high efficiency single junction a-Si:H cells. The graded interface between the a-Si:H buffer and the bulk a-SiGe:H i-layer is employed to reduce recombination of carriers at that interface. An abrupt transition from a-Si:H (1.7eV) to a-SiGe:H (1.57eV) can increase the number of recombination centers at the interface. Further, if the electron affinity does not change as the Ge content is increased in the a-SiGe:H alloys but the valence band moves up in energy, this can create a barrier to the transport of holes at this interface. Figure 2-6 shows the device structure used in the single junction cells. Even with a graded interface there is evidence which suggests that hole transport is relatively poor in these alloys as compared to a-Si:H. Figure 2-7 shows the forward bias dependence of photo-generated carriers as a function of wavelength. In this figure we have plotted the ratio of quantum efficiency at an applied forward bias of 0.6V to that at 0V for an a-Si:H and an a-SiGe:H cell. As can be seen there is no wavelength dependence on the collection of carriers in the forward bias in the case of a-Si:H cell whereas in the case of a-SiGe:H cell there is a strong wavelength dependence. Carriers generated in the bulk of the a-SiGe:H i-layer (long wavelength) where holes have to traverse the entire thickness of the i-layer are collected less efficiently than carriers generated at the front of the cell (short wavelength). This is also seen in the quantum efficiency measurements made at reverse bias. Figure 2-8 shows a plot of the ratio of quantum efficiency at -3V to that at 0V for the cell shown in Figure 2-7. Clearly, the long wavelength response is more bias dependent indicating hole transport limitation which may be due to the low product of holes and/or due to a low field region (dead region) in the i-layer.

We have studied the effect of i-layer thicknesses on the photovoltaic parameters of a-SiGe:H single-junction solar cells in which the optical bandgap of the i-layer was approximately 1.55eV. We find that as the i-layer thickness is

FIGURE 2-6. DEVICE STRUCTURE OF a-SiGe:H SINGLE JUNCTION CELL.

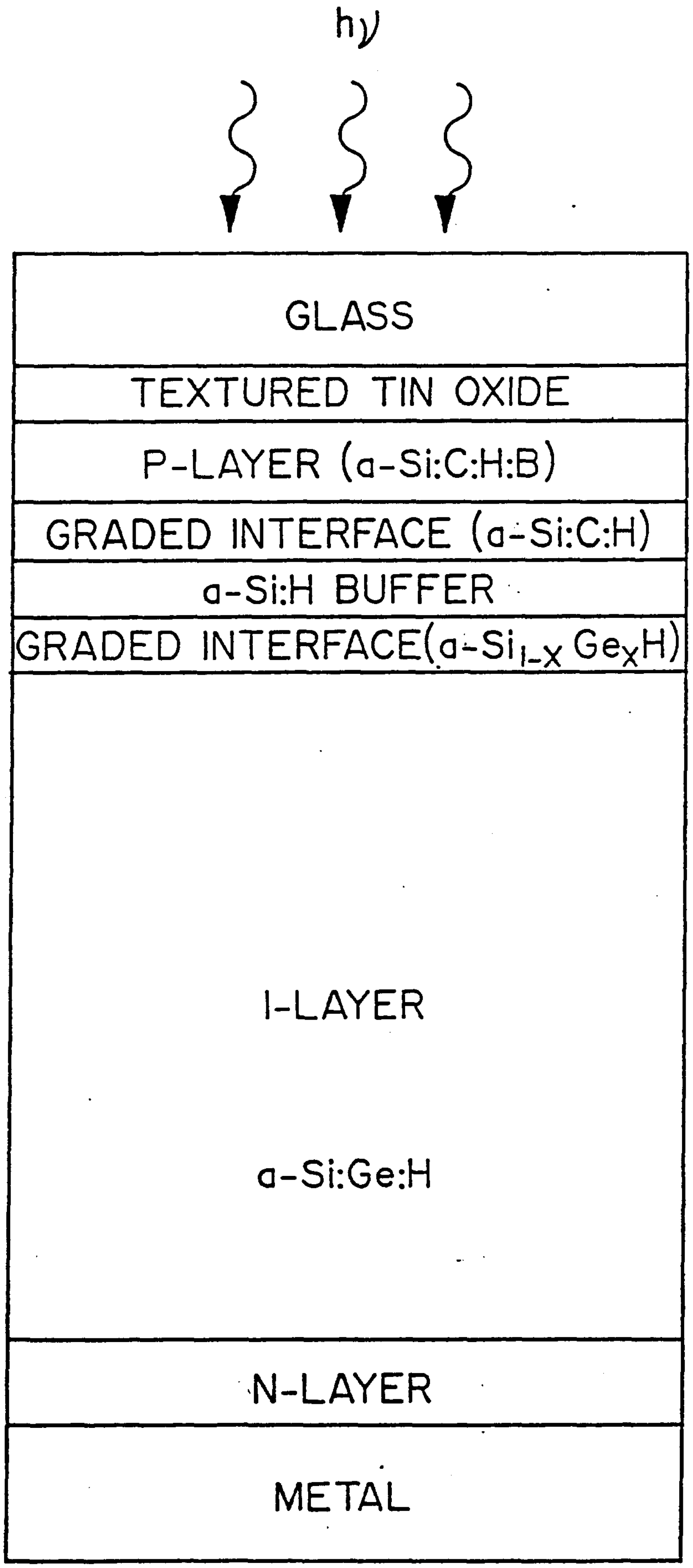

FIGURE 2-7. RATIO OF QUANTUM EFFICIENCY (0.6V/0V) AS A FUNCTION OF WAVELENGTH.

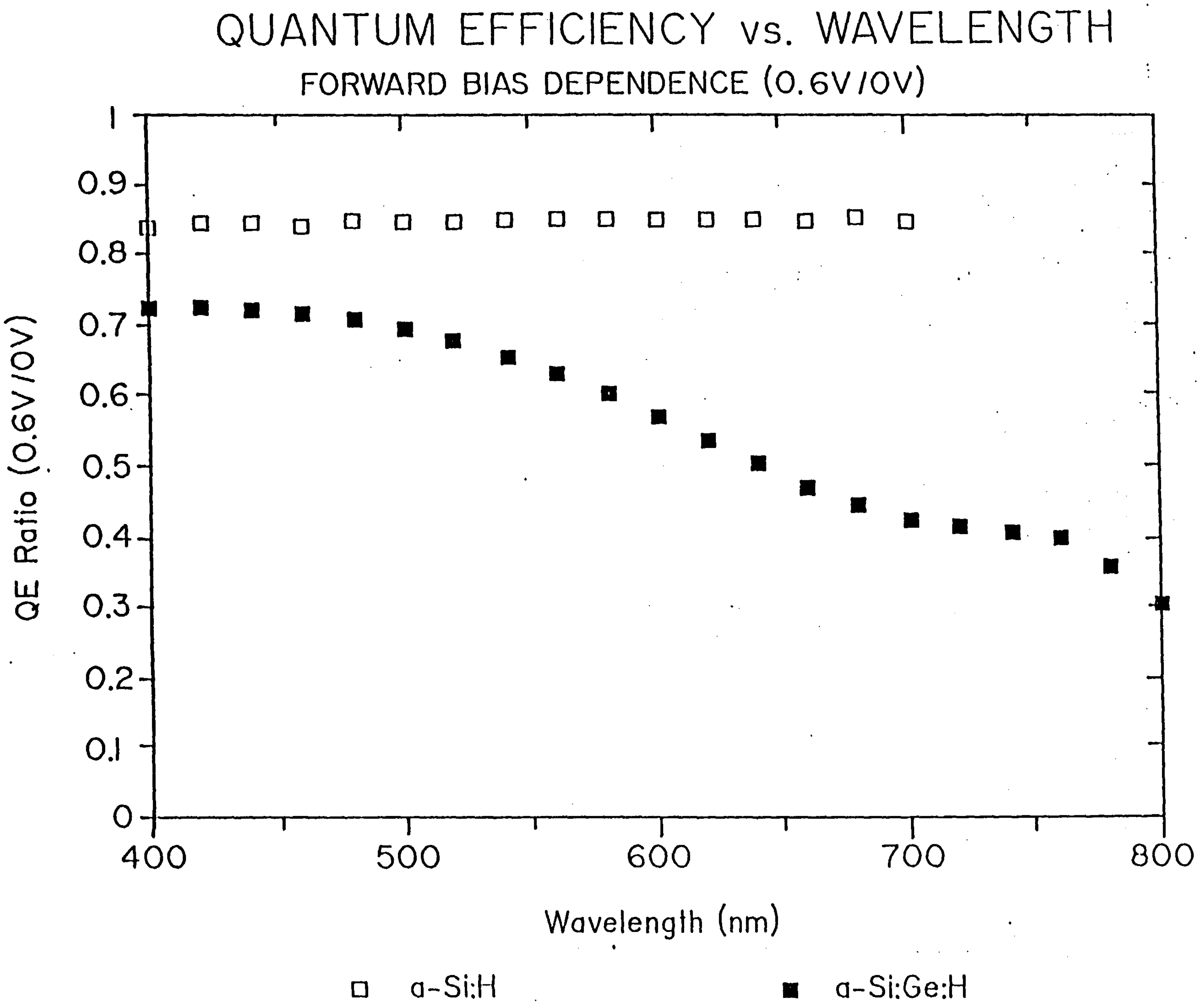

FIGURE 2-8. RATIO OF QUANTUM EFFICIENCY (-3V/0V) AS A FUNCTION OF WAVELENGTH.

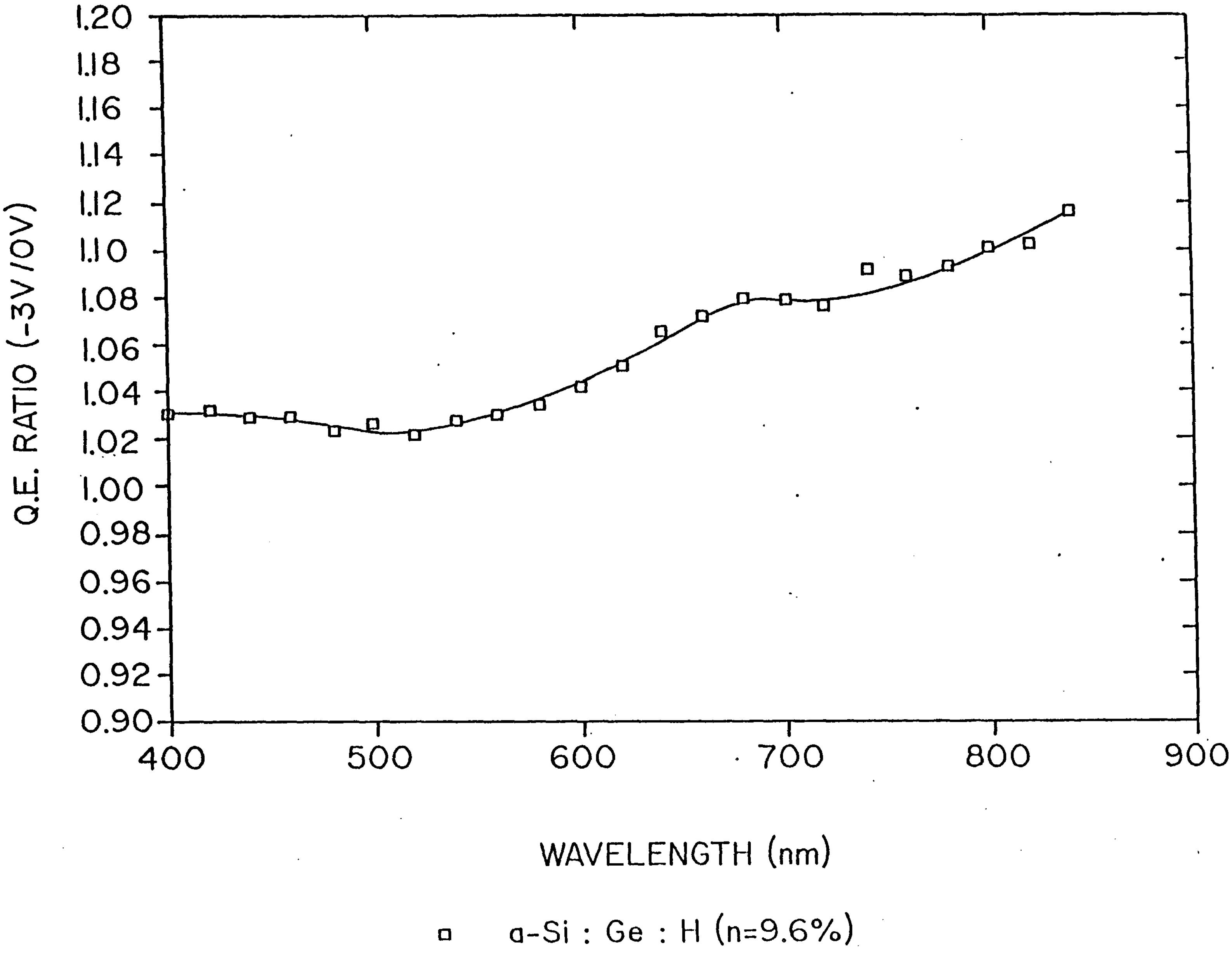

increased from 1000Å to 5000Å, J_{sc} increases from 14.1mA/cm^2 to 19.9mA/cm^2, the fill-factor decreases from 0.68 to 0.58, and the response at 800nm increases from 2% to about 20%. Figure 2-9 shows the changes in the photovoltaic parameters as a function of the i-layer thickness. The thinnest cell of this series is remarkable - it exhibited 14.1mA/cm^2 current density with a conversion efficiency of 7.77%. This is probably the highest efficiency observed in an a-Si based single-junction cell with a 1000Å thick i-layer. Figure 2-10 shows the J-V characteristics of this cell and Figure 2-11 shows the quantum efficiency vs. wavelength measurement on this device. The highest efficiency single- junction a-SiGe:H cell in which the bandgap of the i-layer was 1.61eV was 10.77% and that for which the bandgap of the i-layer was 1.55eV was 9.6%. The J-V characteristics of these two cells are shown in Figure 2-12 and 2-13. Figure 2-14 shows a comparison of the quantum efficiencies of these two cells with that of the highest efficiency a-Si:H cell. It is clear from the QE measurements that the improvements in the J_{sc} comes from the long wavelength response of the narrower bandgap alloy cells. The highest J_{sc} values that we have measured are 20.5mA/cm^2. The photovoltaic parameters of a-SiGe:H single-junction cells are tabulated in Table 2-7.

2.2.3.1 n-Type a-SiGe:H Doped Layers

In a-SiGe:H single-junction p-i-n solar cells, the i/n interface and the effect of phosphorus doping of a-SiGe:H has been studied. Devices with a-SiGe:H i-layers (E_g = 1.57eV) were fabricated which had a-Si:H n-layers, and a-SiGe:H n-layers. The photovoltaic parameters of these two types of cells are tabulated in Table 2-8. We find that the V_{oc}, the J_{sc}, and the FF of cells with an a-Si:H n-layer is far superior to that with an a-SiGe:H n-layer. A study of the electrical and optical properties of these two n-layers revealed that the dark conductivity of a-SiGe:H n-layer is about an order of magnitude lower than that of a-Si:H. Moreover, the activation energy (E_a) of this film was 0.299eV as compared to 0.207eV of that of a-Si:H. The optical and electrical properties are tabulated in Table 2-9. In the devices the difference in the J_{sc} values can be explained in terms of the light absorbed in the respective n-layers (E_g = 1.54eV versus 1.71eV). The lower values of V_{oc} and FF are probably due to the

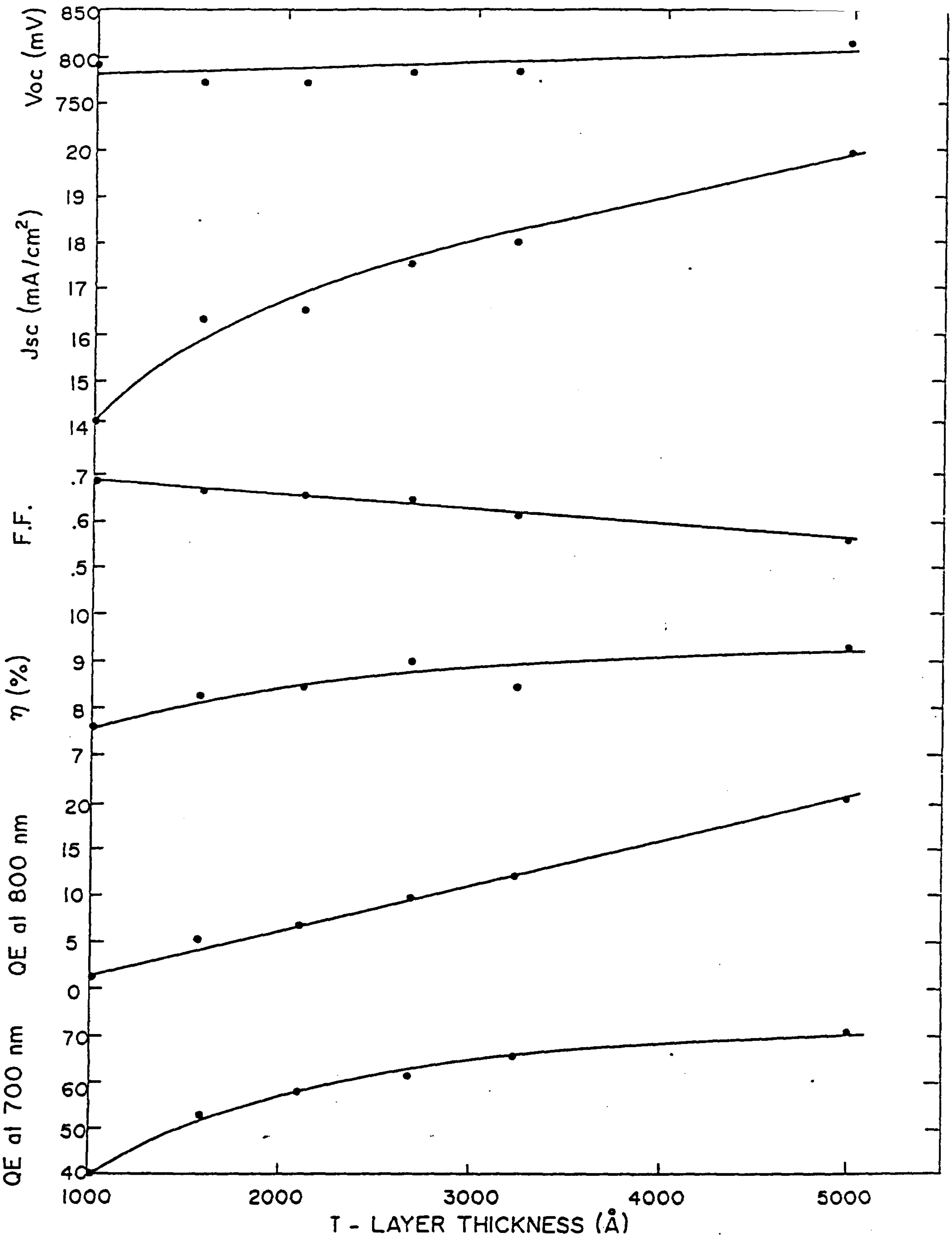

FIGURE 2-9. PHOTOVOLTAIC PARAMETERS OF a-SiGe:H SINGLE-JUNCTION CELLS AS A FUNCTION OF I-LAYER THICKNESS.

Cell No. LL7182-I-I SIRR

Voc = -.790 Volts

F.F. = .679

Power = 7.77 mw/cm^2

V max = -.655 Volts

Bs = 5.08E + 00 ohm-cm^2

Bscc = .99

Temp. = 25.1 deg. C

Date 070687

Jsc = 14.49 mA/cm^2

Eff = 7.77%

Illum. = 100.73 mW/cm^2

J max = 11.87 mA/cm^2

Rsh = 1.45E + 03 ohm/cm^2

Rshcc = 0.00

ITO = 0.00E + 00 ohm/cm^2

Cell Area = .257 cm^2

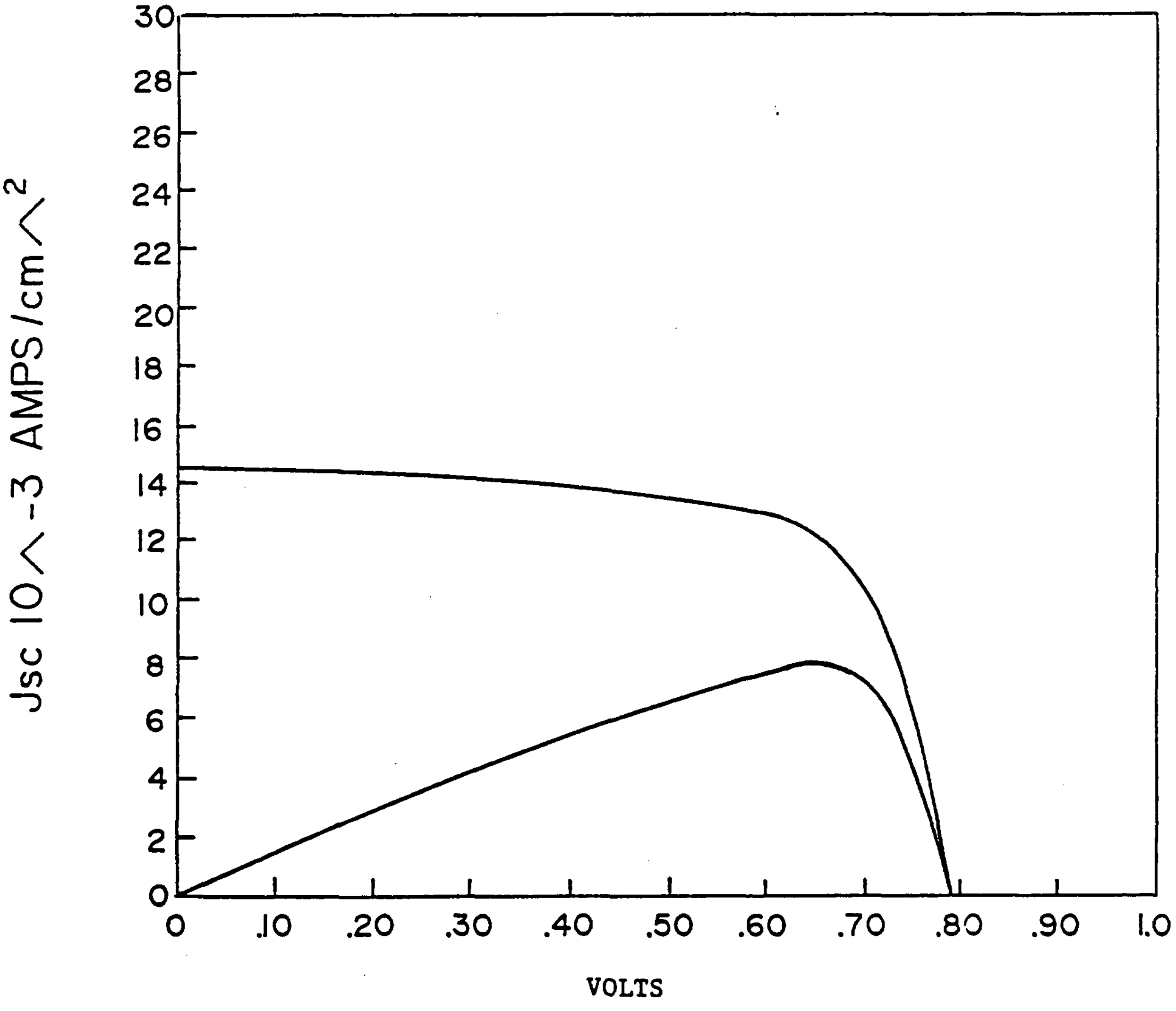

FIGURE 2-10. J-V CHARACTERISTICS UNDER AM1.5 ILLUMINATION OF AN a-SiGe:H SINGLE-JUNCTION CELL WITH I-LAYER THICKNESS EQUAL TO 1000Å.

FIGURE 2-11. QUANTUM EFFICIENCY AS A FUNCTION OF WAVELENGTH OF THE CELL SHOWN IN FIGURE 2-10.

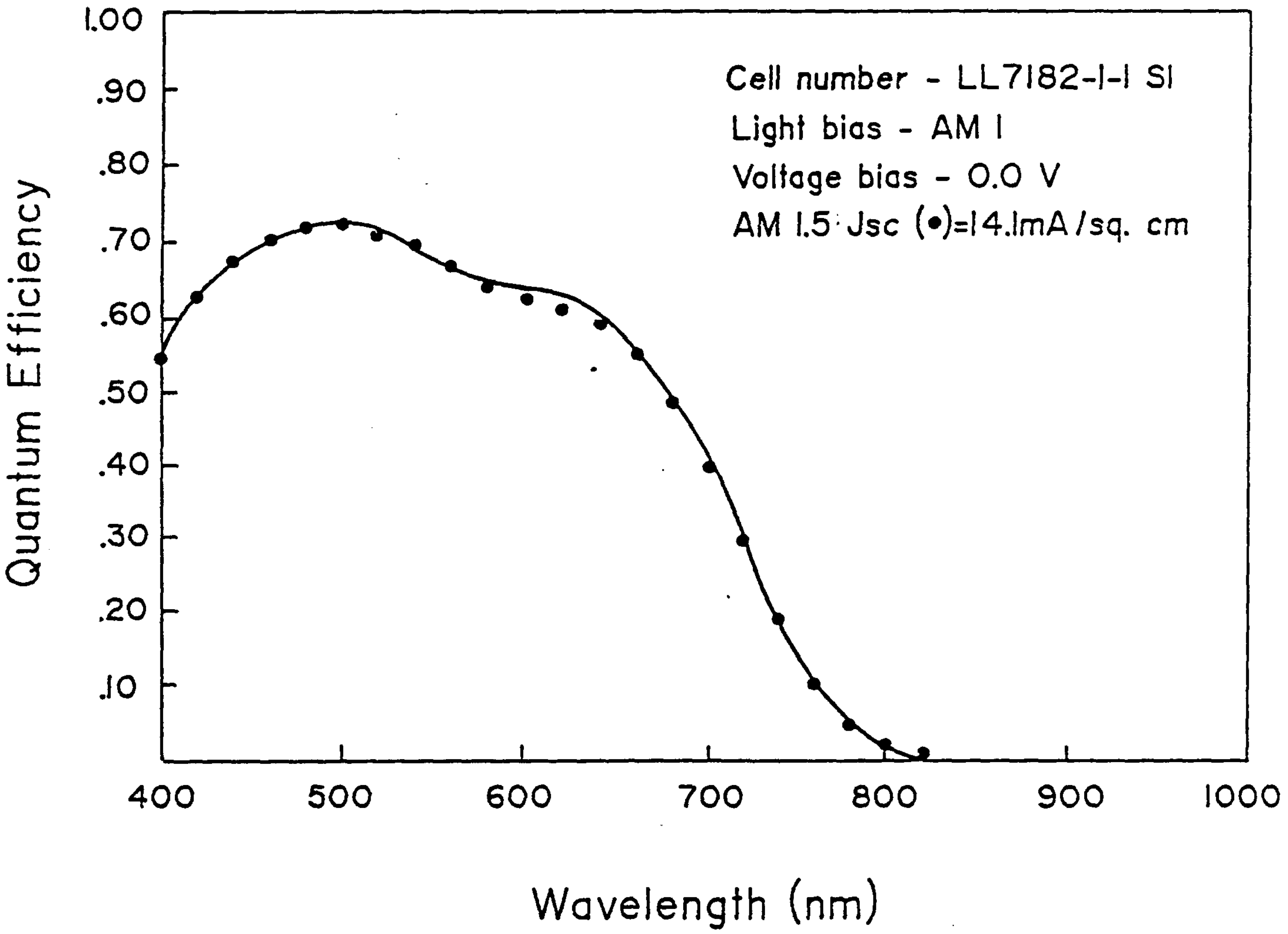

a-Si : Ge : H

Cell No. LL7111-3-2S3
Voc = -.851 Volts
F.F. = .654
Power = 10.77 mW/cm^2
V max = -.637 Volts
Rs = 6.06E+00 ohm/cm^2
Temp. = 23.6 deg. C

Date 042787
Jsc = 19.34 mA/cm^2
Eff = 10.77%
Illum. = 99.34 mW/cm^2
J max = 16.91 mA/cm^2
Rsh = 2.59E+02 ohm/cm^2
Cell Area = .257 cm^2

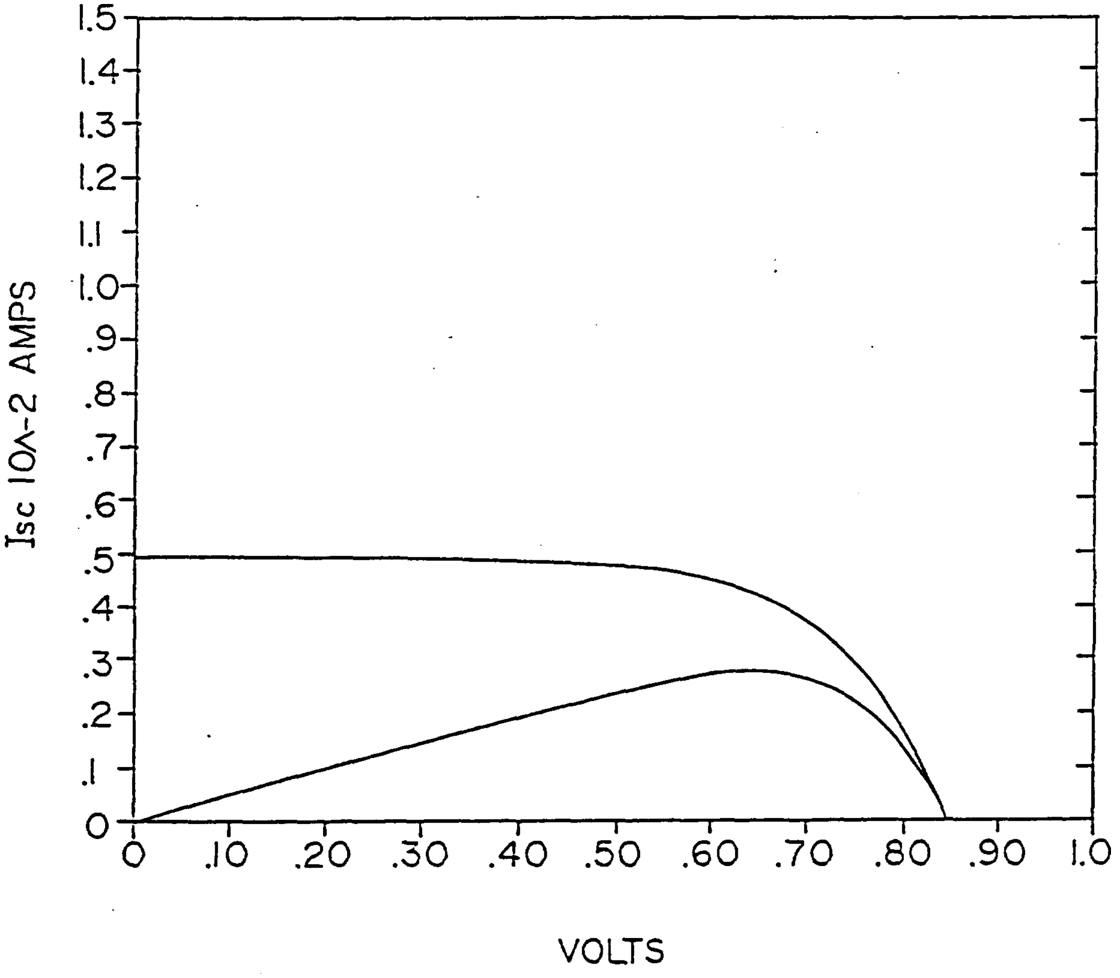

FIGURE 2-12. J-V CHARACTERISTICS UNDER AM1.5 ILLUMINATION OF a-SiGe:H SINGLE-JUNCTION CELL WITH BANDGAP OF 1.61eV.

a-Si : Ge : H

Cell No. LL7111-2-2A S3A
Voc = -.812 Volts
F.F. = .580
Power = 9.59 mW/cm^2
V max = -.566 Volts
Rs = 8.63E+00 ohm/cm^2
Temp. = 26.0 deg. C

Date 051187
Jsc = 20.38 mA/cm^2
Eff = 9.59%
Illum. = 93.56 mW/cm^2
J max = 16.94 mA/cm^2
Rsh = 1.01E+03 ohm/cm^2
Cell Area = .255 cm^2

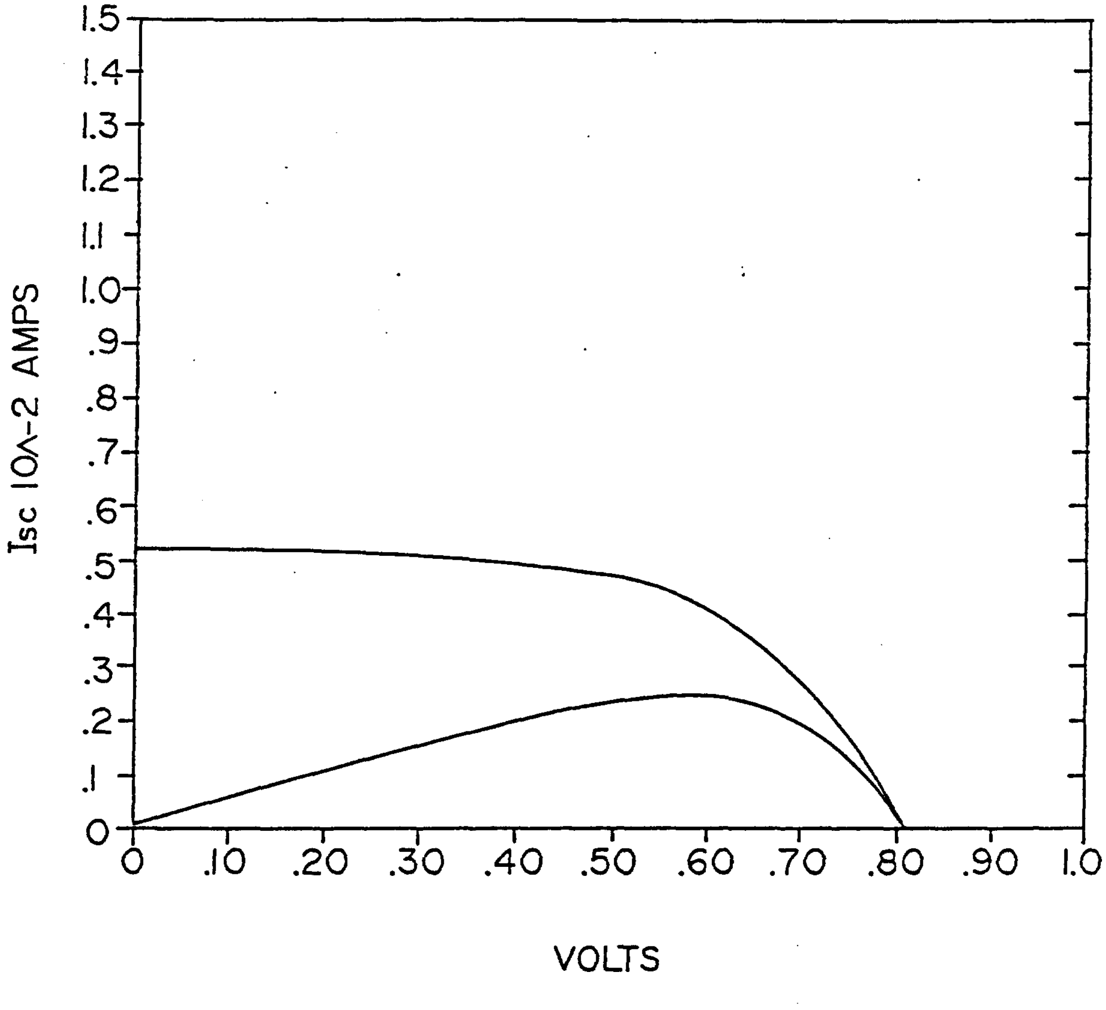

FIGURE 2-13. J-V CHARACTERISTICS UNDER AM1.5 ILLUMINATION OF AN a-SiGe:H SINGLE-JUNCTION CELL WITH BANDGAP OF 1.57eV.

FIGURE 2-14. COMPARISON OF QUANTUM EFFICIENCY VERSUS WAVELENGTH MEASUREMENTS OF CELLS SHOWN IN FIGURES 2-3, 2-12, AND 2-13.

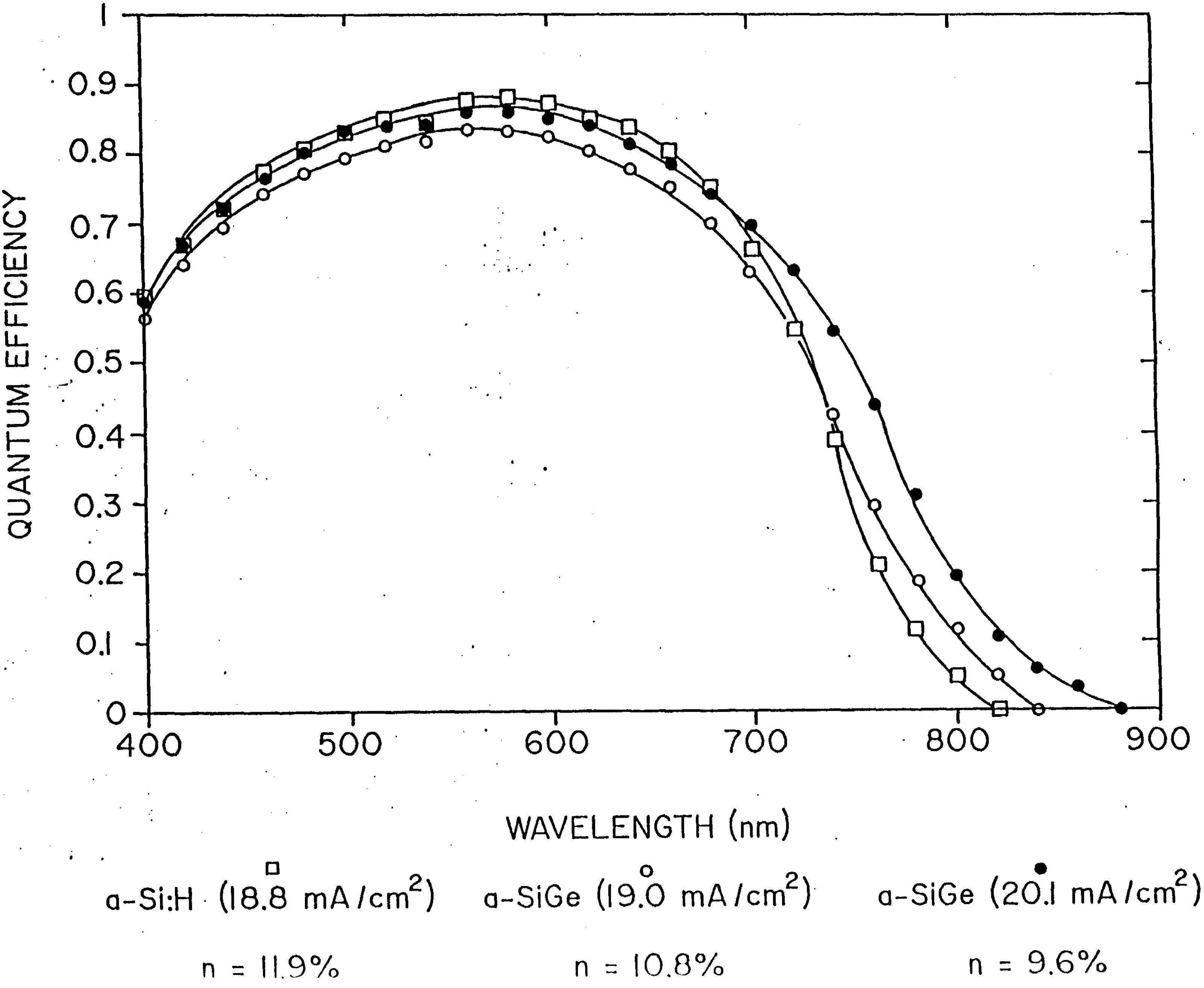

TABLE 2-7

PHOTOVOLTAIC PARAMETERS OF SOME a-SiGe:H CELLS

Cell #	E_g (eV)	V_{oc} (mV)	J_{sc} (mA/cm^2)	FF	%	J_{sc} from QE	Remarks
LL711133S3	1.61	851	19.34	0.654	10.77	19.0	
LL711122S3	1.57	811	20.08	0.566	9.2	19.9	
		805	19.98	0.5511	8.9		SERI
LL71312M1	1.57	808	20.15	0.565	9.22	20.1	
LL711122AS3	1.57	812	20.38	0.58	9.6	20.1	
LL718211S1	1.57	790	14.49	0.679	7.77	14.1	1000Å

TABLE 2-8

COMPARISON OF a-Si:H and a-SiGe:H n-Layers

Cell #	V_{oc} (mV)	J_{sc} (MA/cm^2)	FF	J_{sc} from QE (mA/cm^2)	Efficiency (%)	n-layer
LL724422	834	19.23	0.629	19.0	9.96	a-Si:H
LL724431	822	18.03	0.519	18.0	7.70	a-SiGe:H

TABLE 2-9

COMPARISON OF PROPERTIES OF n-Layers

Property	a-Si:H	a-SiGe:H
Optical Bandgap	1.71eV	1.54eV
Dark Conductivity	$6.4 \times 10^{-3} (\Omega\text{-cm})^{-1}$	$3.1 \times 10^{-4} (\Omega\text{-cm})^{-1}$
Activation Energy	0.207eV	0.299eV

inferior doping characteristics of a-SiGe:H n-layer. A poorer doped n-layer can lead to less band-bending at the i/n interface, a lower value of flat-band voltage, and consequently a lower value of V_{oc} and FF. The increase in the activation energy of a-SiGe:H n-layers is consistent with the formation of defects with an energy level in the mid-gap region which compensates the dopant and pulls the Fermi level towards the mid-gap. The hypothesis of less band-bending at the i/n interface is somewhat evident in the quantum efficiency measurements made under applied forward bias. In forward-bias the built-in field is reduced, and if this reduction in field strength is uniform, one would expect very little wavelength dependence in collection of carriers. In a-SiGe:H devices there is a strong wavelength dependence in collection of carriers. The long wavelength dependence indicates hole transport limitation which may be due to the low $\mu\tau$ product of holes. In these devices the same trend is seen but cells with a-SiGe:H n-layers have a much larger bias dependence than cells with a-Si:H n-layers. This is shown in Figure 2-15 where we have plotted the ratio of quantum efficiency measurements made at 0.6V to that made at 0V.

2.2.4 Multi-Junction (Stacked) Solar Cells

We have fabricated multi-junction solar cells in the configuration of double and triple stacked cells. In double stacked cells the i-layers comprise of a-Si:H, a-SiC:H, or a-SiGe:H. Cells with the following combination have been explored: a-SiC:H/a-Si:H,a-Si:H/a-Si:H, and a-SiC:H/a-SiGe:H. Triple stacked cells with the configuration of a-SiC:H/a-Si:H/a-SiGe:H have also been fabricated. In all these cells we have employed the concept of p/i graded interface and ITO/Ag rear contacts.

2.2.4.1 a-SiC:H/a-Si:H Stacked Cells

These multi-junction cells comprise of the top cell which has an i-layer of a-SiC:H with an optical bandgap between 1.8 and 1.85eV and the bottom cell has a conventional a-Si:H i-layer with an optical bandgap of about 1.7eV. The highest open circuit voltage measured in cells with this configuration is 1.8V. This high value of V_{oc} is attributed to the wider bandgap of the top cell. This cell

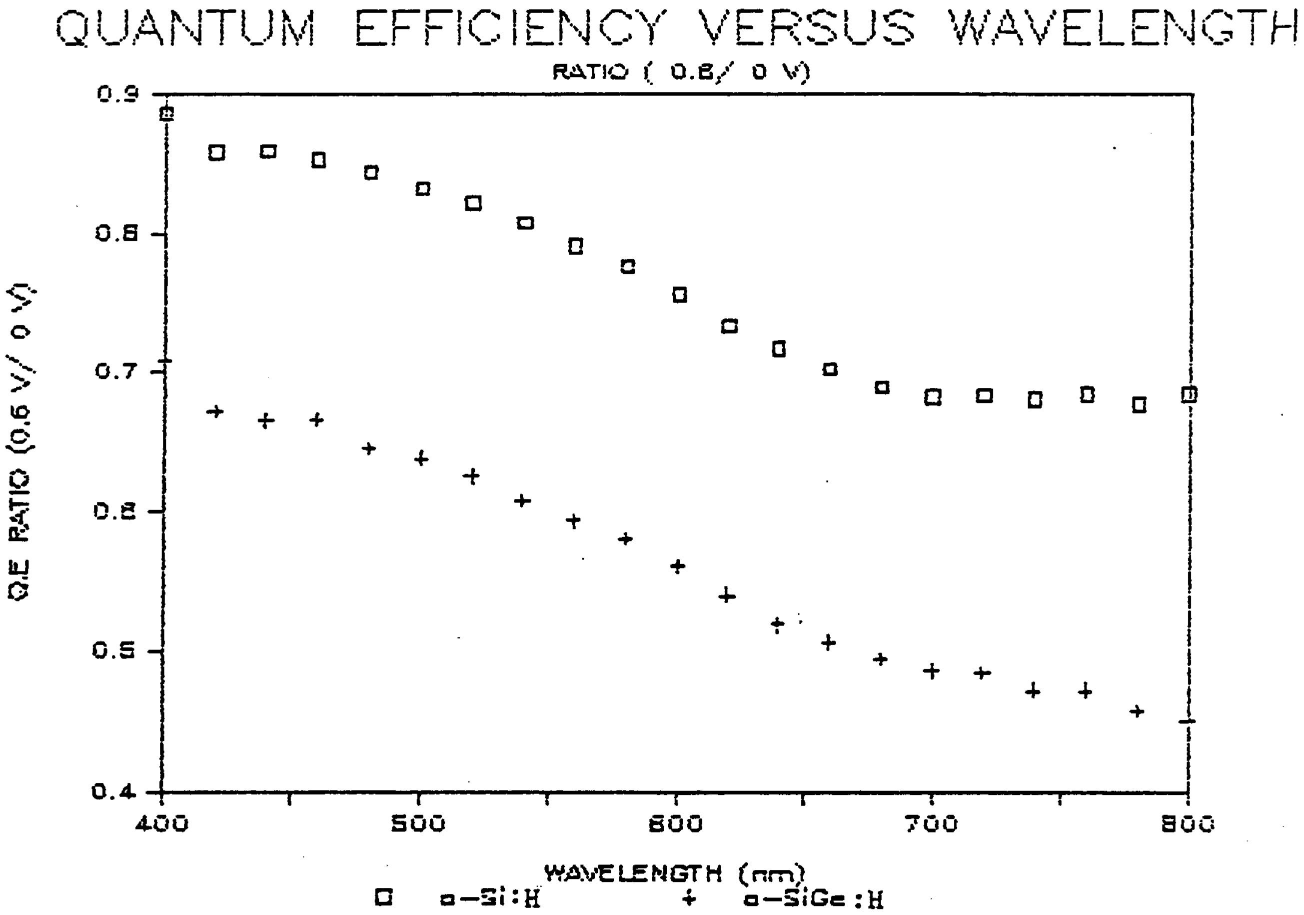

FIGURE 2-15. RATIO OF QUANTUM EFFICIENCY (0.6V/0V) OF a-SiGe:H SINGLE JUNCTION CELLS WITH a-Si:H n-LAYER AND a-SiGe:H n-LAYER.

configuration has resulted in the highest efficiency two stacked cell. We have measured conversion efficiency has high as 10.2% with the following photovoltaic parameters: $V_{oc} = 1.752V$, $J_{sc} = 8.16mA/cm^2$ and fill factor = 0.712. Figure 2-16 shows the J-V characteristics of this cell and Figure 2-17 shows the quantum efficiency versus wavelength of this cell. As can be seen from this figure, the blue response (400nm) of the front cell is about 0.65 which is higher than that normally obtained on single junction a-Si:H cells, and the currents are well matched at about $8.3mA/cm^2$.

2.2.4.2 a-Si:H/a-Si:H Stacked Cells

These cells have conventional a-Si:H i-layers where the thicknesses of the top and bottom cells are designed so that the two cells generate the same current. The highest conversion efficiency with this combination was 9.8% with the following parameters: $V_{oc} = 1.713V$, $J_{sc} = 7.99mA/cm^2$, and fill factor = 0.717. Figures 2-18 and 2-19 show the J-V characteristics and quantum efficiency measurements of this cell. These cells have lower values of V_{oc} than a-SiC:H/a-Si:H cells. Moreover the blue response (400nm) is about 0.55 as compared to 0.65 for silicon-carbide stacked cells. The currents match in this case at about $8.0mA/cm^2$.

2.2.4.3 a-SiC:H/a-SiGe:H Stacked Cells

In this device configuration the top cell consists of an a-Si:C:H i-layer with an optical bandgap between 1.8 to 1.85eV and the bottom cell consists of an a-SiGe:H i-layer with an optical bandgap of about 1.55eV. The cell with the highest short-circuit current density had a conversion efficiency of 9.2% with the following parameters: $V_{oc} = 1.612V$, $J_{sc} = 9.39mA/cm^2$ and fill-factor = 0.612. Figures 2-20 and 2-21 show the J-V characteristics and the quantum efficiency measurements of this device. The current density generated from the top cell is $9.5mA/cm^2$ and that from the bottom cell is $9.8mA/cm^2$ which means the total current generated in these cells in parallel would be $19.3mA/cm^2$. This is higher than the highest current that we have obtained on a-Si:H single junction cell. Moreover, the bottom cell has a response of about 70% at 700nm and a a-SiC/a-Si

Cell No. L7127-IFS2ITO
Date 052687
Voc = 1.752 Volts
Jsc = 8.16 mA/cm^2
F.F. = .712
Eff = 10.17%
Power = 10.17 mW/cm^2
Illum. = 99.24 mW/cm^2
V max = -1.450 Volts
J max = 7.01 mA/cm^2
Rs = 2.27E + 01 ohm/cm^2
Rsh = 2.85E + 03 ohm-cm^2
Temp = 27.1 deg C
Cell Area = .257 cm^2

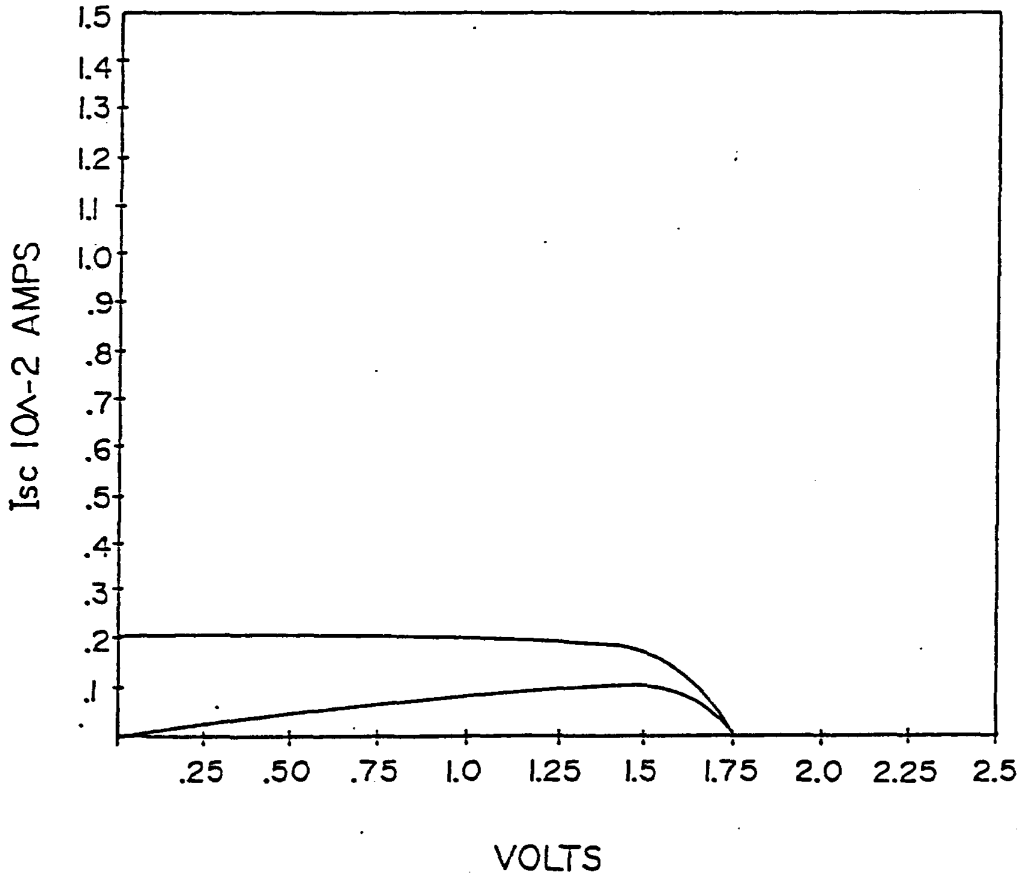

FIGURE 2-16. J-V CHARACTERISTICS OF a-SiC/a-Si:H TWO JUNCTION STACKED CELL UNDER AM1.5 ILLUMINATION.

Date - 05/22/87
Cell Number - L7127-IF-52
Light Bias = Roomlight
Voltage Bias = 0.0 V
AMI.5 Jsc (△) = 8.3 mA/sq. cm
AMI.5 Jsc (□) = 8.4 mA/sq. cm
Comment - STACK

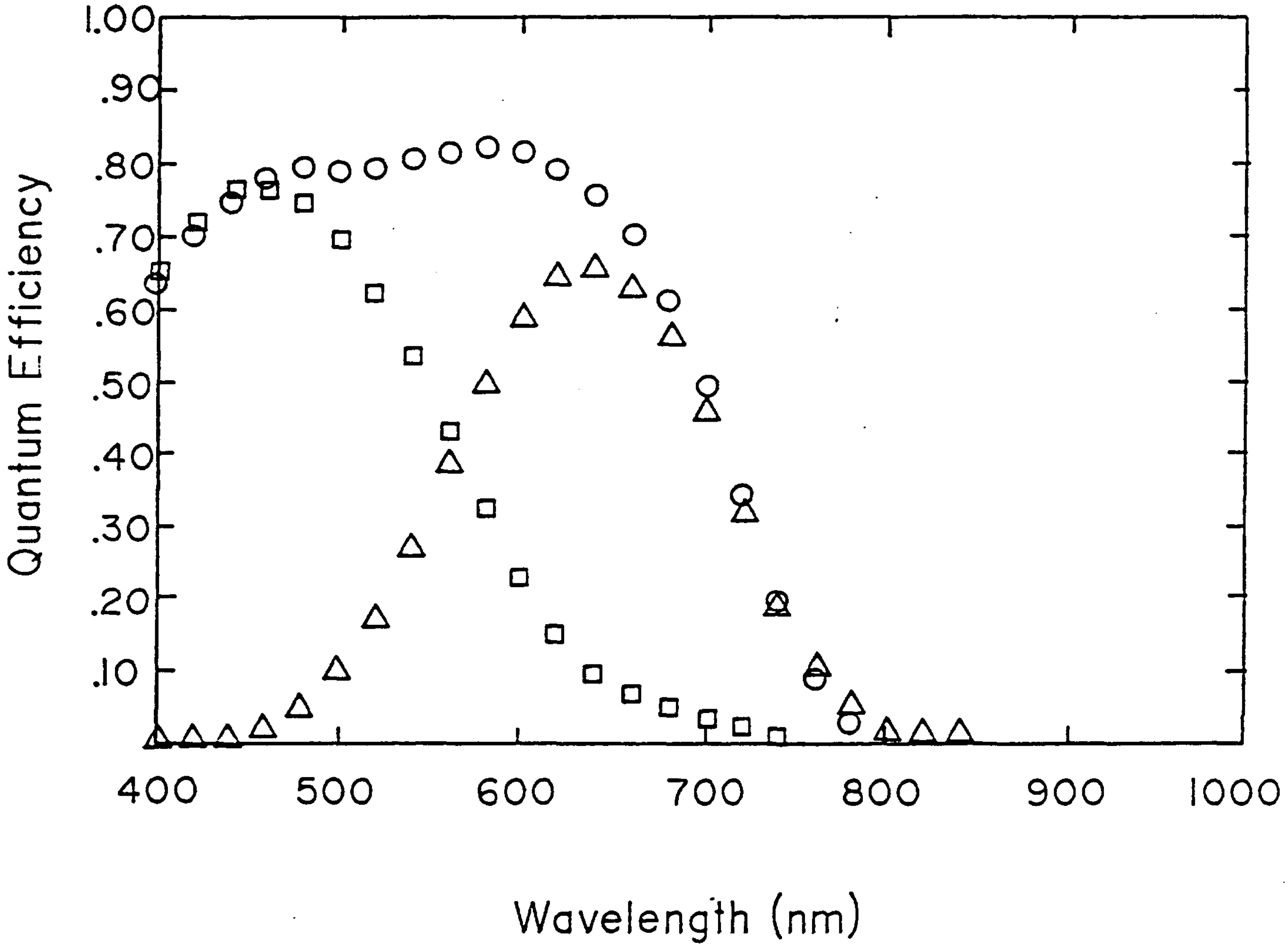

FIGURE 2-17. QUANTUM EFFICIENCY AS A FUNCTION OF WAVELENGTH OF THE CELL SHOWN FIGURE 2-16.

a-Si/a-Si

Cell No. LL7103-3-1 L1 Date 870429
Voc = -1.713 Volts Jsc = 7.99 mA/cm^2
F.F. = .717 Eff = 9.81%
Power = 9.81 mW/cm^2 Illum. = 99.99 mW/cm^2
V max = -1.391 Volts J max = 7.05 mA/cm^2
Rs = 2.59E+01 ohm/cm^2 Rsh = 9.97E+03 ohm/cm^2
Temp. = 25 deg. C Cell Area = 1.050 cm^2

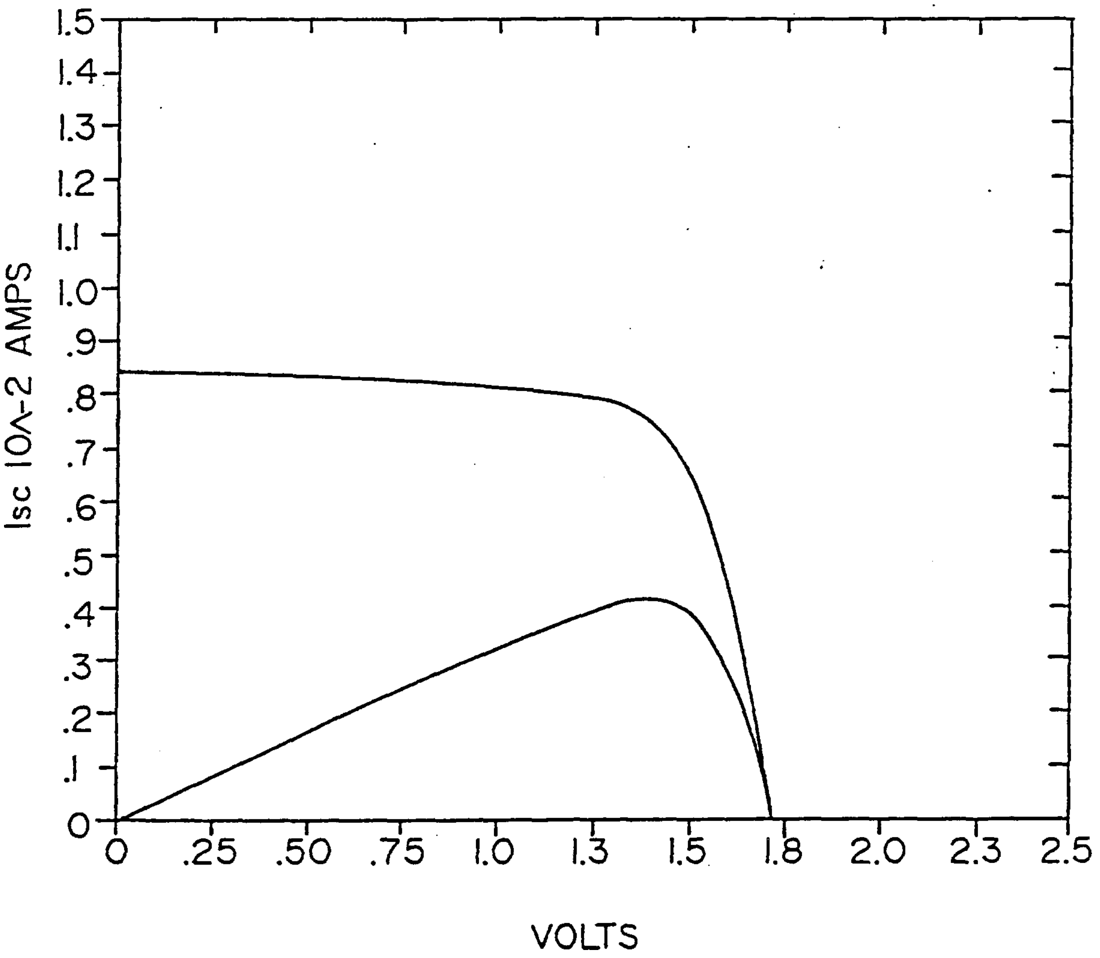

FIGURE 2-18. J-V CHARACTERISTICS OF a-Si:H/a-Si:H TWO-JUNCTION STACKED CELL UNDER AM1.5 ILLUMINATION.

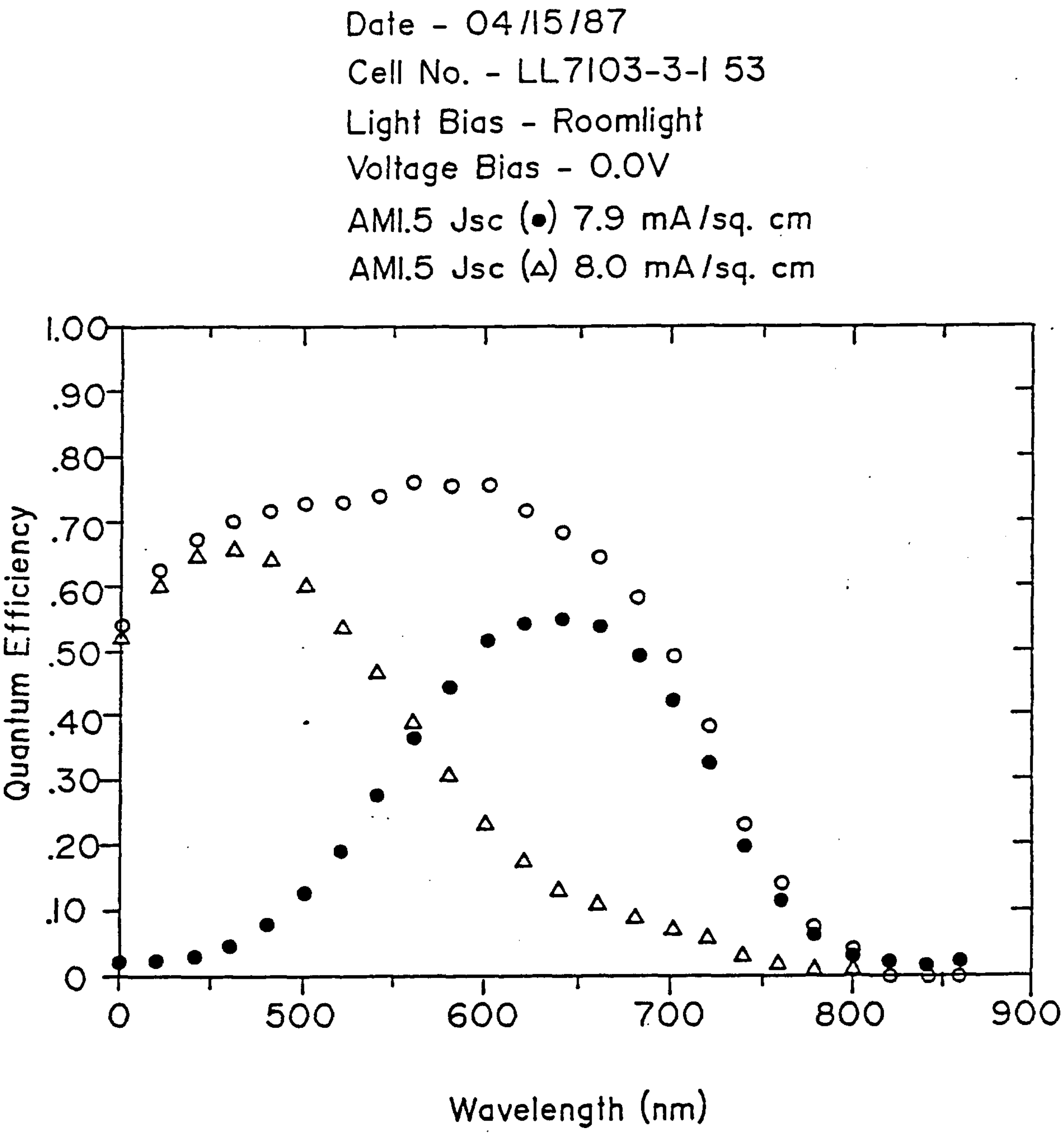

FIGURE 2-19. QUANTUM EFFICIENCY AS A FUNCTION OF WAVELENGTH OF THE CELL SHOWN IN FIGURE 2-18.

a-SiC/a-SiGe

Cell No. LL7127-2-3S3ARR Date 052687
Voc = -1.612 Volts
Jsc = 9.39 mA/cm^2
F.F. = .611
Eff = 9.24%
Power = 9.24 mW/cm^2
Illum. = 97.83 mW/cm^2
V max = -1.211 Volts
J max = 7.63 mA/cm^2
Rs = 3.16E + 01 ohm/cm^2
Rsh = 1.27E + 03 ohm/cm^2
Temp = 25 deg C
Cell Area = .256 cm^2

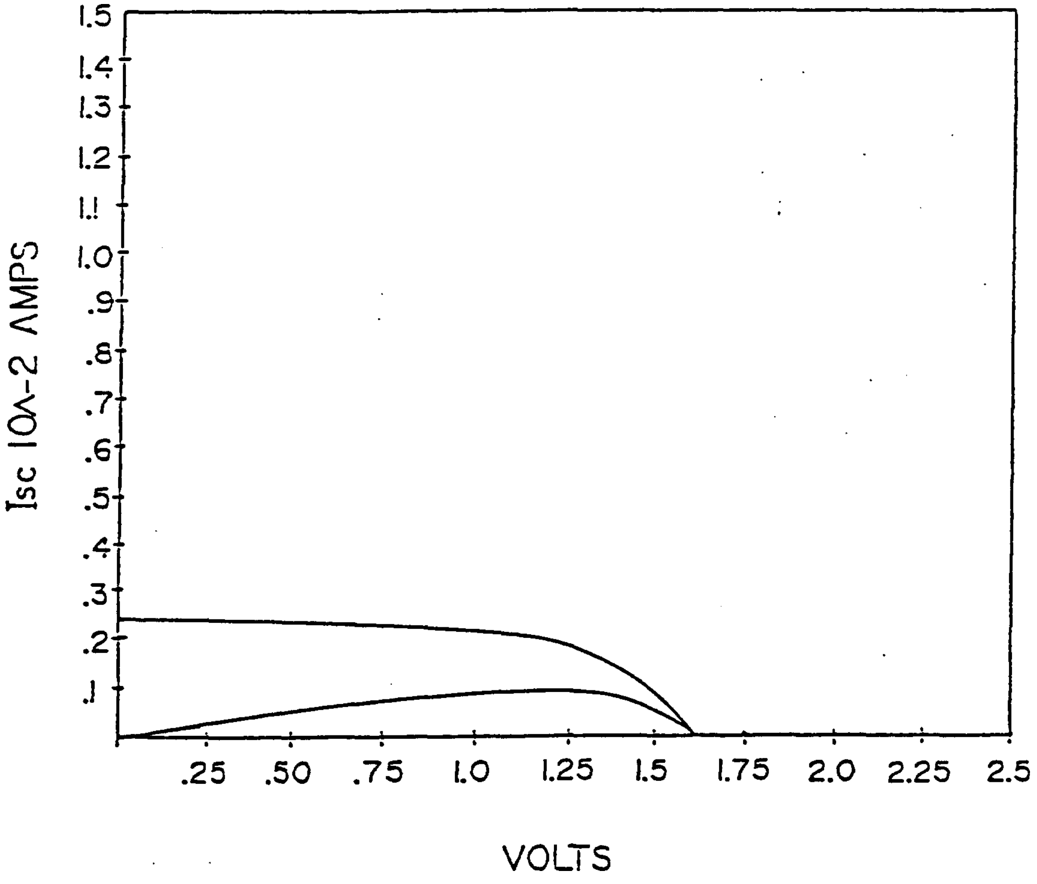

FIGURE 2-20. J-V CHARACTERISTICS OF a-SiC/a-SiGe TWO-JUNCTION STACKED CELL UNDER AM1.5 ILLUMINATION.

Date - 05/27/87
Cell Number - LL7127-2-3 53
Light Bias = Roomlight
Voltage Bias = 0.0 V
AMl.5 Jsc (△) = 9.8 mA/sq. cm
AMl.5 Jsc (□) = 9.5 mA/sq. cm
Comment - RBHT2 AR

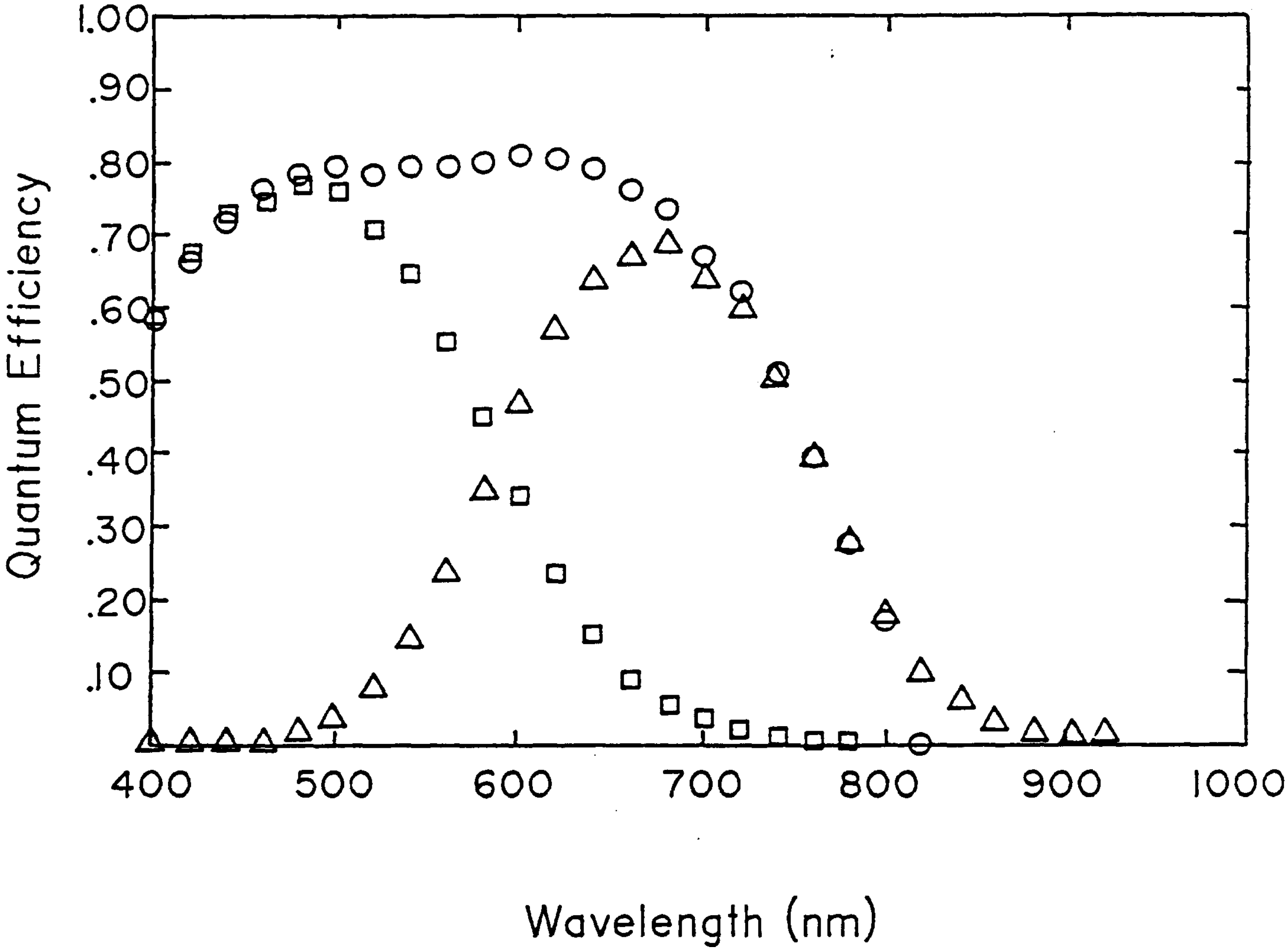

FIGURE 2-21. QUANTUM EFFICIENCY VERSUS WAVELENGTH OF THE CELL SHOWN IN FIGURE 2-20.

response of 17% at 800nm which clearly demonstrates that the bottom cell is collecting carriers generated beyond the a-Si:H regime. The highest conversion efficiency obtained with this device configuration was 10.51% with the following photovoltaic parameters: $V_{oc} = 1.722V$, $J_{sc} = 9.11mA/cm^2$ and FF = 0.67. Figures 2-22 and 2-23 show the J-V characteristics and the quantum efficiency measurements of this cell. The cell measurements were verified at SERI where a conversion efficiency of 10.3% was measured. Table 2-10 shows a comparison of measurements made at Solarex and SERI.

2.2.4.4 Triple Stacked Cells

We have fabricated a few exploratory triple stacked cells with the following device configuration: a-SiC:H/a-Si:H/a-SiGe:H where the optical bandgap of the top cell is about 1.85eV and that of the bottom cell is about 1.55V. The best triple stacked cell had a conversion efficiency of 8.28% with the following parameters: $V_{oc} = 2.481V$, $J_{sc} = 4.99mA/cm^2$ and fill-factor = 0.669. Figure 2-24 shows the J-V characteristics of this cell and Figure 2-25 shows the corresponding quantum efficiency versus wavelength measurements. It is clear that the cells are not current matched and further optimization is needed.

2.2.5 A Note of Caution on Microcrystalline Doped Layers

Recently some p-i-n solar cells were fabricated at Solarex which had microcrystalline n-layers. These cells had an anomalous high value of short-circuit current density (J_{sc}) when measured under AM1.5 illumination. There was a large discrepancy in J_{sc} measured by the simulator with the integration of the external quantum efficiency with the AM1.5 spectrum (example: the simulator measured $18.5mA/cm^2$ whereas the QE measurements gave $14.4mA/cm^2$. A careful examination of these cells revealed that due to the extremely high lateral conductance of the microcrystalline n-layers, the active area of the cell was no longer being defined by the rear metal contact i.e., current collection was occurring beyond the metal contact area. After the a-Si:H was etched away from areas around the cell, the rear contact correctly defined the ctive area of the cell and the discrepancy between solar J-V measurements and

FIGURE 2-22. J-V CHARACTERISTICS OF HIGHEST EFFICIENCY a-SiC/a-SiGe TWO STACKED JUNCTION CELL UNDER AM1.5 ILLUMINATION.

Cell No. LL7217-3-3 TIAR
Date 870810
Voc = -1.722 Volts
Jsc = 9.11 mA/cm^2
F.F. = .670
Eff = 10.51%
Power = 10.51 mW/cm^2
Illum. = 101.01 mW/cm^2
V max = -1.354 Volts
J max = 7.76 mA/cm^2
Rs = 2.26E+01 ohm/cm^2
Rsh = 6.67E+03 ohm/cm^2
Temp = 24.1 deg. C
Cell Area = .755 cm^2

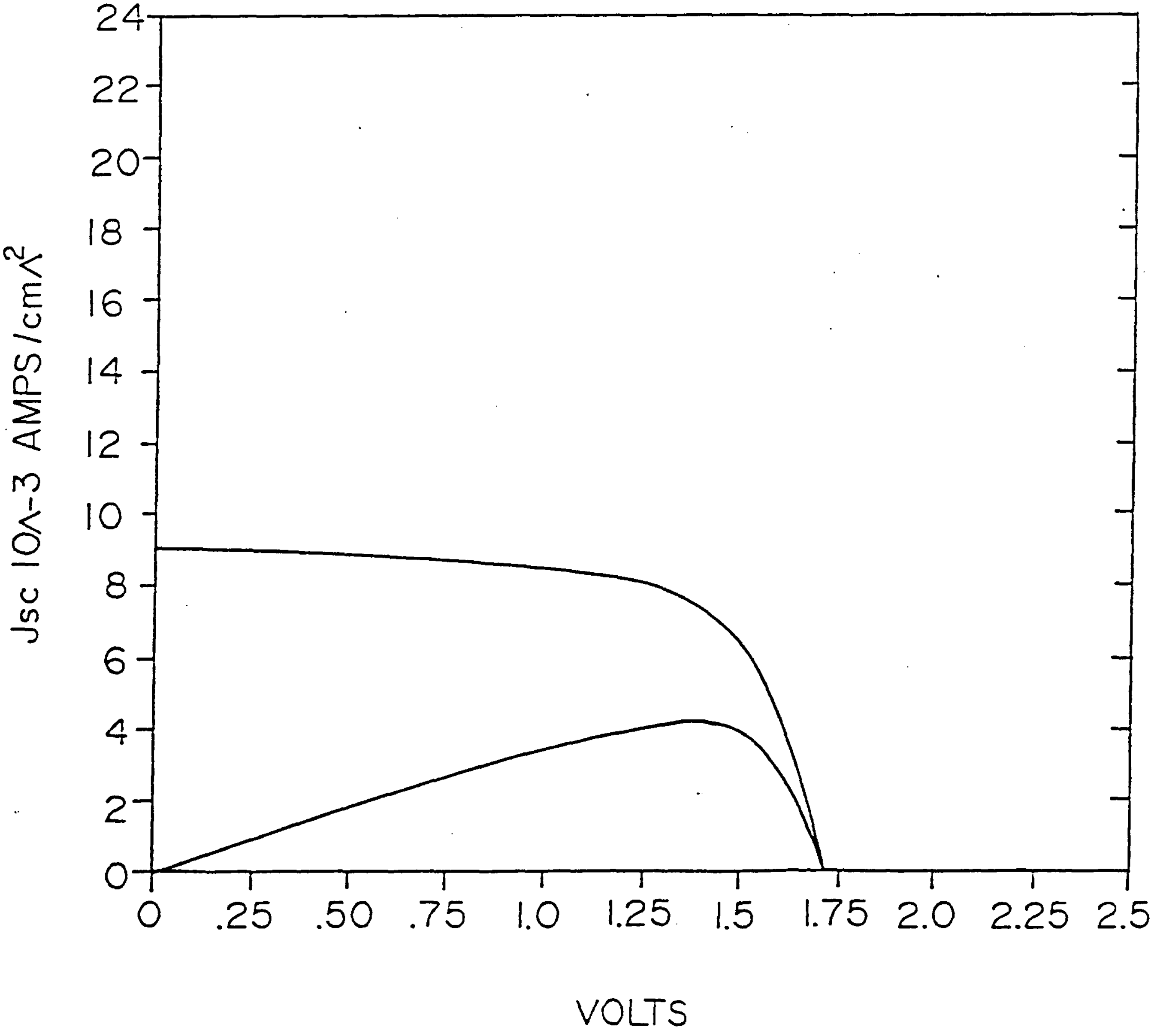

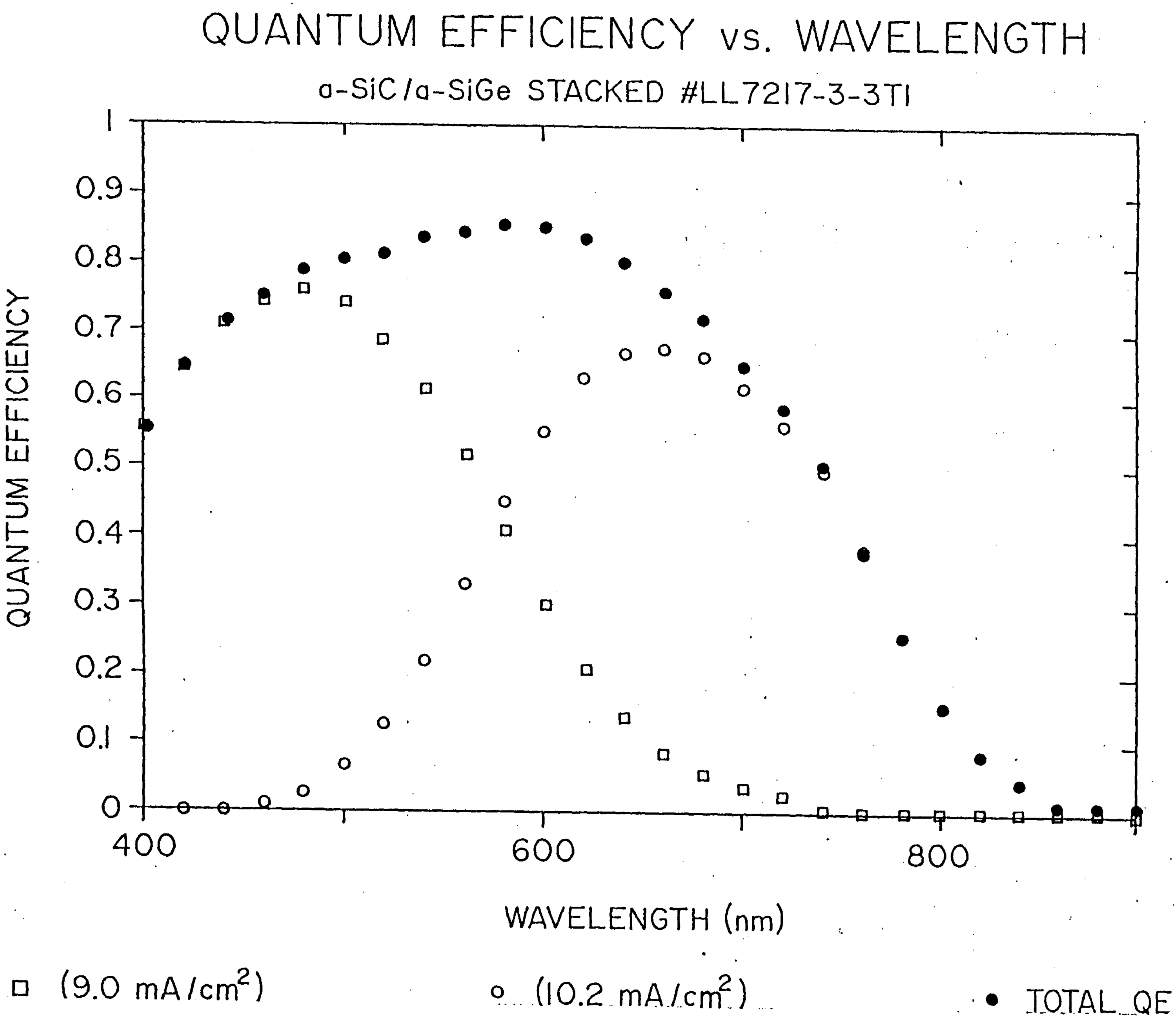

FIGURE 2-23. QE MEASUREMENTS OF CELL SHOWN IN FIGURE 2-22.

TABLE 2-10

COMPARISON OF a-SiC:H/a-SiGe:H STACKED CELLS MEASURED AT SOLAREX AND SERI

Cell #	Area (cm^2)	V_{oc} (V)	J_{sc} (mA/cm^2)	FF	Efficiency (%)	Measured at
LL721733T1	0.755	1.722	9.11	0.670	10.51	Solarex
LL721733T1	0.758	1.666	9.032	0.6856	10.31	SERI

Cell No. LL7215-3-3 SIRR
Voc = −2.481 Volts
F.F. = .669
Power = 8.28 mW/cm^2
V max = -1.953 Volts
Rs = 6.68E+01 ohm/cm^2
Temp = 25.5 deg. C

Date 080687
Jsc = 4.99 mA/cm^2
Eff = 8.28%
Illum. = 99.38 mW/cm^2
J max = 4.24 mA/cm^2
Rsh = 5.51E+03 ohm/cm^2
Cell Area = .257 cm^2

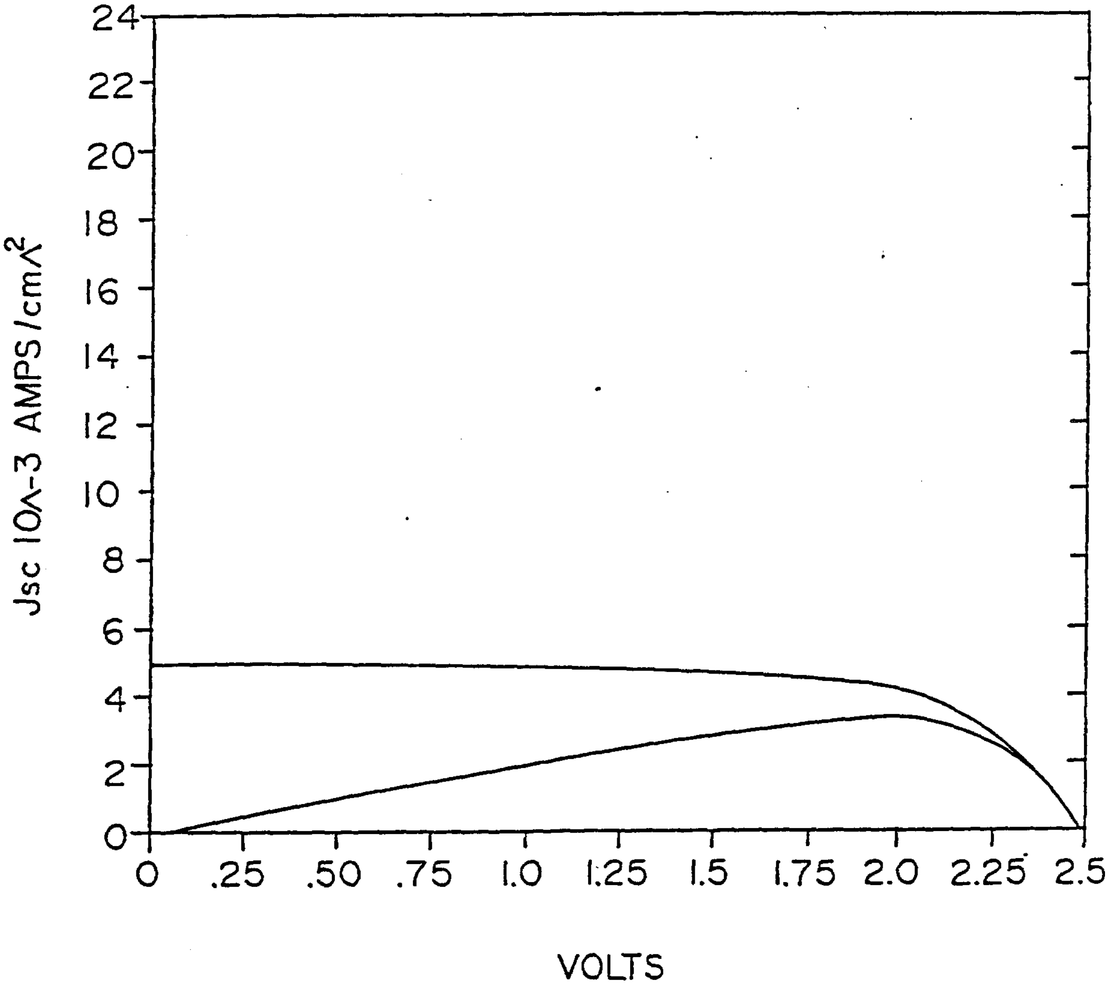

FIGURE 2-24. J-V CHARACTERISTICS OF a-SiC/a-Si/a-SiGe TRIPLE-STACKED CELL UNDER AM1.5 ILLUMINATION.

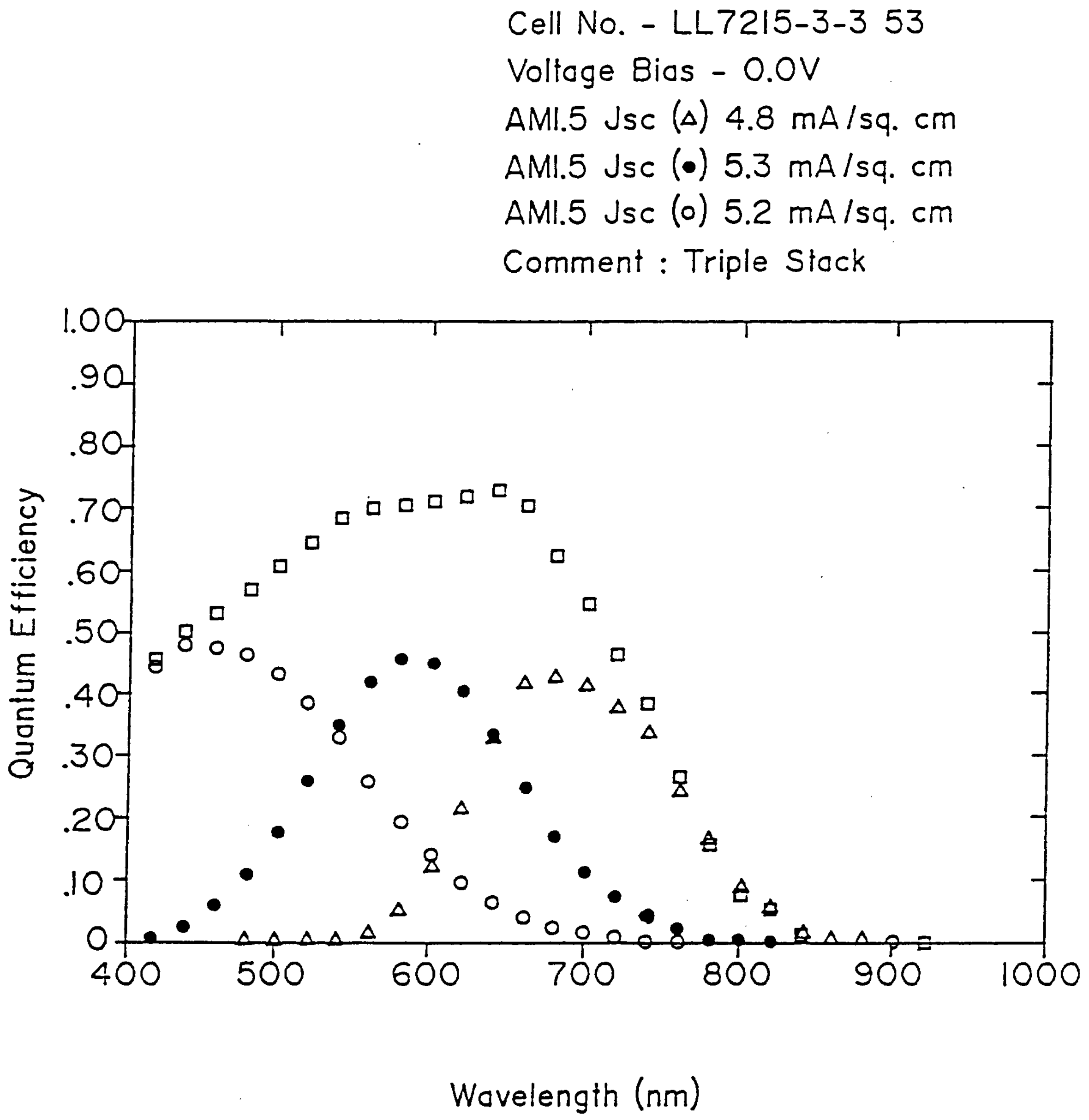

FIGURE 2-25. QUANTUM EFFICIENCY VERSUS WAVELENGTH OF THE CELL SHOWN IN FIGURE 2-24.

QE measurements was eliminated. This also resulted in an increase in the shunt resistance which improved the fill-factor of the cell. These results are tabulated in Table 2-11.

These results show that the active area of the cell cannot always be defined by the rear metal contact. Results like these elucidate the importance of verification of J_{sc} values by external quantum efficiency measurements since the latter measurements are independent of the area of the cell.

2.3 a-SiGe ALLOYS

All of these alloys were deposited using plasma-enhanced CVD in the temperature range 265-275°C.

Three series of SiGe:H films with different feedstocks have been made: 1) silane + germane, 2) disilane + germane, and 3) silane + germane diluted with hydrogen (H_2/total deposition gas = 0.40). For the films grown from silane and germane, we found that that amount of silicon and germanium incorporated in the films (measured using x-ray fluorescense calibrated with RBS) was approximately three times greater than the amount of germanium in the deposition gas i.e., 5% germane in the deposition gas leads to 15% germanium in the film. This preferential incorporation of germanium presumably arises from the lower bond dissociation energy for germane (86 kcal/mole) than for silane (90. kcal/mole). We expected that the use of disilane, with a bond dissociation energy of 74 kcal/mole, would increase the relative amount of silicon incorporated; however, no change was observed.

PDS measurements indicate that, regardless of feedstock, all of these films have the same density of midgap states (within the accuracy of this measurement) as long as comparisons are made among films containing the same amount of germanium (see Figure 2-26). However, the Urbach edge in the film made with disilane + germane (74meV for the film shown in Figure 2-26) is not as steep as that in the silane + germane film (67meV).

TABLE 2-11

PHOTOVOLTAIC PARAMETERS OF CELLS WITH MICROCRYSTALLINE n LAYERS

Cell #	V_{oc} (mV)	J_{sc} (mA/cm^2)	FF	η (%)	J_{sc} from QE	R_{sh} (Ω-cut)	Remarks
D7149S3	852	18.52	0.604	9.53	14.4	175	Unmasked, as deposited
	852	14.47	0.672	8.31	14.4	853	Masked, after Si etch
D7149S2	843	18.35	0.583	9.01	14.3	461	Unmasked, as deposited
	851	14.68	0.656	8.16	14.3	2800	Masked, after Si etch

FIGURE 2-26. PDS MEASUREMENTS ON a-SiGe:H FILMS DO NOT SHOW SIGNIFICANT DIFFERENCES IN THE DENSITY OF MIDGAP STATES WHETHER THE SILICON FEEDSTOCK IS SILANE OR DISILANE.

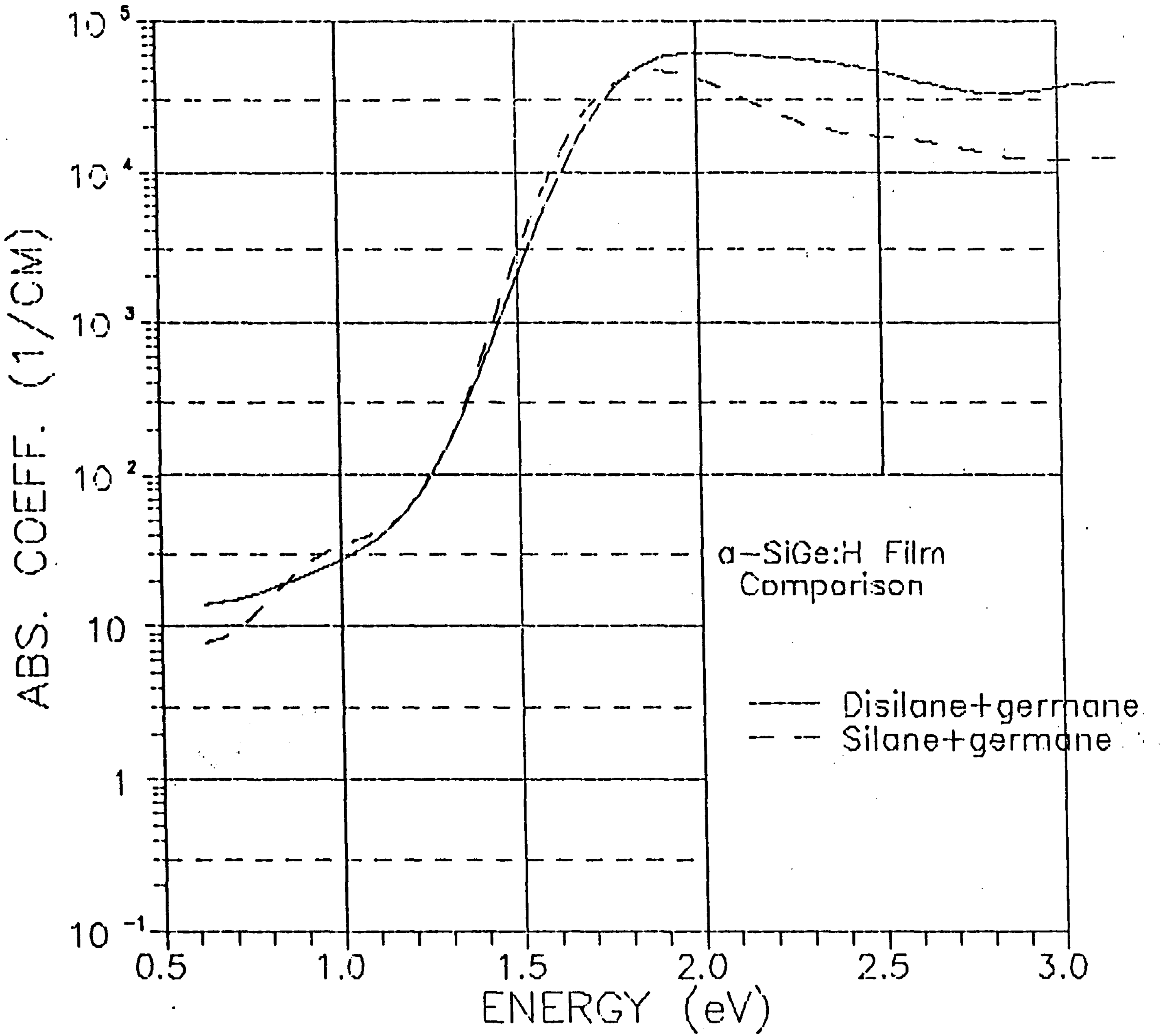

Greater differences between films were apparent in the FTIR results. For films containing small amounts of germanium, the films made with disilane contained more hydrogen and had more dihydride bonding than the corresponding films made with silane. However, as the germanium content was increased, the differences between films made with different feedstocks diminished until no differences were observed.

The photo-conductivity of a film containing ∿25% germanium (E_g ∿ 1.58eV) is about 1.5 orders of magnitude lower than that of a film containing no germanium (E_g ∿ 1.70eV). Using higher values of hydrogen dilution, we hope to improve on the photoconductivity of films containing significant amounts of germanium.

2.4 SiC ALLOYS

A series of a-$Si_{1-x}C_x$:H films has been grown to study the use of this material as a wide bandgap i-layer for the top cell of a stacked cell. The films were deposited at 265°C using DC plasma-enhanced CVD of silane and methane without hydrogen dilution. As the amount of methane in the deposition gas was increased from 0 to 50%, the amount of carbon incorporated in the films increased linearly from 0 to 17%, while the Tauc bandgap increased from 1.70eV to 2.27eV.

PDS measurements on these films (see Fig. 2-27) show a decrease in the slope of the Urbach edge corresponding to an increase in the characteristic energy of the valence band tail states from 65meV to 105meV. The PDS results also show a significant increase in the density of midgap states as the carbon content of the films is increased. Not surprisingly, the conductivity of these films was very poor.

The growth rate of some films was varied from 3 to 8Å/sec. PDS and Tauc bandgap measurements both show that the bandgap is increased by ∿65meV for the film grown at the fastest rate. RBS measurements confirm that higher growth rates do lead to slightly more carbon incorporation, although RBS is not sensitive enough to always detect this increase for small increases in growth rate. Increased hydrogen incorporation at higher growth rates may also play a role in increasing

the bandgap, although FTIR measurements on these films do not give a clear indication of this. We also found that increasing the growth rate from 3 to 8Å/sec was not sufficient to allow the expected increased in the amount of polymer-like bonding to be observed by FTIR.

Our immediate plans are to use alternate feedstocks and hydrogen dilution in an attempt to improve the midgap density of states and the conductivity of these films.

2.5 MICROCRYSTALLINE FILMS

2.5.1 p^+ Microcrystalline Si:H Films

The development of highly conductive (10_{Ω}-cm^{-1}) p^+ microcrystalline Si which can be dc plasma deposited has been reported previously by Solarex [1]. One impediment to the direct use of this material in p-i-n single junction cells is the difficulty encountered in producing this material in the thin (~200Å) layers required for the solar cell. The coplanar conductivity diminishes dramatically whenever the layer thickness is decreased below about 800Å (Fig. 2-28).

Three possibilities can be put forth to explain the observed decrease in conductivity with decreasing thickness: depletion of mobile carriers by surface states, percolation phenomena, or nucleation phenomena. Band bending due to surface states is well known in semiconductors, and conceivably could deplete an entire film of mobile carriers depending on surface state density and energy location, free hole density and film thickness. If the microcrystalline p^+ material exhibits "island" growth during initial stages, then the coplanar conductivity could change rapidly as the film becomes thicker and the islands coalesce, the so called percolation effect. Finally, it is possible that a critical thickness or time of deposition is required before the nucleation of silicon microcrystals can occur.

Recent evidence indicates that the conductivity is primarily governed by nucleation. Sample films of thickness 200Å, 800Å and 6300Å (marked on Fig.

FIGURE 2-28. CONDUCTIVITY VS. FILM THICKNESS FOR p^+ Si:H FILMS GROWN UNDER STANDARD CONDITIONS FOR MICROCRYSTALLINE FILM GROWTH. (⊛ DENOTES CELLS SUBMITTED FOR RAMAN ANALYSIS)

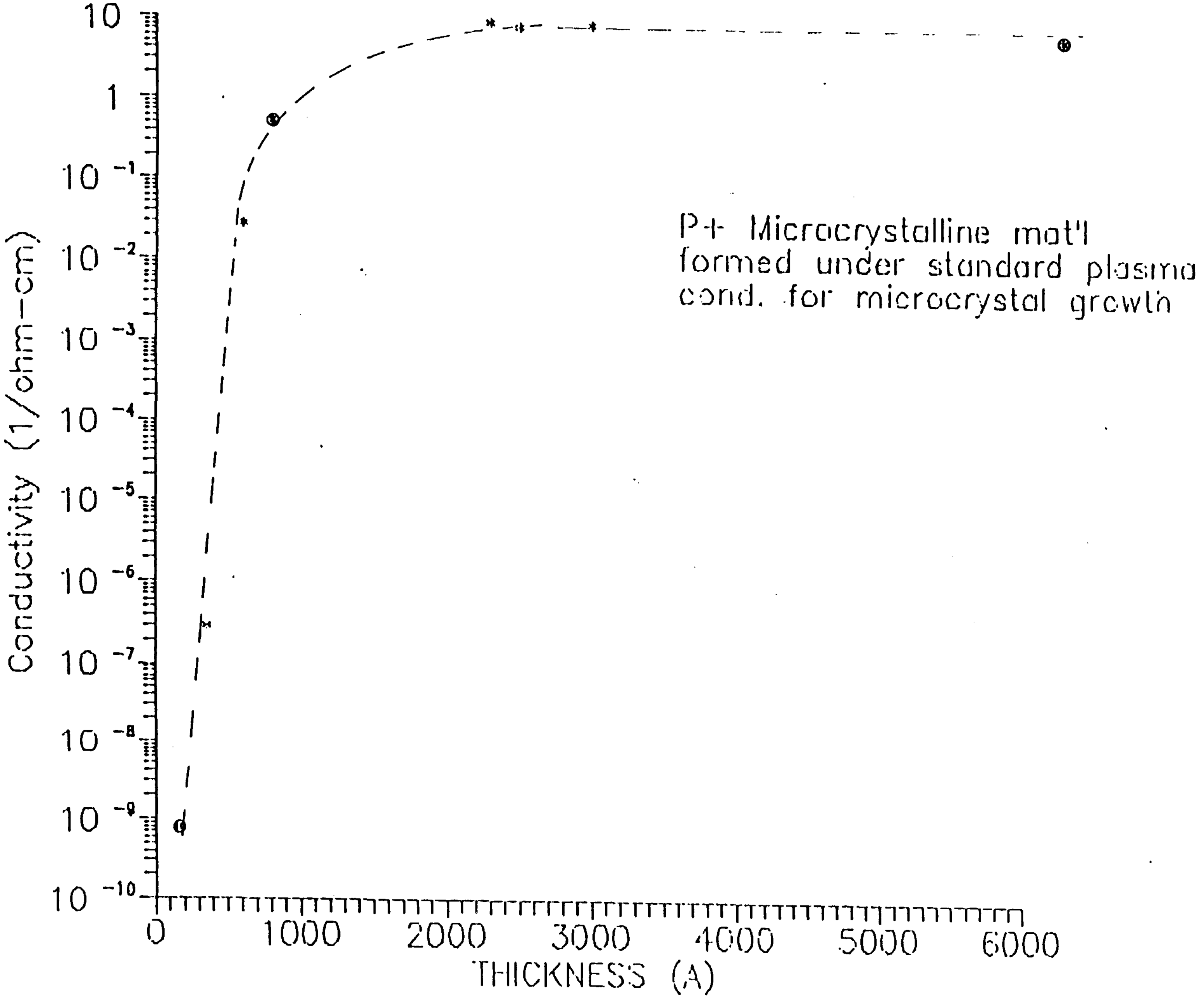

2-28) were found to contain volume fractions of <10%, 70% ± 10% and 90% to 100% microcrystalline material respectively. The Raman spectra in the region of the Si-Si bond for these three different thickness films is shown in Fig. 2-29. Increasing microcrystallinity is indicated by a narrowing of the peak as well as a slight shift in the centroid of the peak.

Presumably, as thickness decreases below 800Å, an increasing fraction of the material exists as poor quality amorphous p^+ silicon. Microcrystalline p^+ Si:H is not expected to be significantly depleted by surface band bending on the basis of its high free hole concentration, however, it is reasonable to expect that the amorphous p^+ Si may be depleted in thin layers. The coplanar conductivity of p^+ a-Si vs. thickness was measured to confirm this assertion (see Fig. 2-30) and the expected decrease in conductivity with decreasing thickness is observed.

It is also reasonable to expect the nucleation of the Si microcrystals to proceed differently on different substrates. So far, however, the volume fraction material in the microcrystalline phase, as judged by Raman analysis for a given film thickness, appears to be about the same on a CTO/glass substrate as it is on quartz. To sum up, it appears that the first deposited material is poor quality amorphous p^+ which is depleted of free holes, and thus exhibits extremely low conductivity [$10^{-10}(\Omega cm^{-1})$ at thicknesses less than 200Å]. As deposition continues, less of the amorphous material is depleted, and the conductivity rises, approaching the bulk conductivity of amorphous p^+ Si. At thicknesses between 500 and 1000Å however, the microcrystals of Si begin to nucleate and the conductivity posts a large increase due to the increasing volume fraction existing in the microcrystalline phase. The microcrystalline material, per se, is assumed to have such high conductivity due to a much increased free hole concentration coupled with a higher hole mobility as compared to amorphous material. The conductivity of the aggregate is likely raised by the presence of even a small amount of microcrystalline material due to proximity doping. In the limit of complete microcrystallinity the conductivity is probably limited by an effective hole mobility which is reduced compared to that of p^+ crystalline silicon due to grain boundary effects.

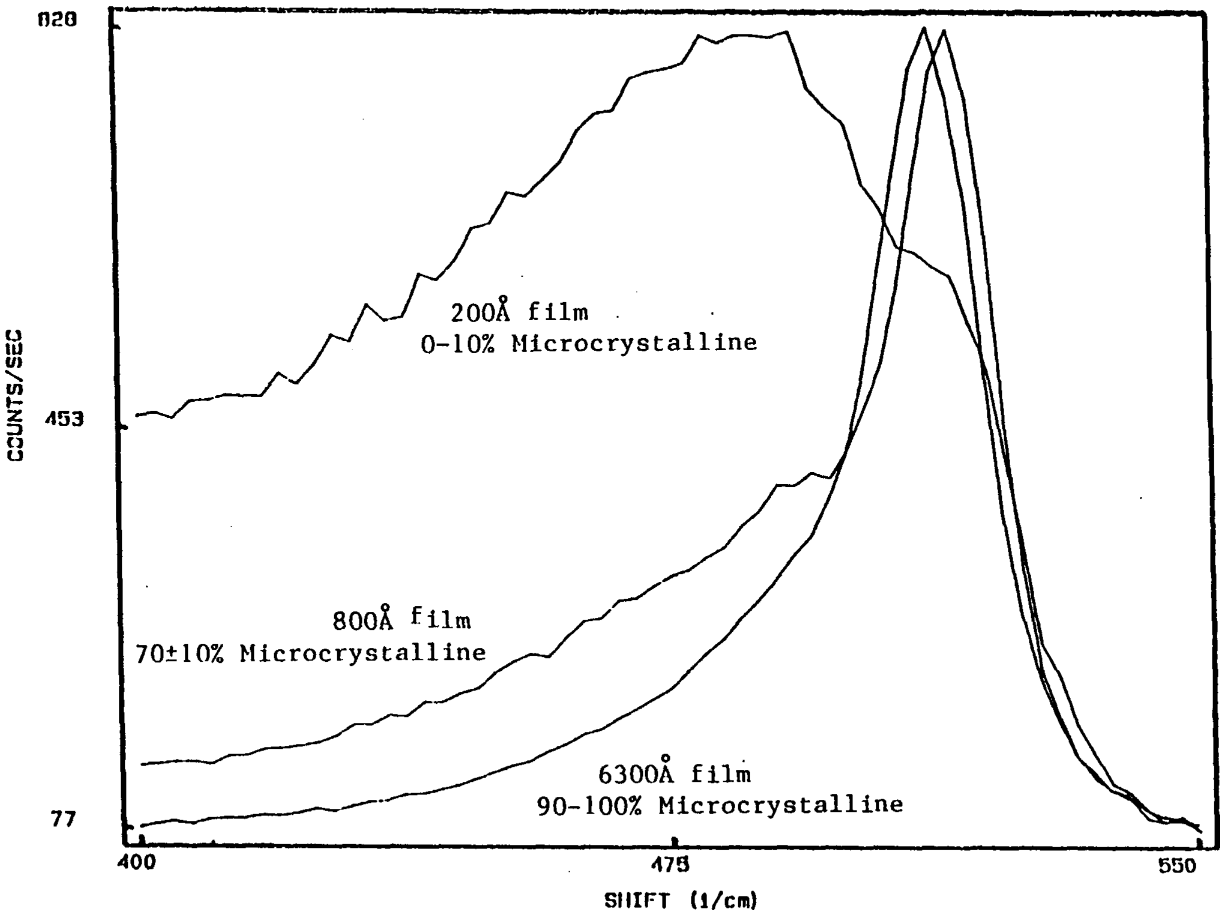

FIGURE 2-29. RAMAN SPECTRA FOR THE THREE FILMS OF DIFFERENT THICKNESSES INDICATED IN FIGURE 2-28.

FIGURE 2-30. COPLANAR CONDUCTIVITY VS. THICKNESS FOR p^+ AMORPHOUS SILICON.

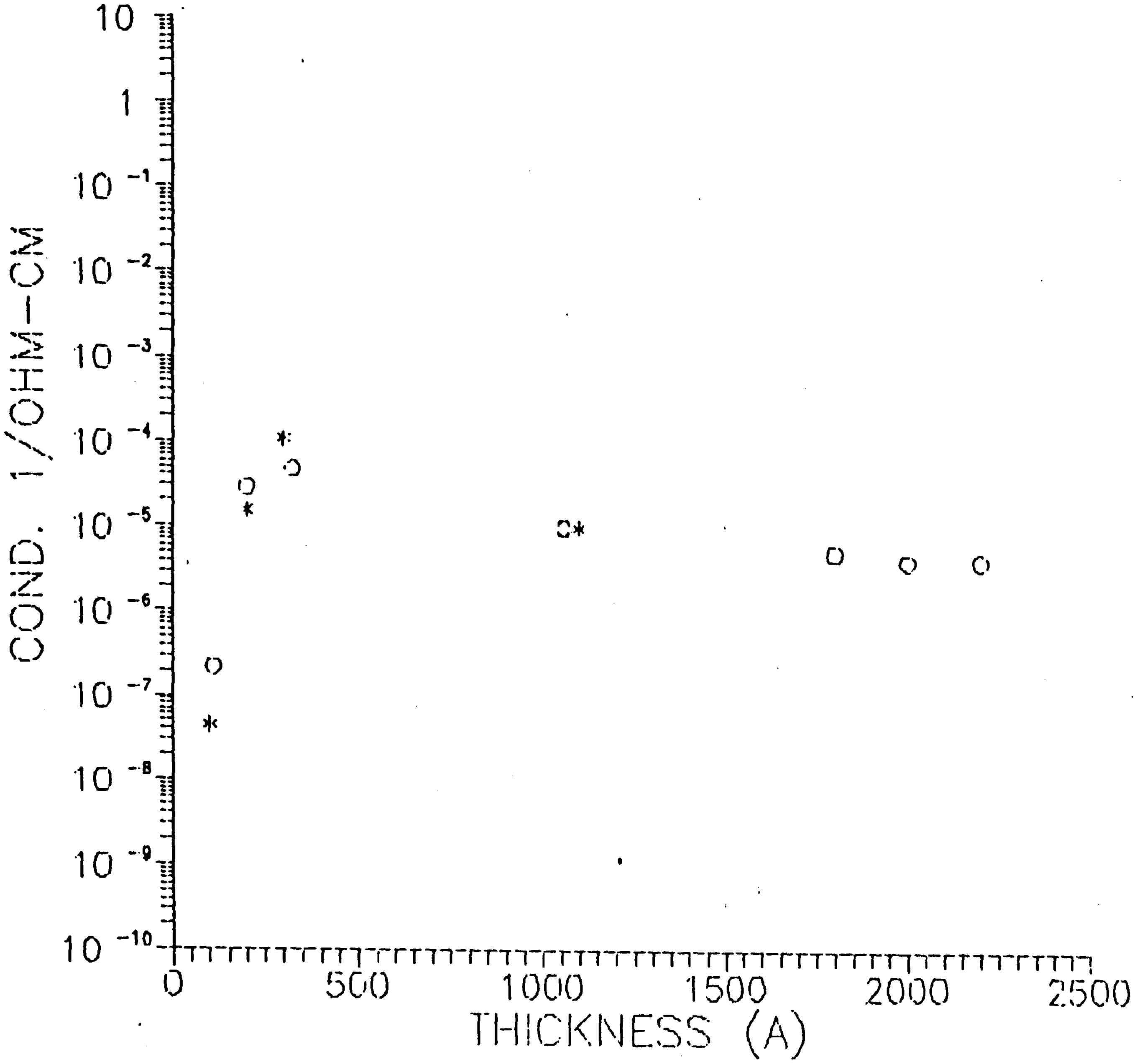

A preliminary search of deposition parameter space which will encourage rapid formation of the microcrystalline phase has involved the variation of deposition temperature, power, pressure, hydrogen dilution, and total gas flow rate. It appears that at least the first 4 of these variables are significant in controlling the nucleation of p^+ Si microcrystals. Although the p^+ layers are still too thick to allow good J_{sc} in a p-i-n cell, it has been possible to produce V_{oc}'s in p-i-n structure cells in the 870 to 890mV range using only the microcrystalline p^+ layer (see Fig. 2-31). This is very encouraging, as historically it has been impossible to produce p-i-n cells with such high V_{oc} without the incorporation of carbon into the p^+ layer, and/or a p^+-i buffer layer. Since these cells using the microcrystalline p^+ layer contain no carbon, and carbon incorporation has been linked to an increased rate of light induced degradation, it is possible that these cells may be more resistant to light-induced degradation.

Present effort is directed toward understanding the relationship between rapid microcrystal nucleation and plasma deposition conditions for the p^+ microcrystalline material, and toward further improvement in the open-circuit voltage of the p-i-n devices which use the p^+ microcrystalline layer instead of the usual a-p^+ a-SiC:H top contact.

2.5.2 n^+ Microcrystalline Si:H Films

Interest in using n^+ microcrystalline Si:H for the rear contact of the p-i-n cell has been stimulated recently by preliminary results indicating improved device performance and thermal stability [5]. The higher conductivity of the n^+ microcrystalline layer should reduce the contact resistance at the n^+/metal contact and should also lead to larger built-in potentials (and hence higher values of V_{oc}). Concurrently, J. Morris and J. O'Dowd [6] have pointed out that a microcrystalline n^+ layer, via a reduced real refractive index, may afford

```
Cell No. S7116E2B          Date 111187                   Cell Area   .075 cm2
Voc  =  -.883 Volts        Jsc  = 10.42  ma/cm2          No. of Segments  1
F.F. =   .664              Eff  =  6.11  %               Voc(I) =   -.889 volts
Power=  6.11  mw/cm2       Illum=102.08  mw/cm2
Vmax =  -.688 Volts        Jmax =  8.88  ma/cm2
Rs   =  1.10E+01 ohm-cm2   Rsh  =  1.74E+03 ohm-cm2
Rscc =  1.00               Rshcc=  0.00
Temp = 25.1 deg C          ITO  =  0.00E+00 ohm/cm2
```

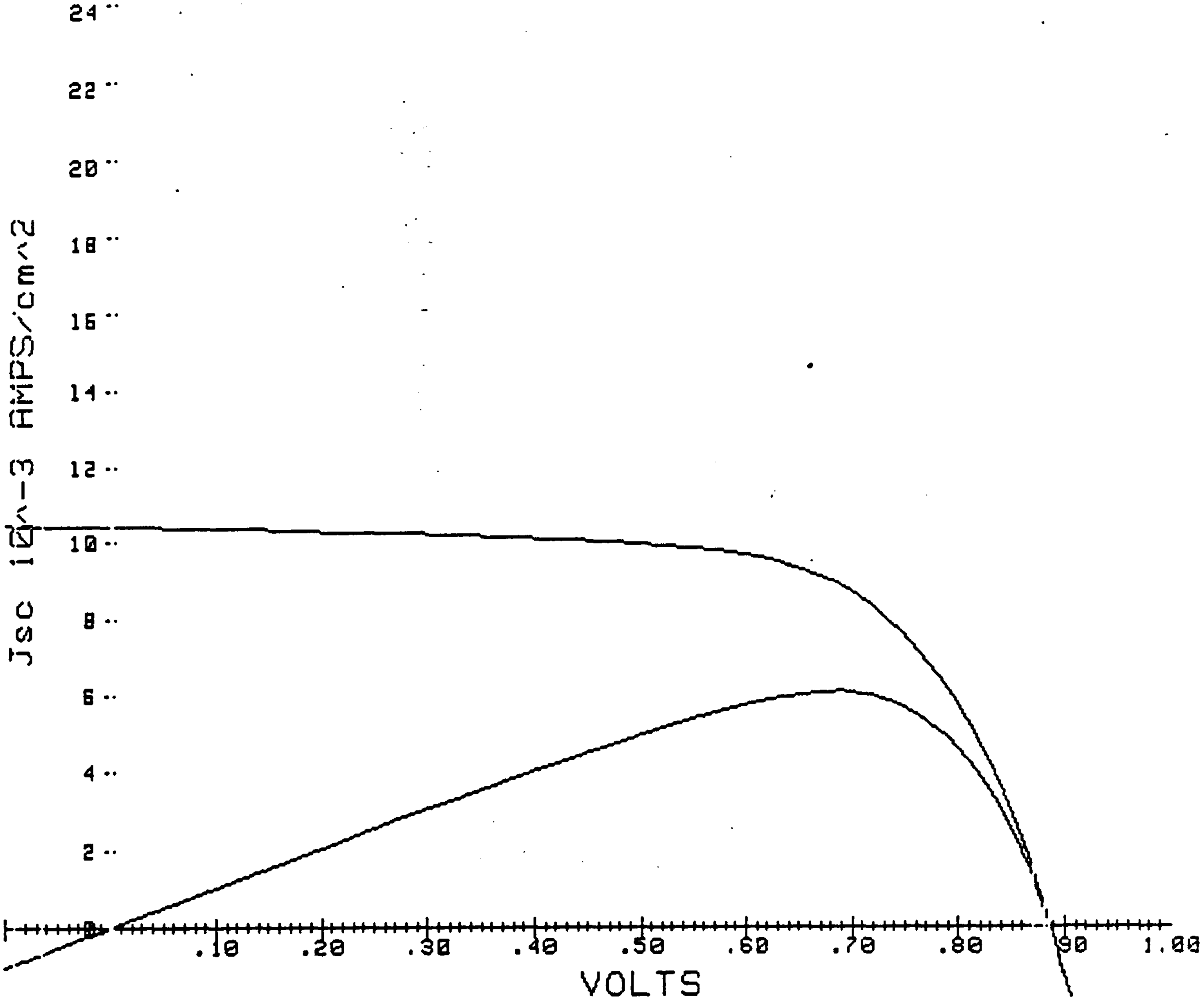

FIGURE 2-31. CURRENT-VOLTAGE CHARACTERISTICS (AM1.5) OF A p-i-n CELL USING A MICROCRYSTALLINE p^+ LAYER WITHOUT CARBON OR A SiC BUFFER LAYER.

better optical reflectivity at the n^+/metal rear contact, thus producing better long wavelength response and improved J_{sc}.

Toward this end, the deposition parameters required to produce highly conductivity $[10(\Omega cm^{-1})]$ n^+ microcrystalline Si:H using dc plasma deposition have been developed (see Fig. 2-32). Because many of the optical properties of microcrystalline silicon lie between those of amorphous and crystalline silicon, the real part of the refractive index at 700nm for microcrystalline silicon could be expected to be between 3.6 and 3.8. Preliminary measurement of this quantity, however, for the dc plasma deposited microcrystalline n^+ material reveals a refractive index of about 2.4, an anomalous but potentially useful result.

Further experiments have confirmed an improved thermal stability [5], i.e., that p-i-n cells using an n^+ microcrystalline layer and aluminum back contacts withstand high temperatures (∿200°C) for extended time (∿20 hours) without apparent degradation, unlike cells using an amorphous n^+ layer. It must be pointed out, however, that these cells also had a much thicker n^+ layer (about 2000Å) than the all amorphous cells (∿400Å n^+ layer) and that the difference in these experiments may be partially or totally responsible for the increased tolerance to high temperature. On this note, it is encouraging, however, that the long wavelength response for the microcrystalline n^+ cells was identical to that of the cells using the standard amorphous n^+ layer, despite the thickness handicap associated with the cell using the microcrystalline n^+ layer.

Initial effort to produce p-i-n cells incorporating a thin microcrystalline n^+ layer demonstrate the same difficulty encountered with p^+ microcrystalline material. That is, nucleation and growth of the microcrystalline material in thin rather than thick layers is much more difficult. However, the constraint on the maximum thickness of the n^+ layer is not nearly so severe as for the p^+ layer, and the problem of producing a microcrystalline n^+ layer of reasonable thickness is likely to be solved quickly. Further testing will then continue to quantify any optical and thermal processing advantages of this approach.

FIGURE 2-32. CONDUCTIVITY VS. 1000/T FOR A DC-PLASMA DEPOSITED MICROCRYSTALLINE MATERIAL WITH ROOM TEMPERATURE CONDUCTIVITY OF ~$10\Omega^{-1}CM^{-1}$ AND AN ACTIVIATION ENERGY OF ~0.02eV.

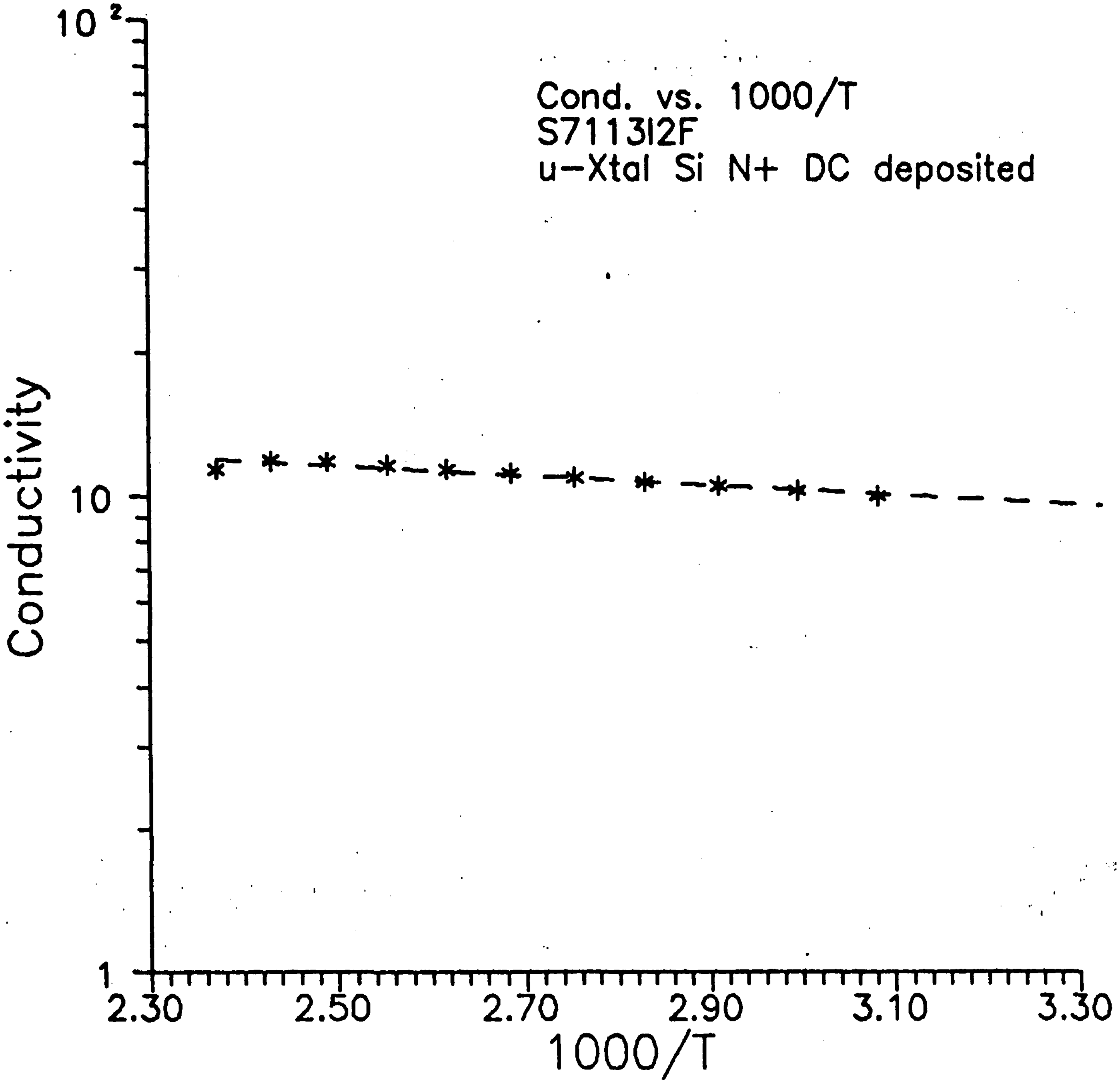

2.5.3 Microcrystalline Silicon-Carbon Alloys

In this section we report the results of a program initiated to study the properties of p-type, microcrystalline, hydrogenated silicon-carbon alloys (μc-SiC:H) for use as p-layers in p-i-n solar cells. Our purpose is to develop such layers having a wide bandgap, high conductivity, and a shallow Fermi level. The advantages of using such material as the p-layer of a p-i-n solar cell are well known.

The films we will be discussing are several thousand Angstroms thick and are deposited onto quartz substrates for electrical, optical, and SIMS (Secondary Ion Mass Spectroscopy) analyses. In addition, other substrates are used that are tailored for specific analytical measurements, e.g., graphite for Rutherford Backscattering compositional analysis, and Si for FTIR (Fourier Transform Infra-Red Spectrometry) lattice vibrational measurements. The principal method used for determining the degree of microcrystallinity in the films is that of Raman Spectroscopy, performed in collaboration with Professor P. Fauchet at Princeton University.

The fundamental electrical properties of these microcrystalline films as a function of increasing carbon concentration are shown in Fig. 2-33 in terms of conductivity on a logarithmic plot vs. reciprocal absolute temperature. The carbon concentration was varied by varying the carbon feedstock gas flow rate while holding constant all other deposition parameters. We have also included in Fig. 2-33 a plot for a film of a-SiC:H (10%C) to be used as a reference standard. In Fig. 2-34 we show a corresponding series of Raman spectra for these films, indicating the degree of microcrystallinity in terms of the ratio of the narrow crystalline Si-Si vibrational line at $517 \mathrm{cm}^{-1}$ to the much broader amorphous Si-Si vibrational line at $476 \mathrm{cm}^{-1}$. In examining Figs. 2-33 and 2-34 several important trends are immediately apparent, as follows: the greater the microcrystallinity, the better the electrical properties in terms of both higher conductivity and lower activation energy ΔE (shallower Fermi level). Increasing carbon, however, acts to suppress the microcrystallinity which, in turn, tends to worsen the electrical properties. Furthermore, carbon may additionally

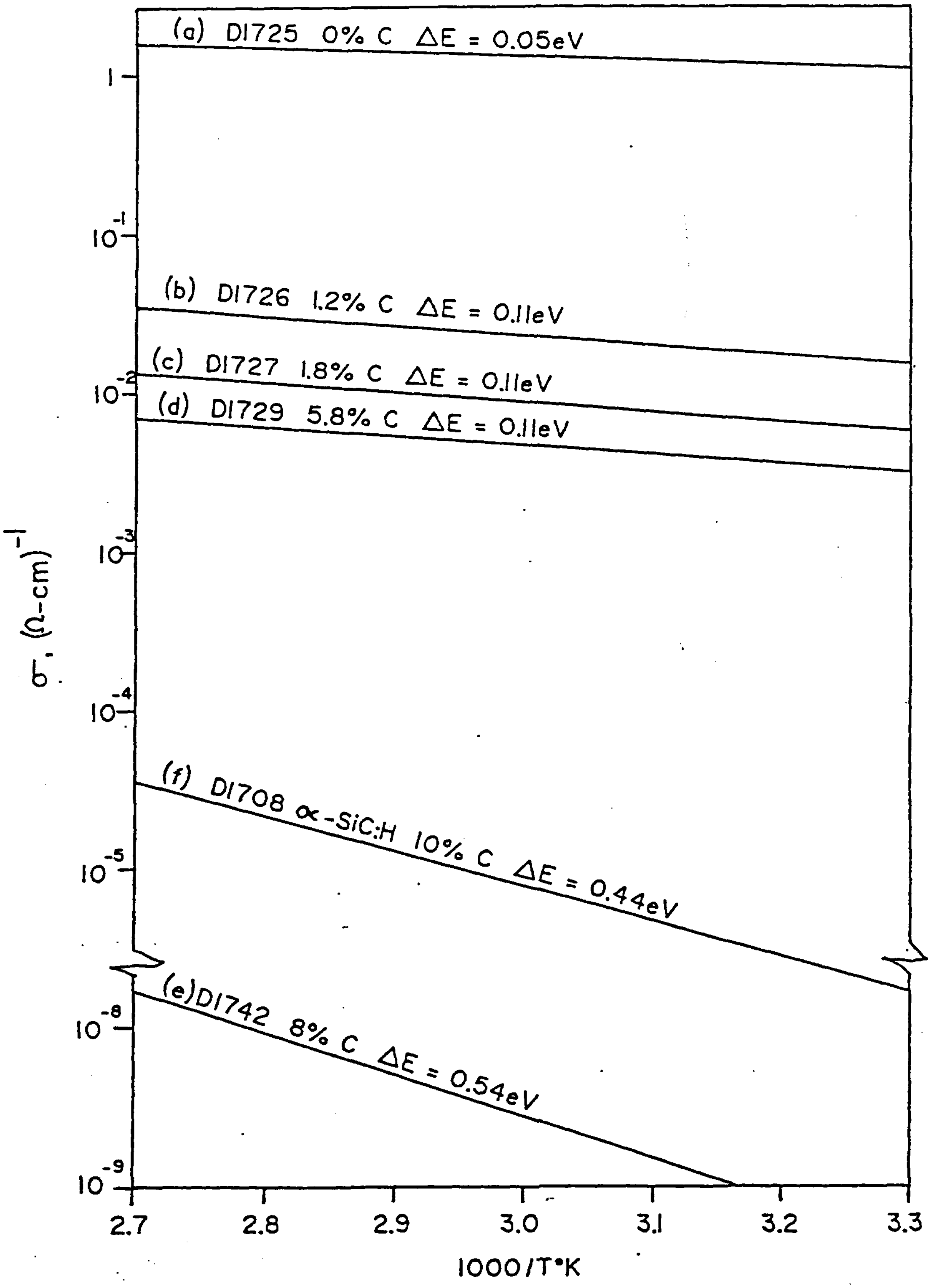

FIGURE 2-33. CONDUCTIVITY VS. RECIPROCAL ABSOLUTE TEMPERATURE OF MICROCRYSTALLINE OR PARTLY MICROCRYSTALLINE FILMS WITH INCREASING CARBON CONCENTRATION, CURVES a-e. NOTE SHARP CHANGE AT 8%C. SAMPLE f IS A REFERENCE FOR A TYPICAL a-SiC:H FILM USED IN SOLAR CELL FABRICATION.

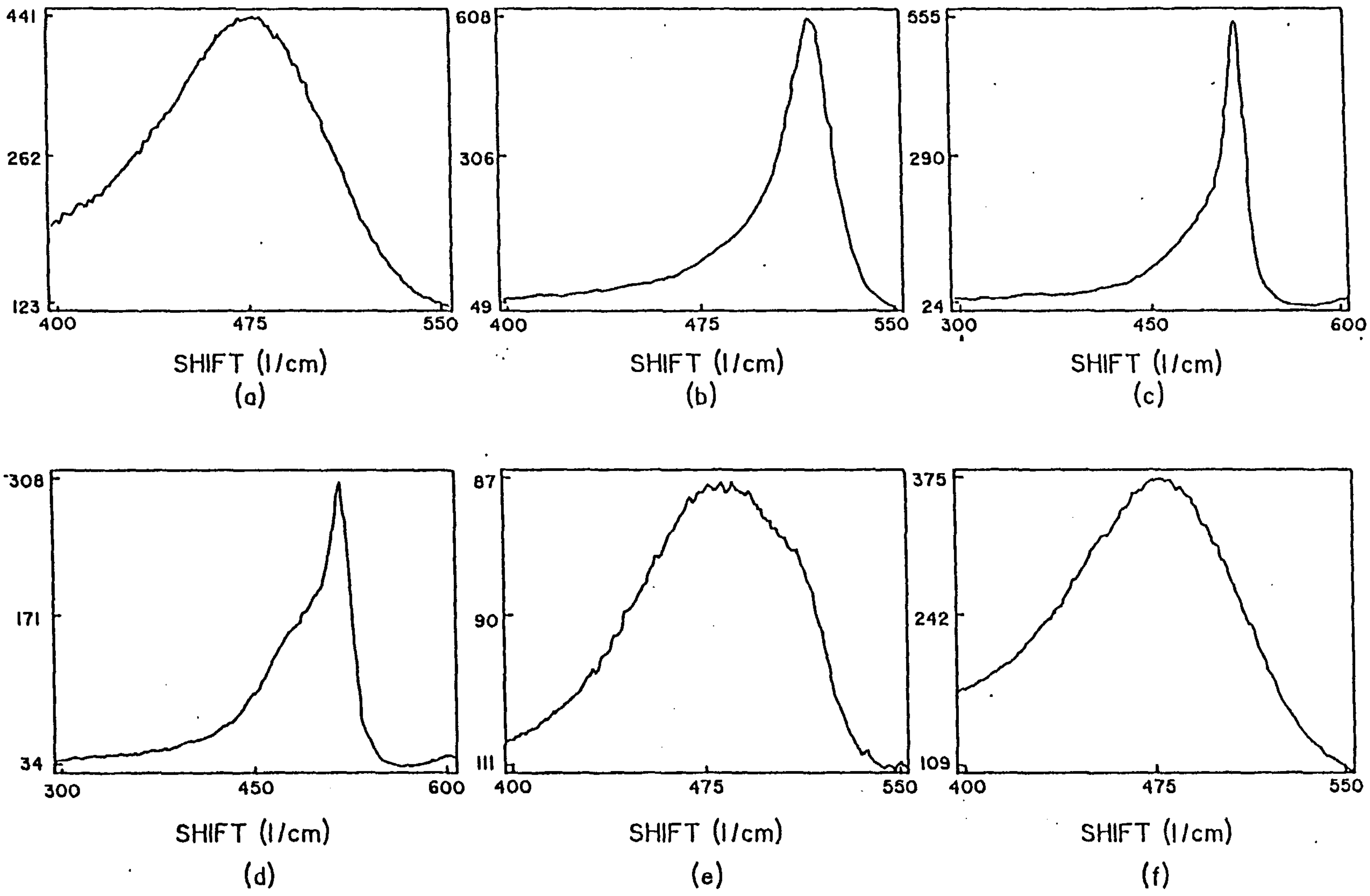

RAMAN SPECTRA SHOWING GROWTH OF AMORPHOUS PHASE WITH INCREASING CARBON
(a) REFERENCE α- SIC:H (10%C) FILM; (b) - (f) μC - SiC:H, C = 0%, 1.8%, 3.6%, 5.8%, 7%

FIGURE 2-34. RAMAN SPECTRA OF SEVERAL FILMS SHOWN IN FIGURE 2-33. NOTE SIMULTANEOUS PRESENCE OF AMORPHOUS AND MICROCRYSTALLINE PHASES, AND THEIR CHANGING RATIO AS CARBON CONTENT INCREASES.

worsen the electrical properties simply by increasing the bandgap (see below). While at carbon concentrations up to 6% there are clear improvements in conductivity and activation energy compared to amorphous SiC, above 6% there is a sharp increase in resistivity and ΔE that is matched by the disappearance of the crystalline Raman line. The degree of microcrystallinity in the films containing carbon can vary from complete, to partial (in which there appear to be microcrystalline grains imbedded in a matrix of amorphous material), to completely absent. As far as application to solar cells is concerned, p-layers with carbon concentrations $\lesssim 6\%$ would be an improvement over amorphous material, while at concentrations $>6\%$ the conductivity is prohibitively low and the activation energy too high. We note that so far we do not know precisely how the carbon is distributed in these microcrystalline films, and the Raman work will attempt to supply this information in the near future.

The changes in optical properties - specifically, the change in bandgap resulting from microcrystallinity and carbon incorporation - is not straightforward to discuss. Analyses of the absorption data are different for microcrystalline and amorphous material because of differences between direct and indirect bandgap material. Furthermore, the presence of routinely high concentrations of boron necessary to produce the required degree of p-type doping introduces tail-state absorption on the order of 10^3-10^4 cm^{-1}, and would thus interfere with band-edge measurements where the intrinsic absorption is low. And, finally, if the partially microcrystalline films (see Fig. 2-34) imply a two-phase material, analyzing the shape of the absorption curve in the vicinity of the band-edge would be accordingly much more complicated. Initially, in order to get some estimate of the relative changes in the optical window properties of these p-layers, we simply plotted transmission vs. wavelength for films of similar thickness in the region where the transmission is not seriously affected by the optical fringes in the spectrum. We show in Fig. 2-35 a series of such transmission curves for microcrystalline films of different carbon content together with a curve of a-SiC:H for relative comparison purposes. (For the spectra in Fig. 2-35, the lateral shift in transmission at 20% between curves (a) and (c) is about 0.3eV.) The trends are clear. In all the microcrystalline films the band edge has moved to higher

FIGURE 2-35. TRANSMISSION VS. WAVELENGTH FOR FILMS OF SIMILAR THICKNESS: (a) a-SiC:H, 10%C; (b) c-SiC:H, 1.8%C; (c) μc-SiC:H, 5.8%C, (d) μc-SiC:H, 7%C, (e) μc-SiC:H, 8%C.

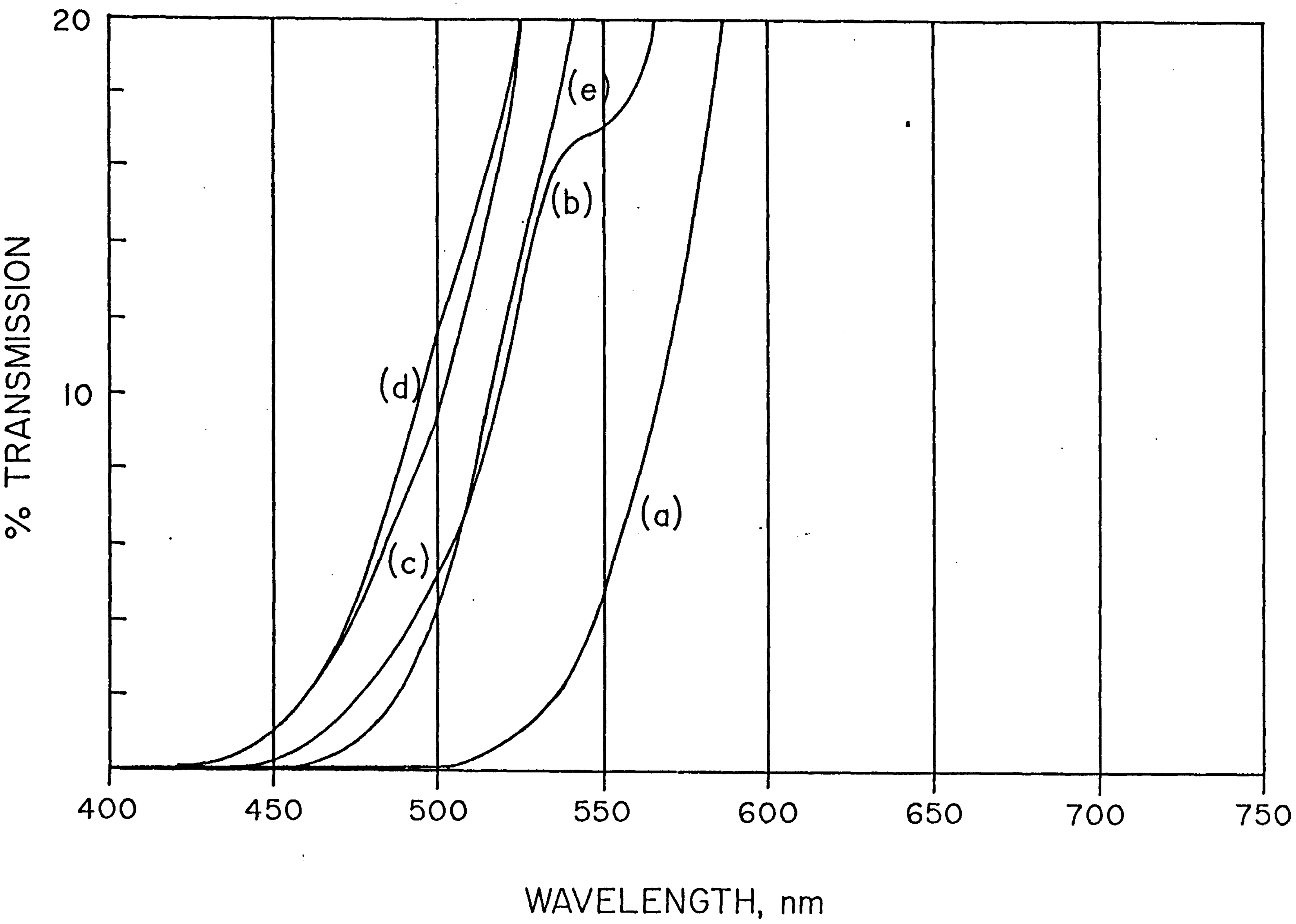

energies; carbon, at first, also has the effect of moving the band edge to higher energies, but when the carbon is greater than 6% the band-edge does not change further, presumably because of the carbon-induced suppression of the microcrystallinity. Indeed, the spectrum for the sample containing 10% carbon has actually shifted back toward that of the 10% carbon a-SiC:H reference sample. Note that the suppression of microcrystallinity (Fig. 2-34), the lack of additional spectral shift (Fig. 2-35), and the sudden increase in resistivity and activation energy (Fig. 2-33) all occur at about 6% carbon.

Some improvement in the plotting of the absorption data can be obtained as follows. Since a "bandgap" for this material is difficult to define accurately and, for doped material, even more difficult to measure accurately (the "Tauc Bandgap" treatment is patently incorrect), we now simply plot the absolute absorption coefficient vs energy for values of α greater than $10^4 cm^{-1}$. This at least lets us evaluate the significant changes in α in the region of interest introduced by our film modifications. Absolute absorption for μc-material is determined by 1) assuming that the film-quartz interface and the quartz itself are optically negligible since a 5000Å film will absorb 92% of the incident light when $\alpha = 5x10^4 cm^{-1}$, and 2) experimentally determining the reflectivity, R. This lets us write simply

$$\text{Transmitted intensity} = (1-R)e^{-\alpha t}$$

and since I, R and t are all known, α can be solved for. A set of curves similar to those shown in Figure 2-35 is shown in Figure 2-36 in terms of α vs energy.

A series of experiments were performed to optimize some of the parameters involved in the deposition process. For each of two different carbon feedstock flow rates (2 sccm and 6 sccm) films were deposited over a temperature range from 150°C to 300°C. Conductivity results are represented by the curves in Fig. 2-37 and a data summary is given in Table 2-12. Once again, basic trends are clear. Films grown at lower substrate temperature have higher resistivities and activation energies; films grown with 6 sccm flow rates exhibit this effect much

FIGURE 2-36. ABSORPTION COEFFICIENT, α, VS ENERGY FOR VARIOUS SAMPLES AS INDICATED. NOTE BREAK IN CURVE (C) DUE POSSIBLY TO BOTH AMORPHOUS AND MICROCRYSTALLINE PHASES. AT 5.8%C CONSISTENT WITH FIGURE 2-34.

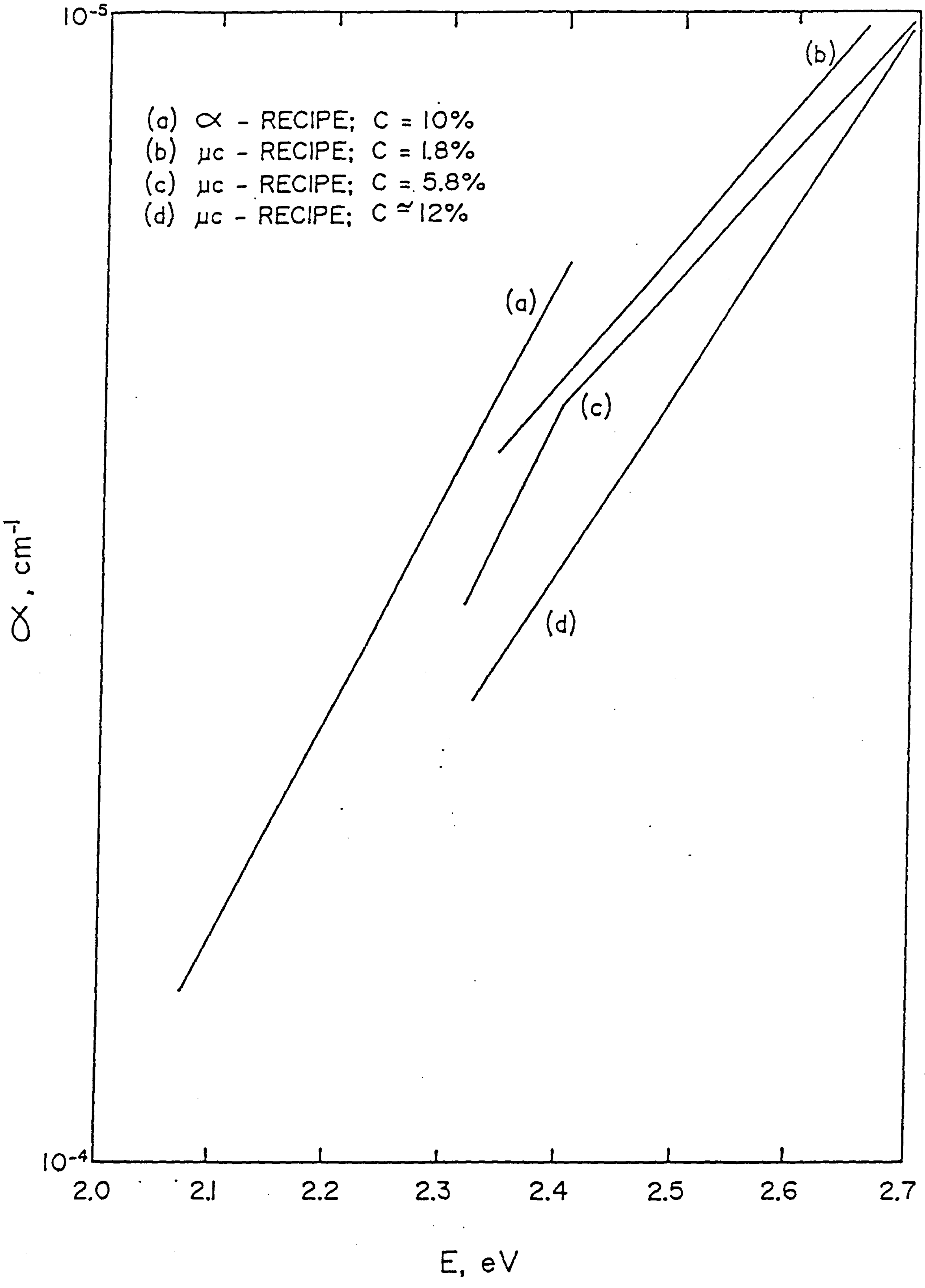

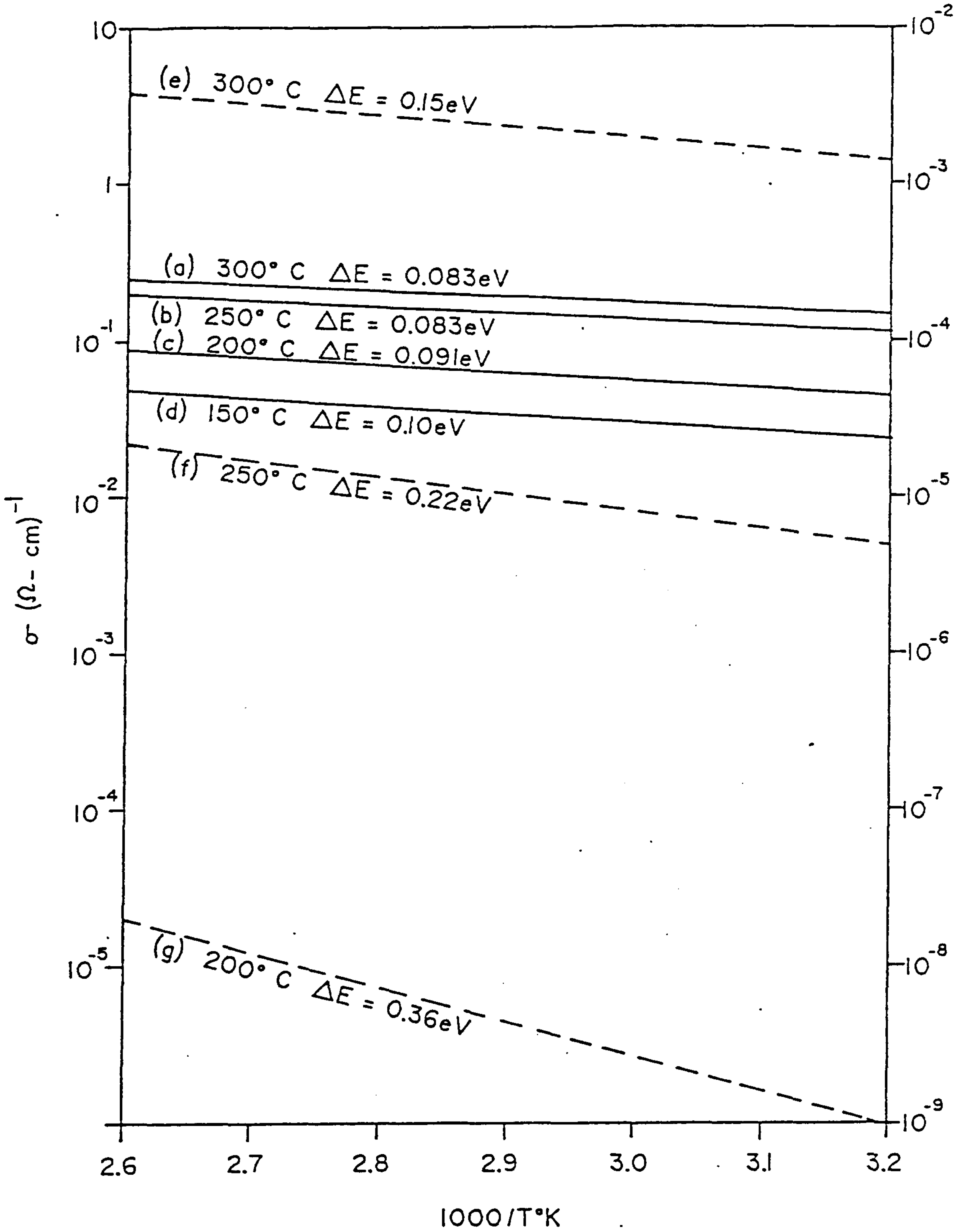

FIGURE 2-37. CONDUCTIVITY AND ACTIVATION ENERGIES FOR FILMS DEPOSITED AT VARYING SUBSTRATE TEMPERATURES FOR CARBON FEEDSTOCK FLOW RATES OF 2 SCCM (SOLID LINES), AND 6 SCCM (DASHED LINES). SUBSTRATE TEMPERATURES AND ACTIVATION ENERGIES ARE AS GIVEN. THE CONDUCTIVITY FOR THE 6 SCCM CURVE AT 150°C WAS LESS THAN $10^{-12}(\Omega\text{-cm})^{-1}$.

TABLE 2-12

DATA SUMMARY FOR FIG. 2-37

Sample #	Curve	Deposition Temperature	Carbon Feedstock Flow Rate (sccm)	$\sigma(\Omega^{-1}cm^{-1})$ Rm. Temp	E (eV)
D1766	(a)	300°C	2	$1.3x10^{-1}$	0.083
D1767	(b)	250°C	2	$1x10^{-1}$	0.083
D1768	(c)	200°C	2	$4x10^{-2}$	0.091
D1769	(d)	150°C	2	$2x10^{-2}$	0.10
D1762	(e)	300°C	6	$1.4x10^{-3}$	0.15
D1763	(f)	250°C	6	$4x10^{-6}$	0.22
D1764	(g)	200°C	6	$1x10^{-9}$	0.36
D1765	(h)	150°C	6	10^{-12}	not meas.

more strongly than do films grown with 2 sccm flow rates. Consistent with these results is the finding that the optical transmission edge moves to higher energies at lower substrate temperatures (all other growth parameters remaining constant) which we take to reflect a widening band gap. A straightforward explanation of these results may be indicated by Fig. 2-38, in which we plot the carbon incorporation as a function of feedstock flow rate. Note that at 6 sccm the data show a significant increase in carbon incorporation for the same flow rate at lower substrate temperature. Thus, the electrical and optical data mentioned above may simply be due to more carbon in the films and its subsequent effects of increasing bandgap and resistivity. Along these lines, recall (Fig. 2-34) that at carbon levels much above 6%, the films become amorphous which would also tend to increase the resistivity.

When microcrystalline p^+ layers were grown only several hundred angstroms thick in order to approximate actual solar cell structures, it was discovered that the desirable electrical properties discussed above worsened dramatically. While at a thickness of 1050Å the conductivity and its activation energy was the same as that at 6000Å, as the thickness decreased below 1050Å, the conductivity decreased and its activation energy increased (see Fig 2-39). For a thickness of 400Å, $\sigma<10^{11}(\Omega\text{-cm})^{-1}$. Scanning Electron Microscope measurements indicated, however, that even at 400Å, the films are still continuous (resolution $\sim$200Å). Raman spectroscopy measurements were ambiguous at this thickness because the quartz substrate lines are surprisingly strong and overpower the microcrystalline thin film lines. However, even at 800Å, where σ had already begun to decrease and ΔE to increase, an increase in the amorphous nature of the film could be observed. Thus, initial nucleation and film growth seemed to be prime contributors to the electrical changes occurring when these layers became very thin.

Two approaches were then tried in an attempt to shed light on this behavior. First, these thin films were annealed at 225°C for further Raman testing, hoping that such anneals would modify the film microstructures. But while the electrical properties significantly improved (in line with work to be described below), no change in the Raman spectrum was observed, indicating a lack of

FIGURE 2-38. ATOMIC PERCENT CARBON INCORPORATED INTO THE FILM VS. CARBON FEEDSTOCK GAS FLOW RATE. NOTE VERY SIGNIFICANT TEMPERATURE DEPENDENCE AT THE 6 SCCM VALUE.

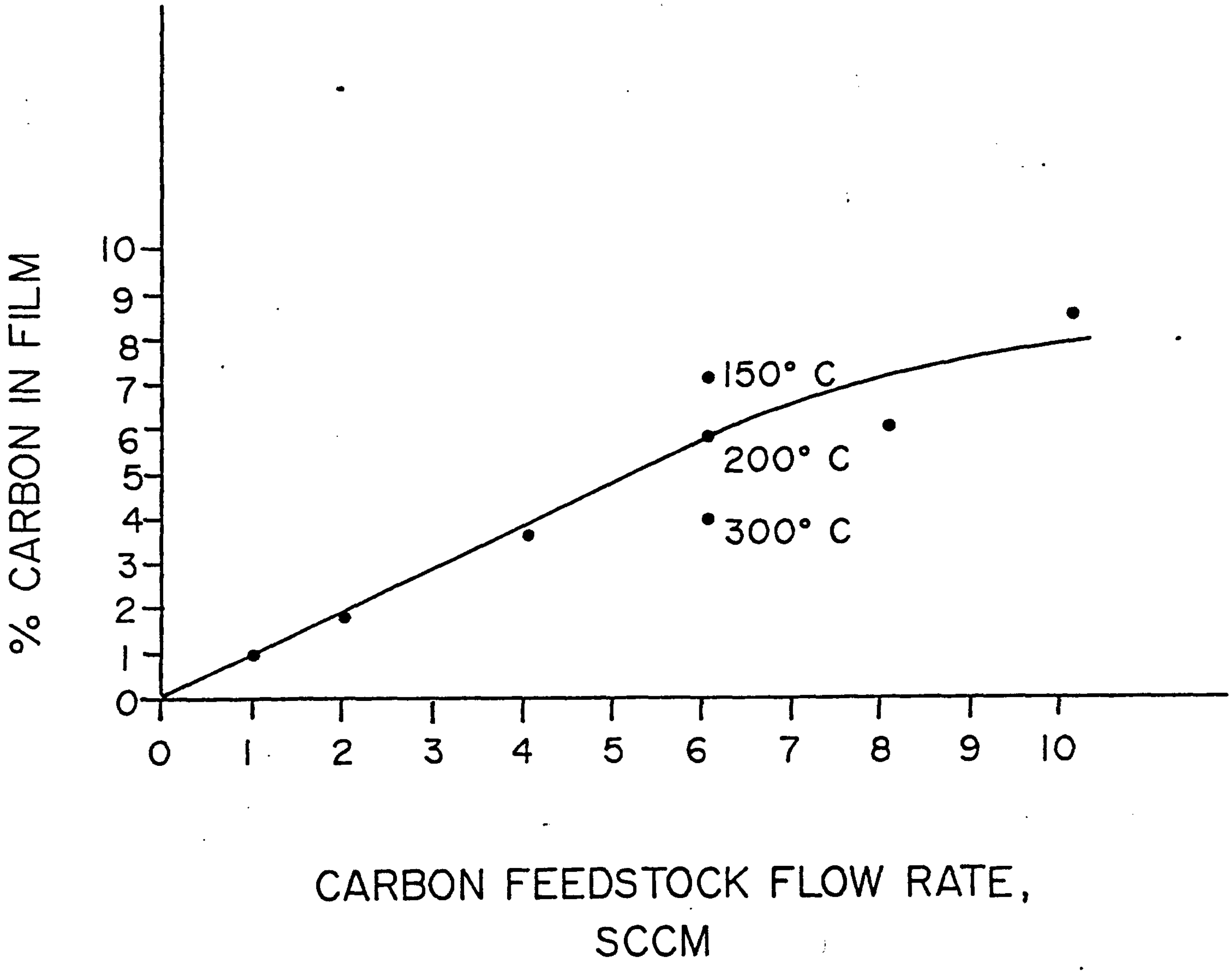

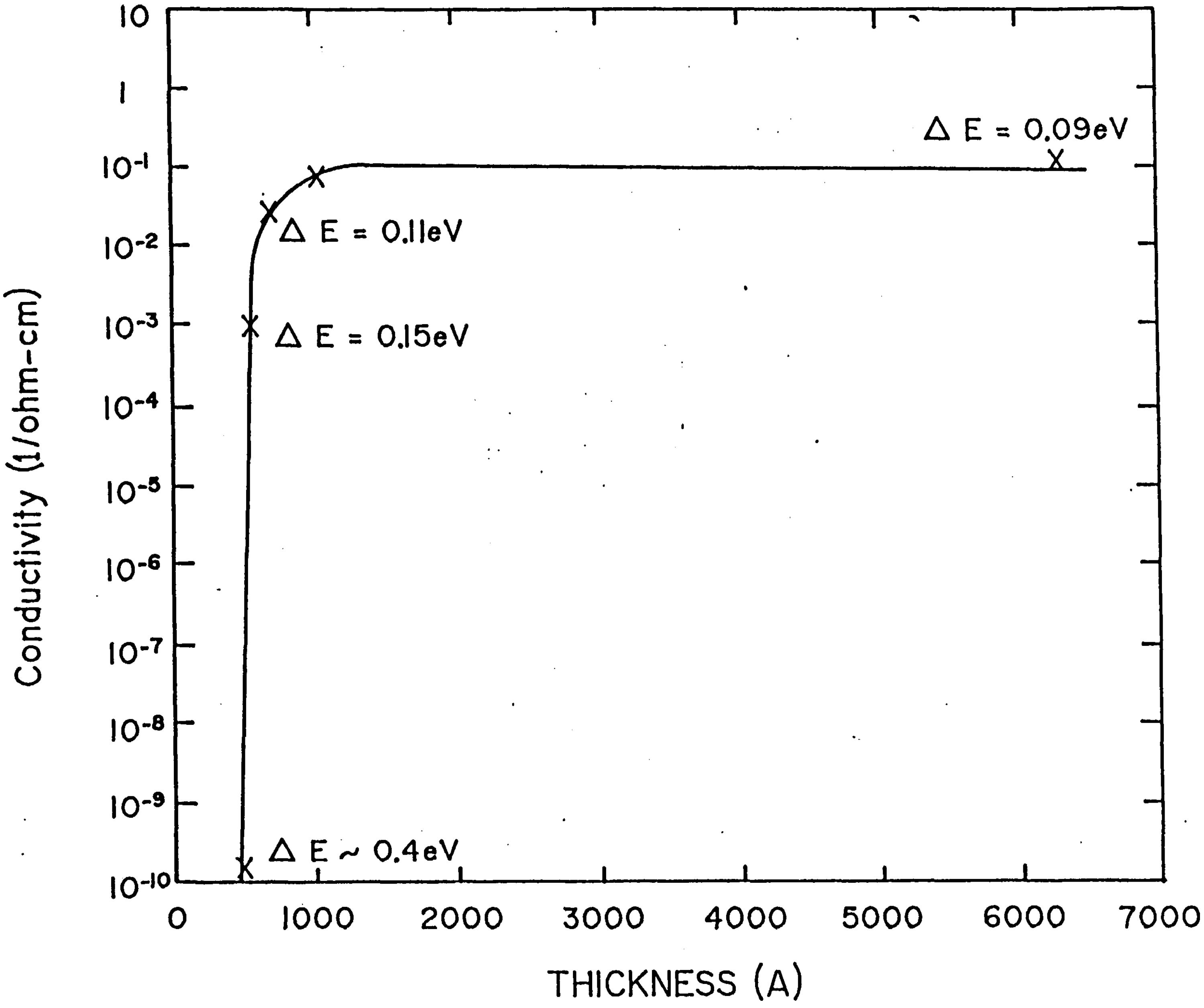

FIGURE 2-39. DARK CONDUCTIVITY AS A FUNCTION OF FILM THICKNESS FOR P+ FILMS DEPOSITED UNDER STANDARD CONDITIONS FOR MICROCRYSTALLINE GROWTH.

change in the microstructure. A second attempt, however, proved more successful. A series of thin films of SiC:H (2%C) were deposited (using the rf "microcrystalline" process) on several substrates that were different from our routine quartz and that might affect initial nucleation. These were 1) single crystal Ge, 2) routine CTO, and 3) routine a-Si:H. The films were about 200Å thick so as to approximate those used in cell structures. Raman spectra were then taken of these films and the results are shown in Figure 2-40.

Curve (a), a reference curve, has the well-known Raman peaks of infinitely thick a-Si:H and μc-Si:H. Curve (b) is that of a thin layer made by the "microcrystalline process" and deposited onto CTO. Curves (c) and (d) are those of identical layers deposited onto single-crystal Ge and routine a-Si:H, respectively. The results are clear. The layer on the CTO substrate is completely amorphous, that on the a-Si:H substrate is almost completely microcrystalline, while even on the single-crystal Ge it is only about 50% μc and 50% amorphous (the should in curve (d) is what some small Raman signal from the substrate should look like).

It appears that in order to grow a thin microcrystalline layer of Si:H or SiC:H from a glow discharge, you must use an a-Si:H substrate (among those that we commonly deal with) to do it on.

Note that this finding readily answeres two disparate questions:

1. Why layers deposited on quartz, glass, and metal begin by growing amorphous material, then suddenly being growing microcrystalline material after several hundred angstroms.

2. Why Hamakawa's group includes an a-SiC:H "buffer" layer over the ZnO layer (as described in their reports) [7] before growing their uc-p^+-i-n cells.

We cannot offer a clear explanation for this effect. It may simply be that a Si:H surface may simply be more conducive to begin forming more of the strong Si-Si bonds that is supposed to be the hallmark of microcrystalline growth.

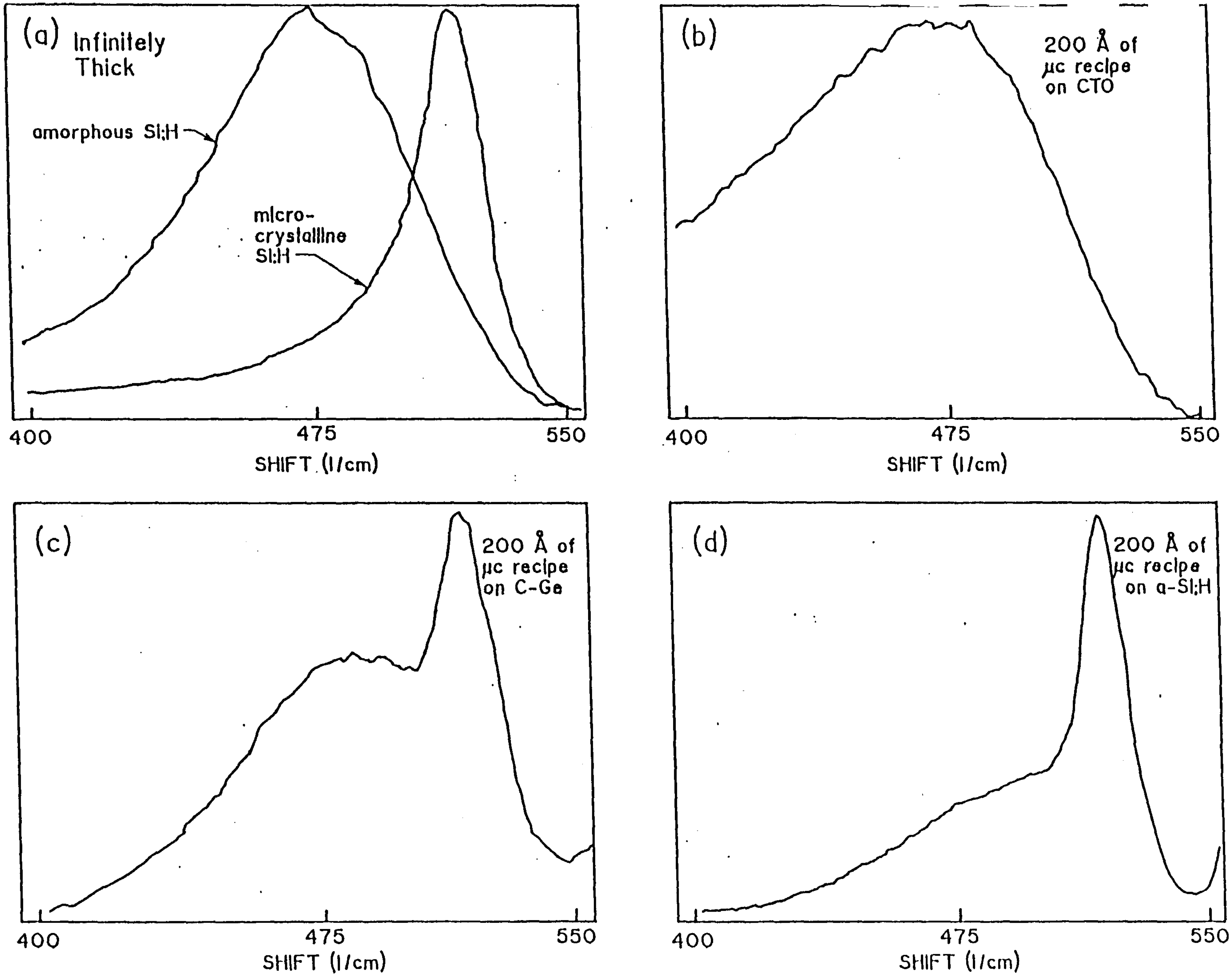

FIGURE 2-40. RAMAN SPECTRA OF 200Å OF SiC(2%C):H FILMS DEPOSITED WITH THE "MICROCRYSTALLINE" PROCESS ON DIFFERENT SUBSTRATES. (a) REFERENCE RAMAN LINES OF INFINITELY THICK SAMPLES OF α- AND μc-Si:H, (b) CTO SUBSTRATE, (c) CRYSTALLINE Ge SUBSTRATE, (d) α-Si:H SUBSTRATE.

If a microcrystalline film of Si:H or SiC:H, or a film formed by the microcrystalline process as described at the beginning of this section, is deposited in the temperature range 115-180°C, then annealing this film in an inert atmosphere at a higher temperature (broadly peaking at 225°C) can increase the conductivity by several orders of magnitude and decrease its activation energy by several tenths of an eV. The absolute magnitude of the changes depends largely on initial values. Typical changes are shown in Fig. 2-41 plotted in terms of conductivity, σ , vs reciprocal absolute temperature. For material that is microcrystalline conductivities greater than $1(\Omega\text{-cm})^{-1}$ and Fermi levels that indicate almost degenerate material have been observed. As a corollary to this effect the highest conductivity films made by the microcrystalline process are those whose deposition starts at a low temperature ∿125°C and then allowing the temperature to rise to ∿ 190°C during deposition. This effect is seen only marginally, if at all, in films made by the amorphous deposition process (no change in E_F at 0.45eV and a change in σ of less than a factor of two). The effect is invariably seen when the microcrystalline deposition process is used, whether microcrystalline material is formed or not. (Microcrystalline material may not form, for example, due to too much carbon - see earlier discussions.)

We have sought an explanation for this effect in terms of changes in microstructure or changes in electrically active doping efficiency. However, Raman spectroscopy measurements have clearly shown no change in either microcrystallite grain size or volume fraction. In addition, SIMS measurements have shown no significant change in hydrogen content although, of course, hydrogen may move around on an atomic scale at these temperatures. The changes in σ and E_F are such that they can be explained completely and most simply by postulating an increase in the electrically active shallow acceptor concentration, i.e., a change in the doping efficiency from its typically low value of about 1 electrically active boron atom per thousand to much higher values, the change induced somehow by the annealing process. One speculation for such a process might involve the movement of hydrogen on an atomic scale together with neutralization of near mid-gap states.

FIGURE 2-41. IMPROVEMENTS IN CONDUCTIVITY σ AND FERMI LEVEL ΔE PRODUCED BY THE MICROCRYSTALLINE RECIPE AT SUBSTRATE TEMPERATURES T_S. (a) 1.8%C, T_S = 115°C; (b) 5.8%C, T_S = 115°C; (c) 3.8%C, T_S = 103°C.

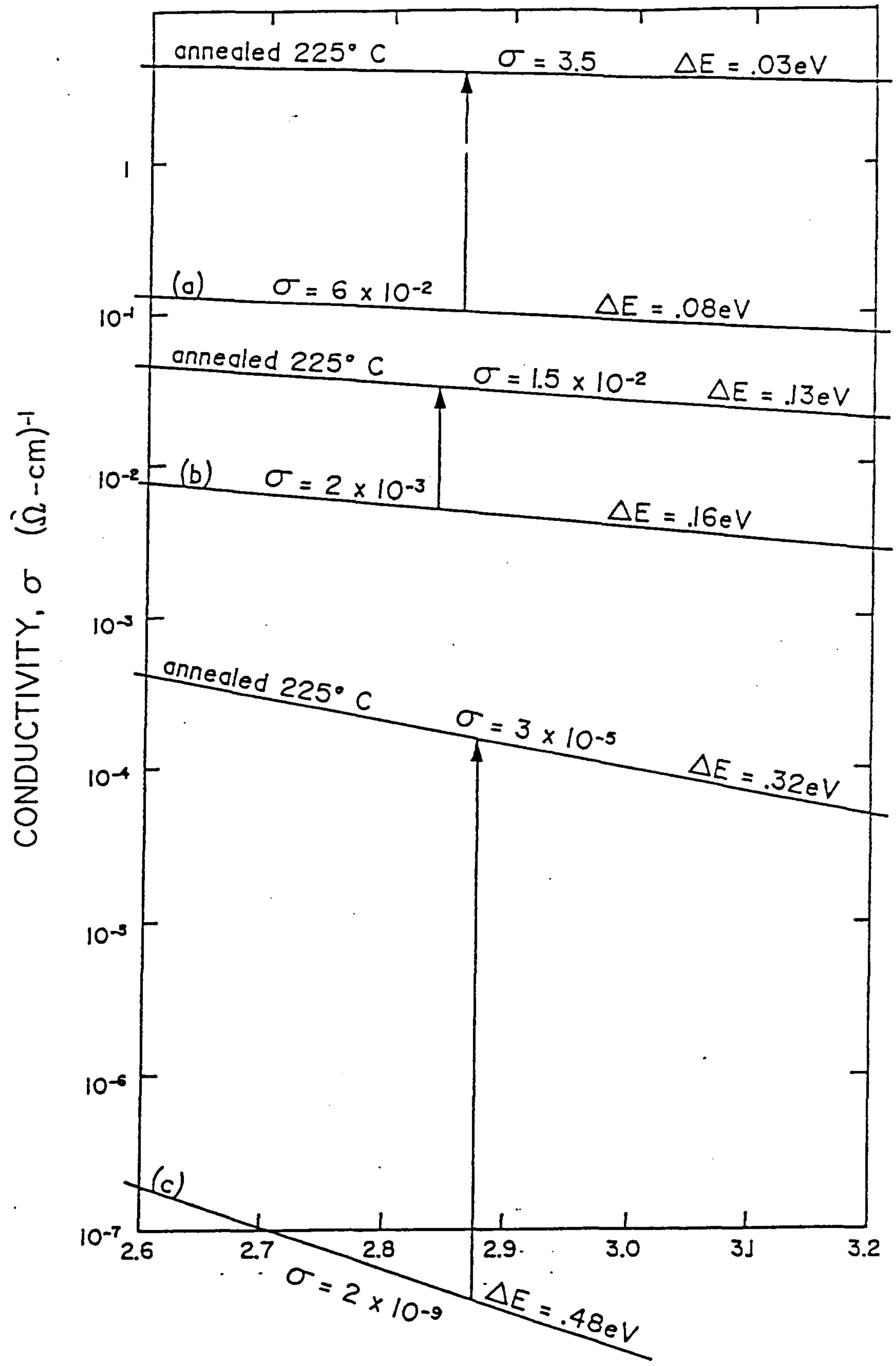

Fig. 2.41

The use of microcrystalline p^+ and n^+ layers in solar cell structures has so far yielded only some initially encouraging results. We have utilized both single-junction p-i-n cells, and double-junction tandem cells (in which the first p^+ layer is kept amorphous so as to eliminate the problem of CTO reduction by the high-power high-hydrogen discharge required for microcrystalline deposition). Of course, we have only recently discovered that depositing thin layers of what we had thought was microcrystalline SiC:H on CTO for the single-junction cells was really amorphous (see Fig. 2-40) so that all our single-junction results had no real bearing on such cell evaluation. Note, however, that working with the remaining possibilities currently available to us, i.e., tandem cells with the first p^+ layer amorphous or single-junction cells with only the n^+ layer microcrystalline, would not give us the available improvement in V_{oc} and carrier collection that might be available when both p^+ and n^+ layers are microcrystalline. Our approach here will be to develop thin buffer layers of α-SiC:H, $\sim$50Å thick, to deposit on the CTO before depositing the microcrystalline p^+-layer.

Results attained so far include the following: (1) Using a microcrystalline n^+ layer of SiC:H in a single-junction cell has increased the red quantum efficiency (at 7000Å) to 0.4 over that of its amorphous n^+ layer counterpart which is typically about 0.28. (2) A non-optimized tandem cell using a microcrystalline tunnel junction and final n^+ layer had a V_{oc} of 1.65V, which was 50-100mV higher than a control cell consisting of only amorphous layers. (3) Tandem cells with mirocrystalline tunnel junction and 5000Å i-layers showing reasonable efficiencies ($\sim$7%) suggest a slower degradation under illumination (and a higher overall efficiency) than its all-amorphous counterpart, see Fig. 2-42.

2.6 LIGHT-INDUCED EFFECTS

2.6.1 Introduction

Studies of the photo-induced changes which occur in a-Si:H and its alloys with C and Ge are continuing on both single and multi-junction cells and on films. Our

FIGURE 2-42. RELATIVE CELL EFFICIENCY OF TANDEM CELLS VS AM1 EXPOSURE TIME. NOTE SUGGESTION THAT CELLS WITH μc-TUNNEL JUNCTION MIGHT DEGRADE MORE SLOWLY THAN ALL-AMORPHOUS CONTROL CELL.

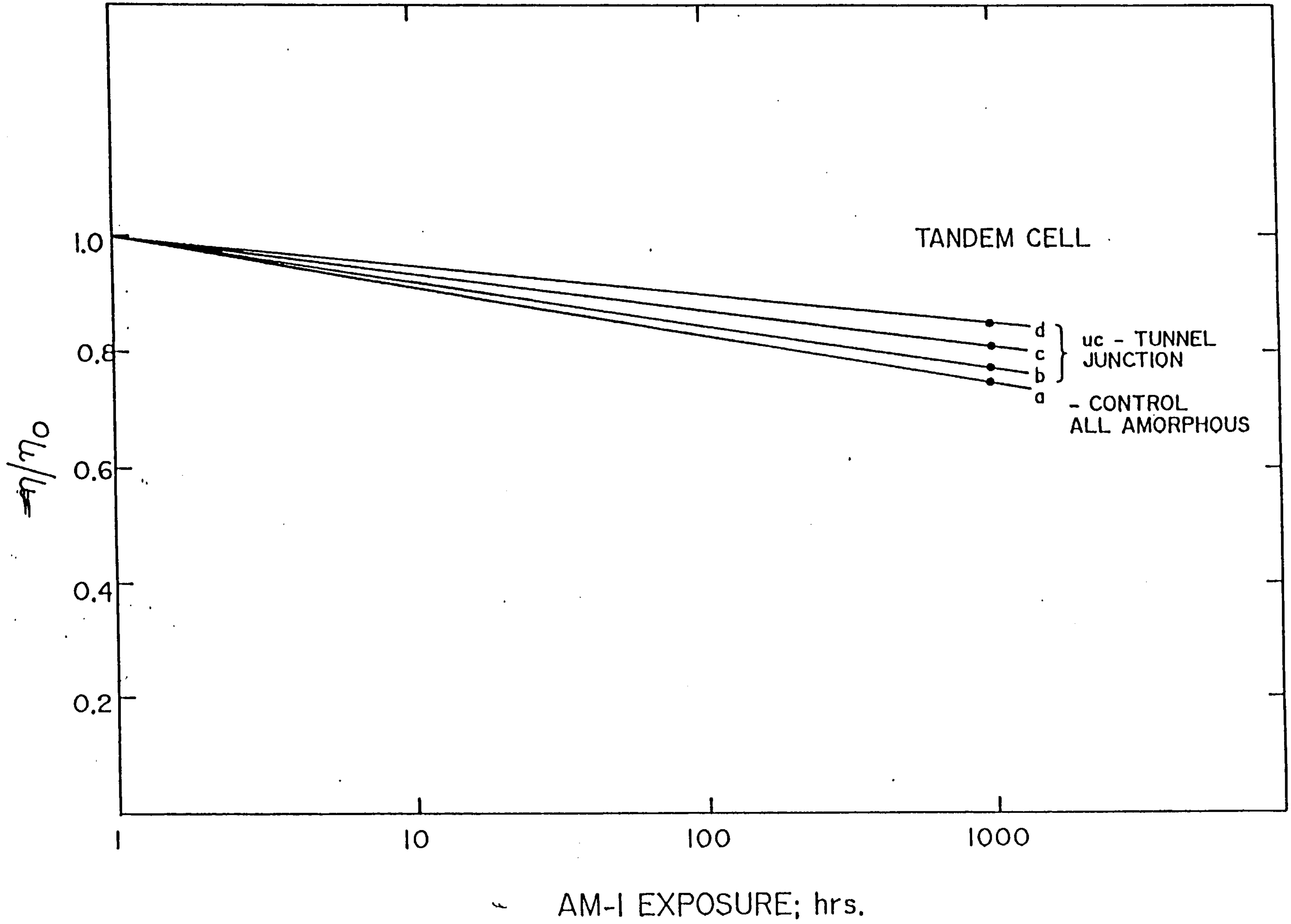

most stable devices to date are Si/Si tandem cells which ave initial efficiencies >8% and which degrade <10% in 240 hours.

With respect to single-junction cells, we have been paying particular attention to the effects of p/i interface grading, both on initial efficiency and on the rate of degradation. We have found the effect of p/i interface grading on stability becomes more important as the i-layer thickness decreases.

We have also begun investigations on the degradation of multi-junction cells. These are being approached from two points of view. The first is simply to make stacked cells and then monitor the efficiency as they are light-soaked. The second is to make single-junction cells corresponding to the possible components of multi-junction cells (i.e., single-junction SiGe cells) to investigate their susceptibility to photodegradation. Simple modeling of tandem cells has also begun.

The goal of these investigations is, of course, to make stable modules. To this end we have expanded and improved our facilities, both outdoor and indoor, for module testing.

The physics of the Staebler-Wronski effect is being studied in a variety of ways. An interesting effect, that of accelerated degradation by forward biasing cells at high temperatures, is being analyzed in terms of a chemical equilibrium phenomenom. As well, the spectral response of cells measured before and after degradation has provided some insights into the fundamental nature of the Staebler-Wronski effect.

Studies of films using photothermal deflection spectroscopy reveal a parallelism between the kinetics of light-induced degradation and thermal recovery of cells and films. A study of the kinetics of the light-induced changes in the absorption coefficient (PDS) of SiC films has been completed.

2.6.2 Continuous vs. Cyclic Degradation

We have made comparisons between the rate of degradation of cells under continuous illumination and under cyclic illumination as specified by SERI (cycles of 8 hours at AM1.5 and 50°C followed by 16 hours in the dark at 24°C). A 3"x3" substrate was taken from each of the 3 different runs and split in half. Cells on one half were degraded according to the SERI procedure, cells on the other half under continuous illumination. There were from 2-4 cells monitored on each half substrate. The results are shown in Figures 2-43, 2-44 and 2-45 where the horizontal axis is the total exposure time. The inserted figure is from the ARCO paper [8] presented at the stability conference in Palo Alto in January 1987. There is no significant difference in the results except that following the cyclic format takes three times as long.

2.6.3. p/i Interfaces

As outlined in Section 2.2.1, interface layers between the p- and i-layers can improve initial efficiencies substantially. However, these layers often, but not always, adversely affect stability. That is, the gain achieved in initial efficiency by adding interface layers is often more than offset after some fairly short period of light soaking as a result of an increased degradation rate. An interface region can be produced in a number of ways, most easily by inserting a SiC layer.

The effects of SiC layers on efficiency are reported in Section 2.2.1 (5000Å i-layer). We have found that the rate of degradation increases slowly as the bandgap of the layer increases for a given interface layer thickness (Figure 2-46), while the efficiency goes through a broad maximum (Figure 2-47). Thus it is possible to benefit slightly by inserting a layer for which the methane content of the deposition gas is about 5%. We found that the thickness of the interface layer had no effect on either the initial efficiency or rate of degradation over the range investigated. There was a difference between using or not using a buffer layer; however, having inserted such a layer, at least in the range of 100-200Å, thickness had no effect.

FIGURE 2-43. COMPARI[illegible] THE RATE OF DE[illegible] OF CELLS LIGHT SOAKED [illegible]HER CONTINUOUSLY OR UNDER CYCLIC CONDITIONS (ACCORDING TO SERI SPECIFICATIONS). THE INSET IS ARCO DATA.

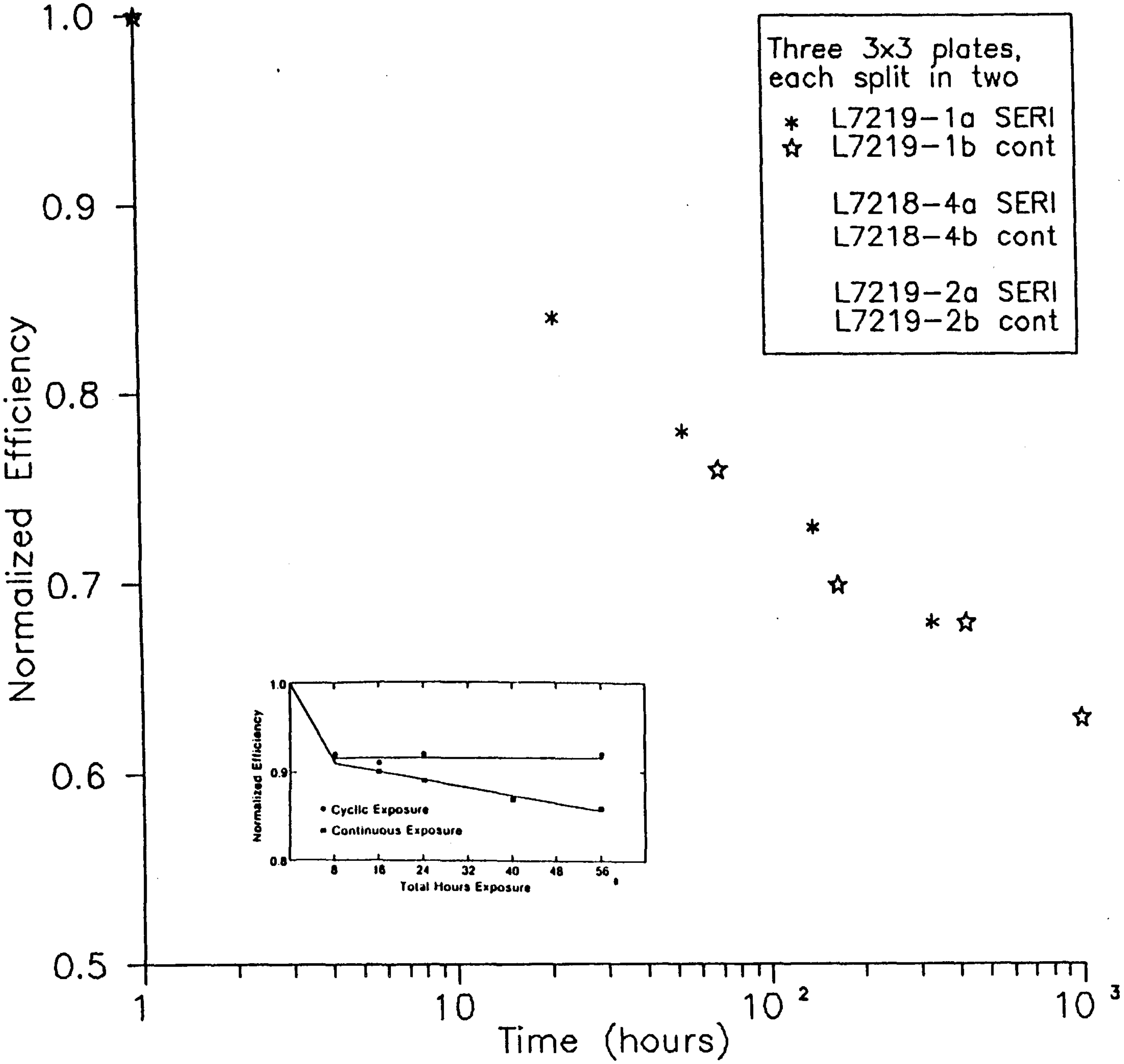

FIGURE 2-44. COMPARISON OF THE RATE OF DEGRADATION OF A SECOND SET OF CELLS LIGHT SOAKED EITHER CONTINUOUSLY OR UNDER CYCLIC CONDITIONS (ACCORDING TO SERI SPECIFICATIONS). THE INSET IS ARCO DATA.

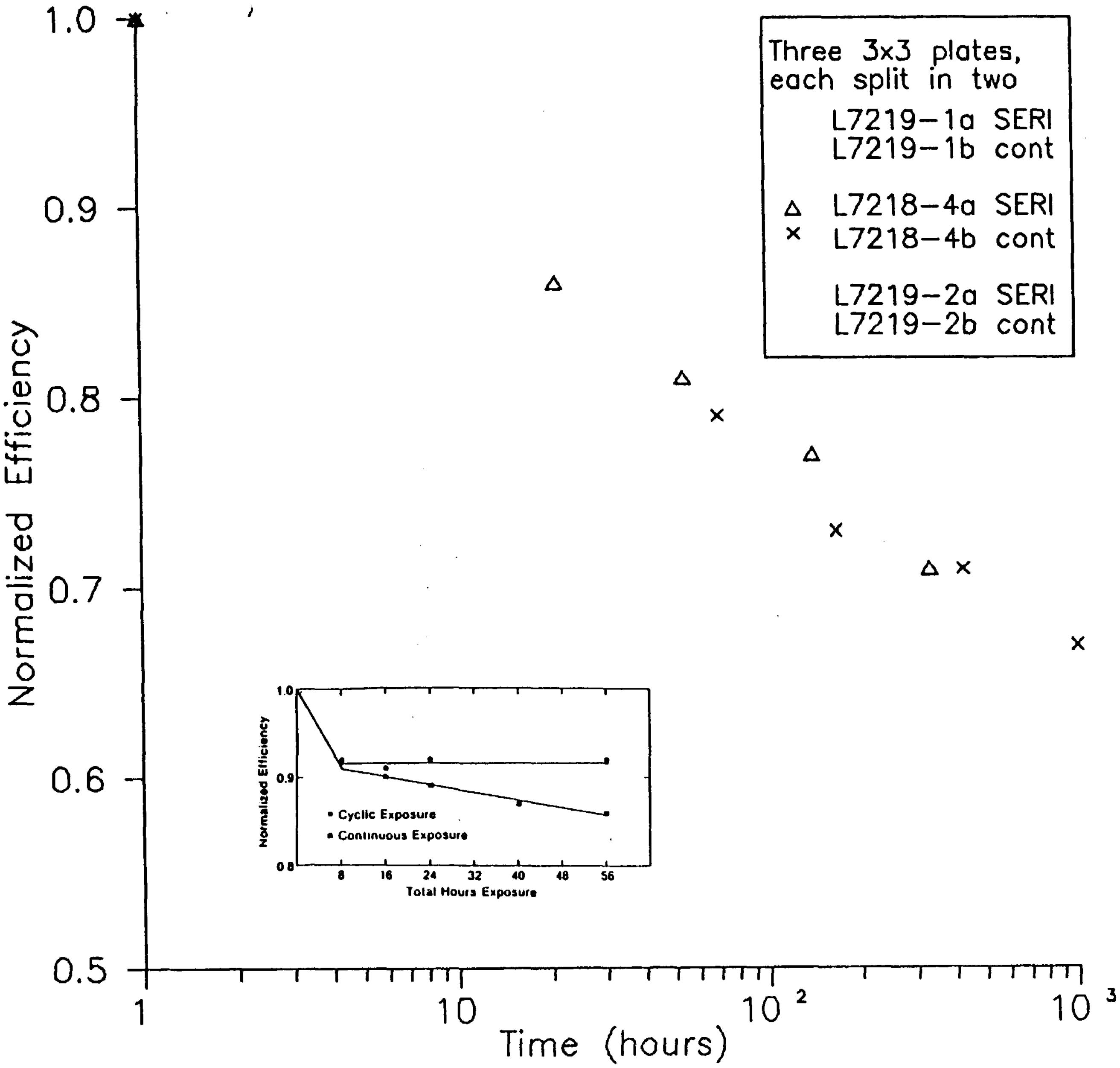

FIGURE 2-45. COMPARISON OF THE RATE OF DEGRADATION OF A THIRD SET OF CELLS LIGHT SOAKED EITHER CONTINUOUSLY OR UNDER CYCLIC CONDITIONS (ACCORDING TO SERI SPECIFICATIONS). THE INSET IS ARCO DATA.

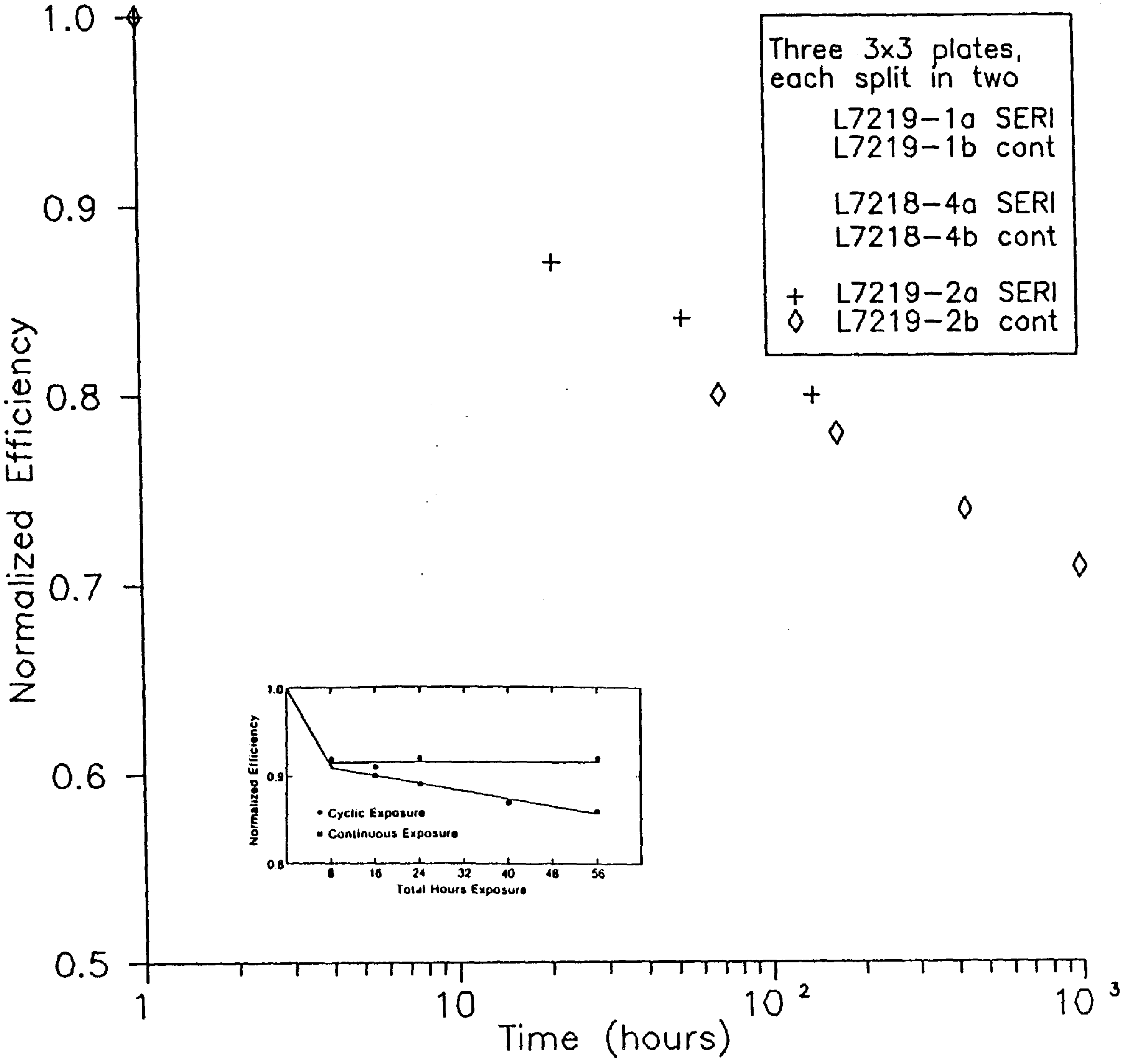

FIGURE 2-46. RELATIVE EFFICIENCY (AFTER 940 HOURS OF LIGHT SOAKING) OF p-i-n CELLS WITH GRADED SiC LAYERS AS A FUNCTION OF CH_4 CONTENT OF THE DISCHARGE ATMOSPHERE AT THE START OF SiC GRADING.

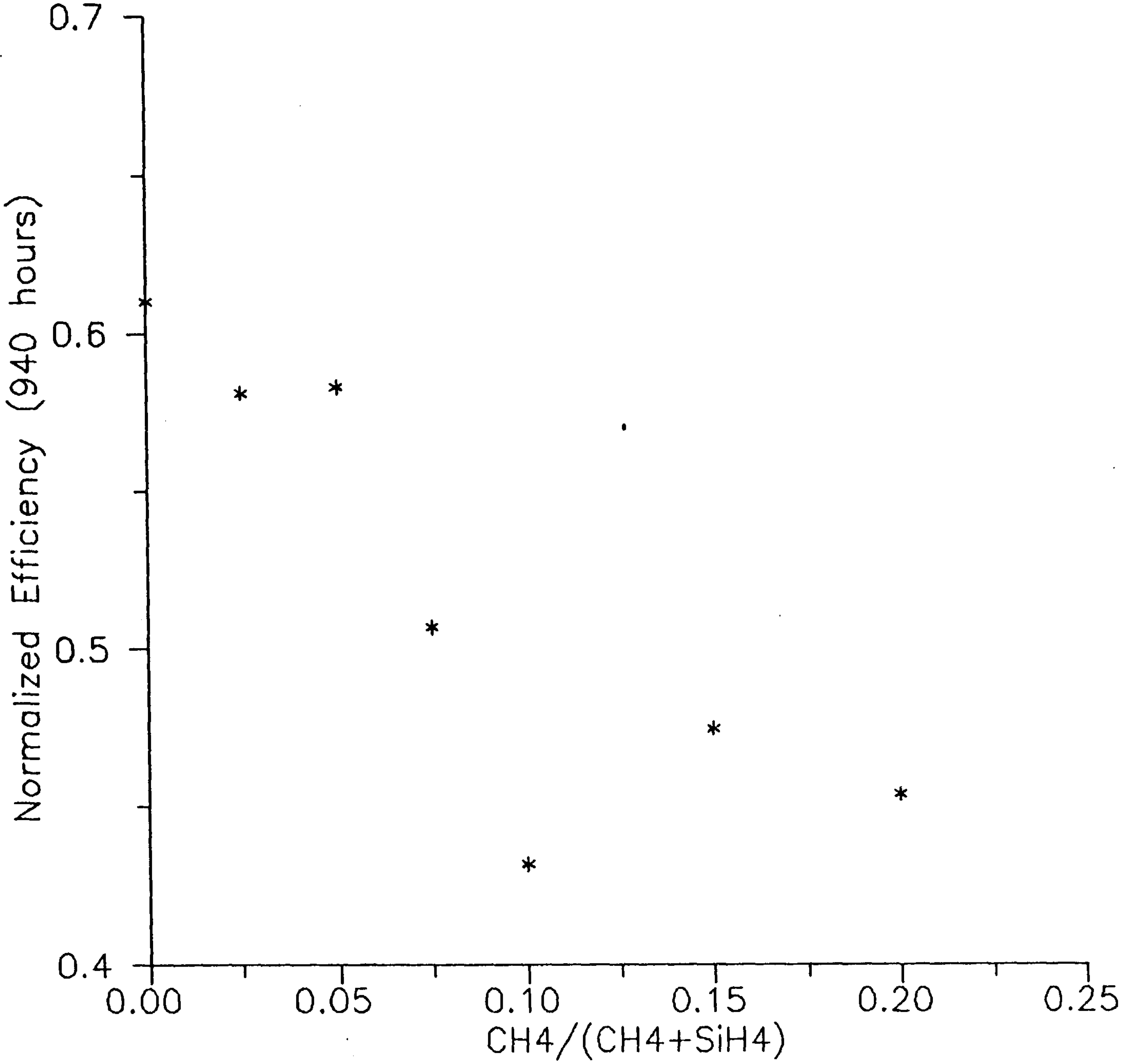

FIGURE 2-47. EFFICIENCY OF p-i-n CELLS WITH GRADED SiC LAYERS AS A FUNCTION OF CH_4 CONTENT OF THE DISCHARGE ATMOSPHERE AT THE START OF SiC GRADING.

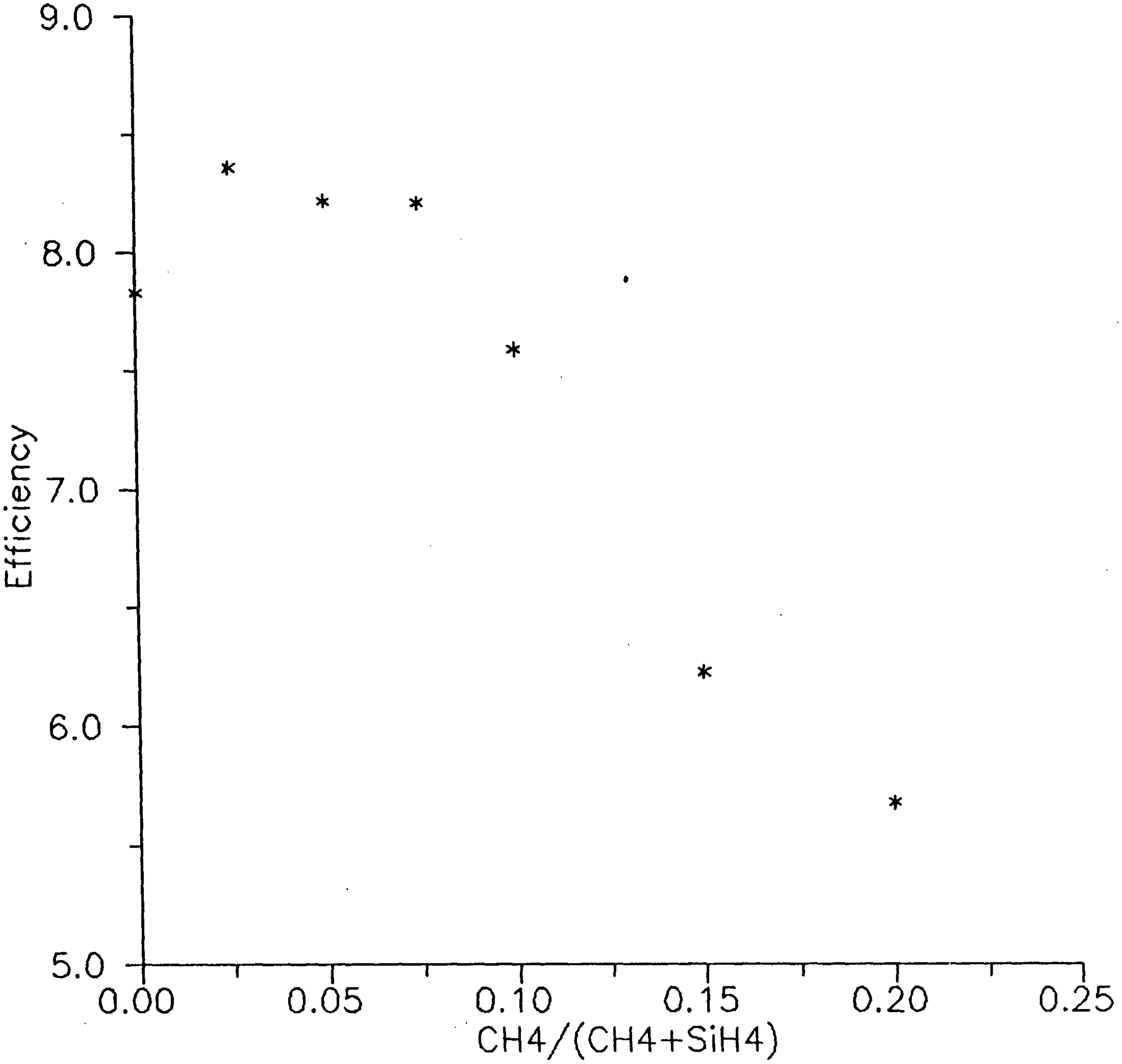

The effect of inserting a SiC layer in thin cells (2000Å i-layer) has also been investigated in a preliminary way. By inserting an interface layer it is possible to increase the initial V_{oc} and efficiency by 5-10%. At the same time, the rate of degradation is increased substantially, as can be seen in Figure 2-48. The cells which lack grading have higher efficiencies after 10-100 hours of light-soaking. Investigations of the effect of interface layer thickness over a wider range (8Å - 200Å) have begun, as have studies of effects of bandgap, and the effects of the details of the structure of the layer (i.e., single homogeneous layer vs. series of layers with varying bandgap).

2.6.4 Thin Single-Junction Cells

Single-junction a-Si i-layer cells have been made with i-layers ranging from 450 to 1750Å. Those cells with i-layers less than about 850Å are essentially stable, at least for the first few hundred hours, which is as long as any tests have been carried out. The normalized efficiency after 100 hours is shown in Figure 2-49 for i-layer thicknesses up to 6500Å.

2.6.5 Single-Junction SiC Cells

Cells with SiC i-layers have a high open-circuit voltage and could act as front junctions in multi-junction devices. We made a large number of SiC single-junction devices, and have investigated the effect of changing the methane fraction (0 to 50%) and growth rate (1 to 10Å/sec). The initial cell characteristics and the rates of degradation are functions of both deposition gas composition and growth rate. Figure 2-50 shows the initial efficiency vs. methane fraction for two growth rates and Figure 2-51 shows the efficiency as a function of exposure time for the cells grown at 4.5Å/sec. Note that for i-layers grown from deposition gases containing more than 15% methane the degradation rate is so fast that no points fall on the graph. This is in spite of the low initial efficiency of these cells. Figure 2-52 shows the change in efficiency with time for two cells grown from different gas compositions and at different rates, but which nonetheless have the same initial characteristics (Table 2-13).

FIGURE 2-48. NORMALIZED EFFICIENCY OF 2000Å THICK p-i-n CELLS WITH OR WITHOUT SiC INTERFACE LAYERS AT THE p/i INTERFACE UNDER 1 SUN ILLUMINATION.

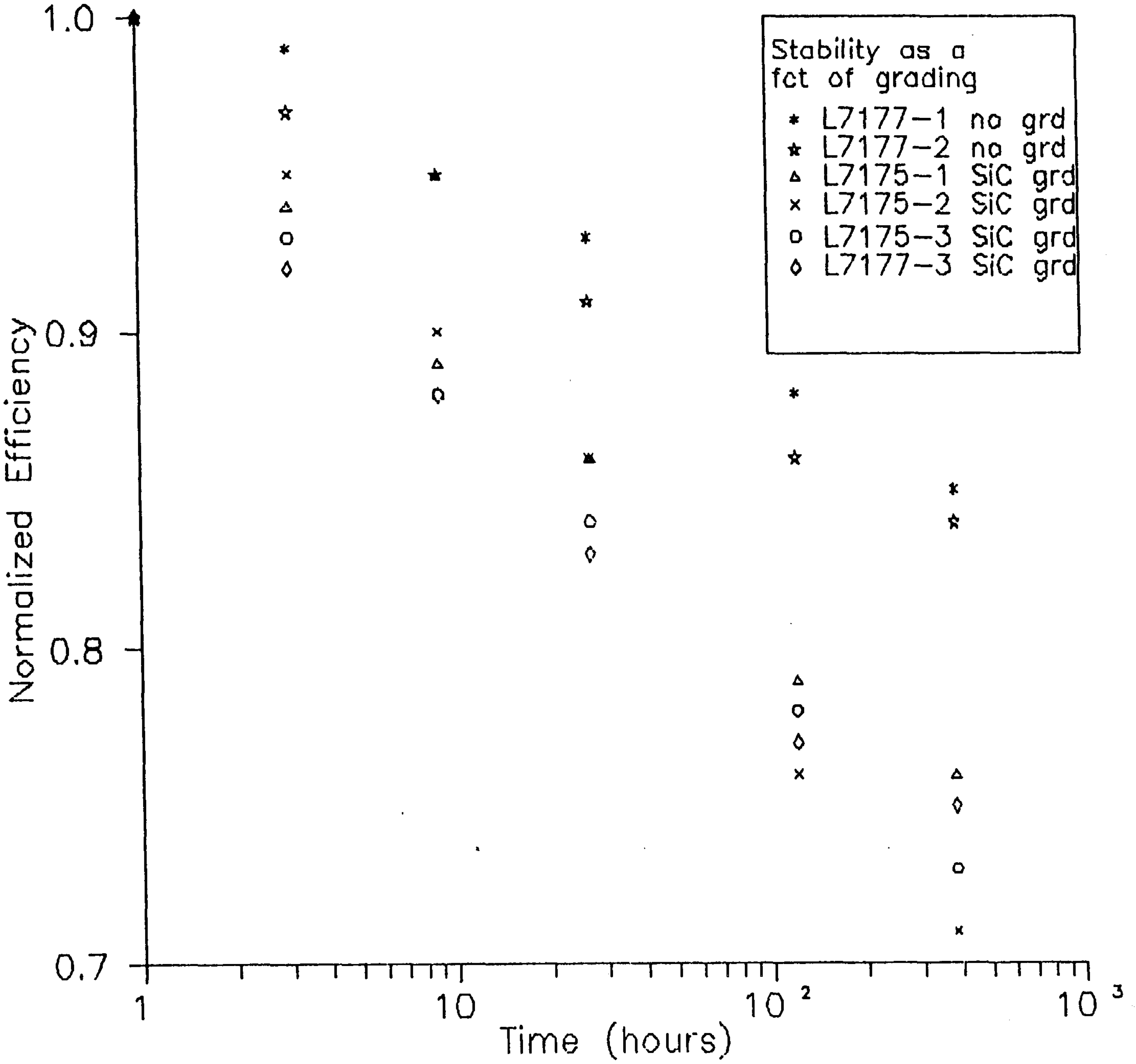

FIGURE 2-49. NORMALIZED EFFICIENCY AFTER 100 HOURS OF LIGHT SOAKING AS A FUNCTION OF i-LAYER THICKNESS.

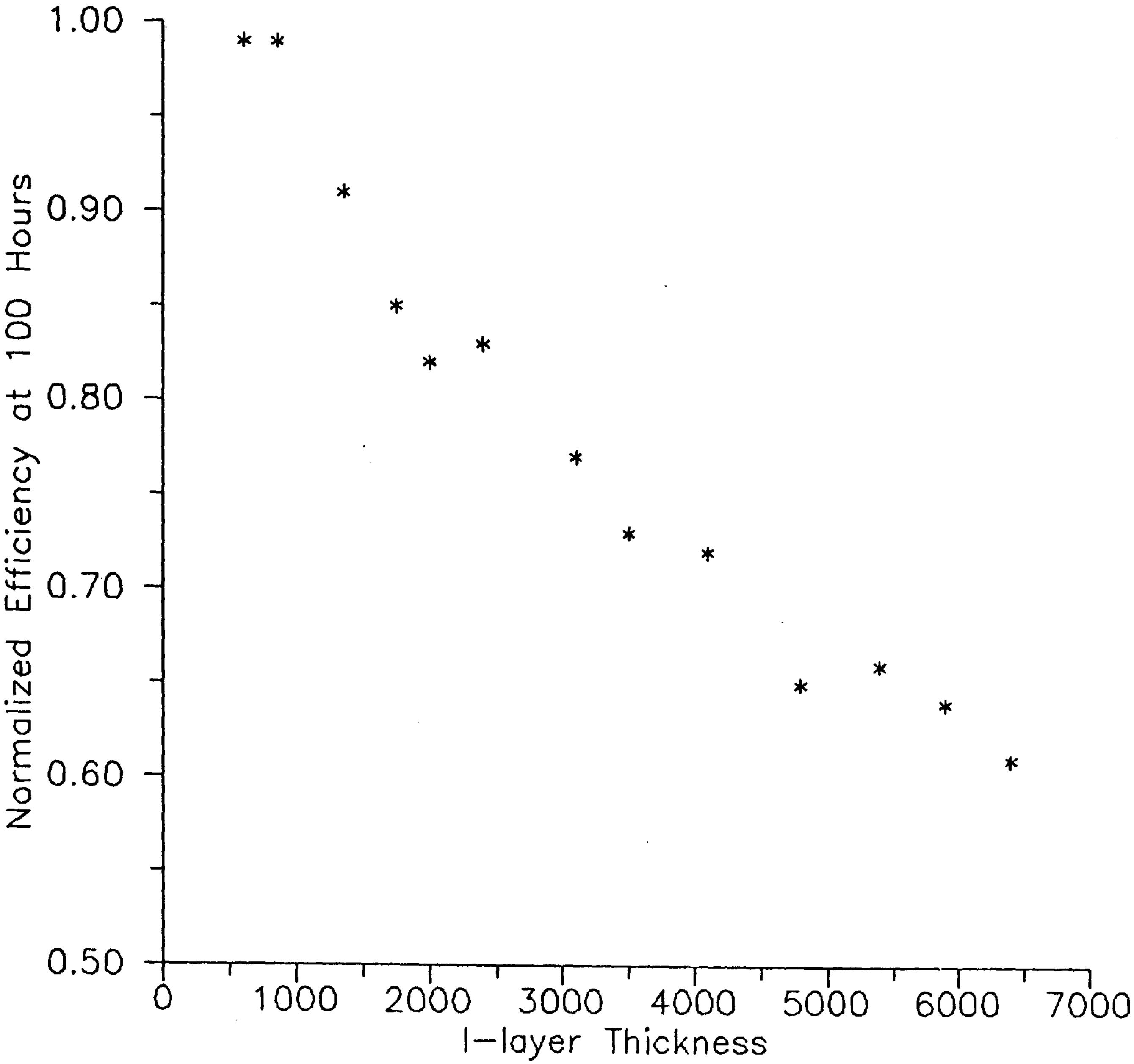

FIGURE 2-50. INITIAL EFFICIENCY OF p-i-n CELLS WITH SiC i-LAYERS AS A FUNCTION OF GROWTH RATE AND CH_4 CONTENT IN THE DISCHARGE ATMOSPHERE.

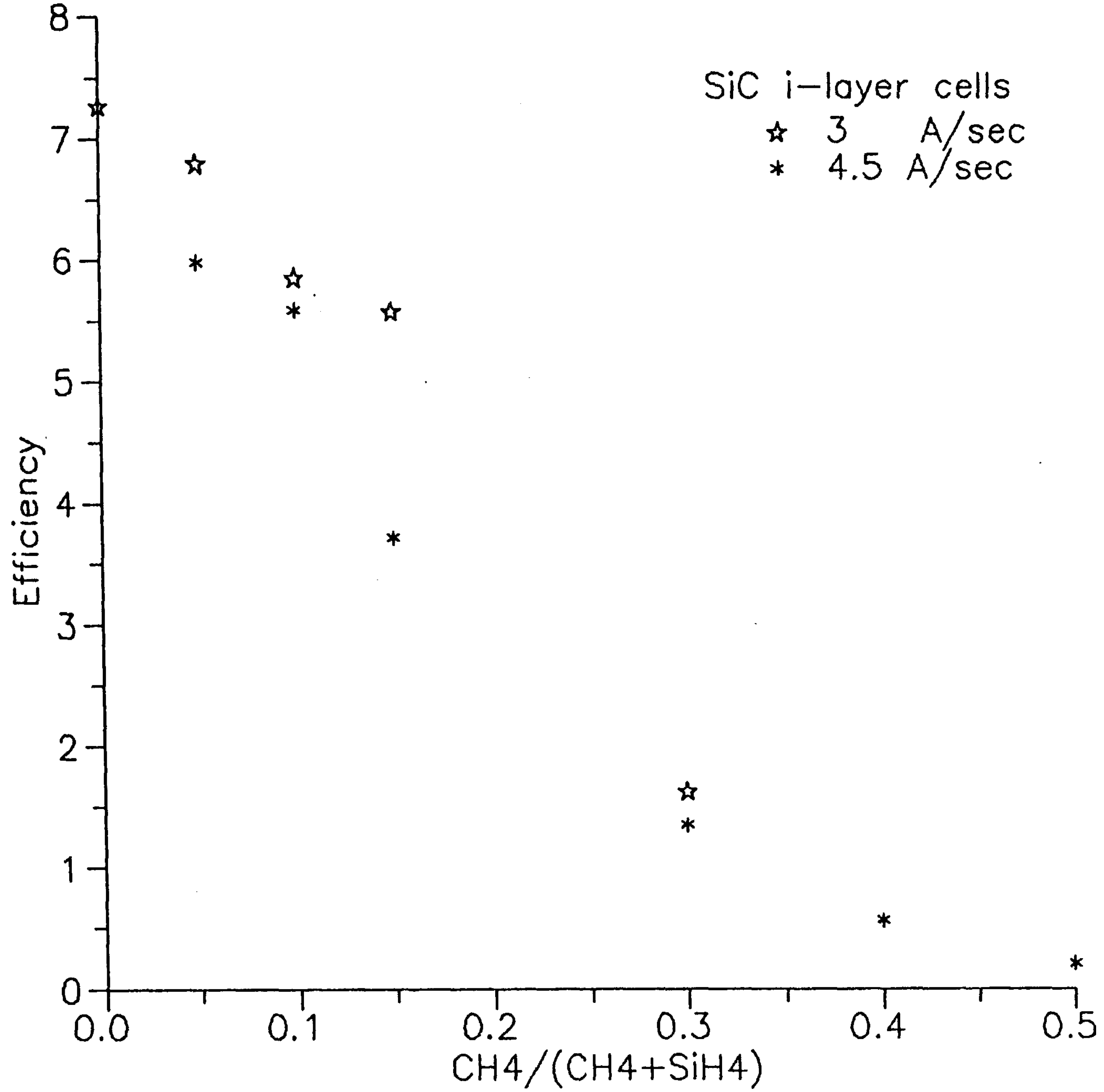

FIGURE 2-51. NORMALIZED EFFICIENCY AS A FUNCTION OF EXPOSURE TIME (AM1.5) FOR p-i-n CELLS WITH SiC i-LAYERS DEPOSITED IN DISCHARGE ATMOSPHERES HAVING VARIOUS METHANE FRACTIONS.

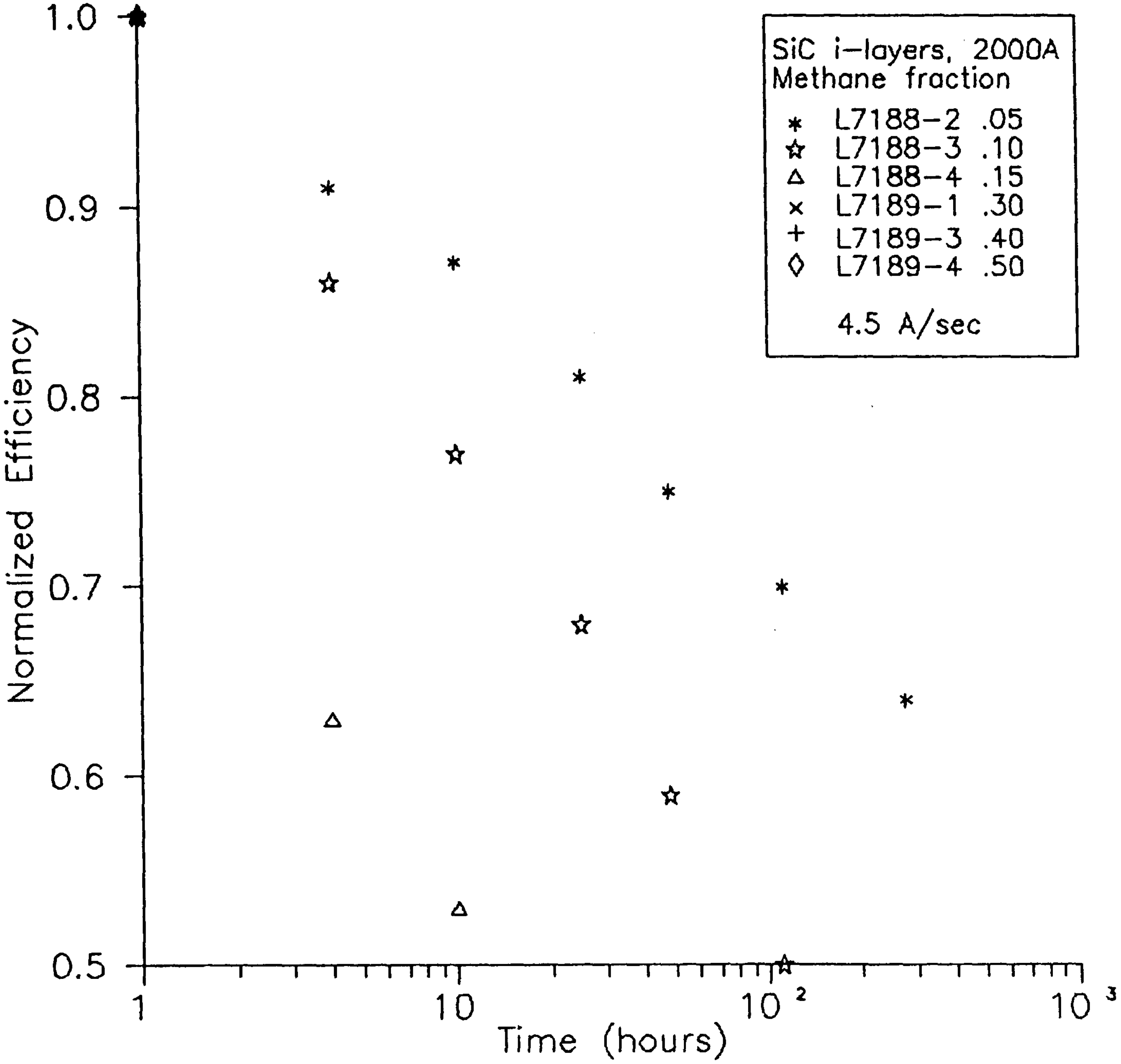

FIGURE 2-52. A COMPARISON OF THE RATE OF CHANGE OF EFFICIENCY OF TWO CELLS HAVING THE SAME INITIAL EFFICIENCIES BUT WHICH WERE GROWN UNDER DIFFERENT CONDITIONS.

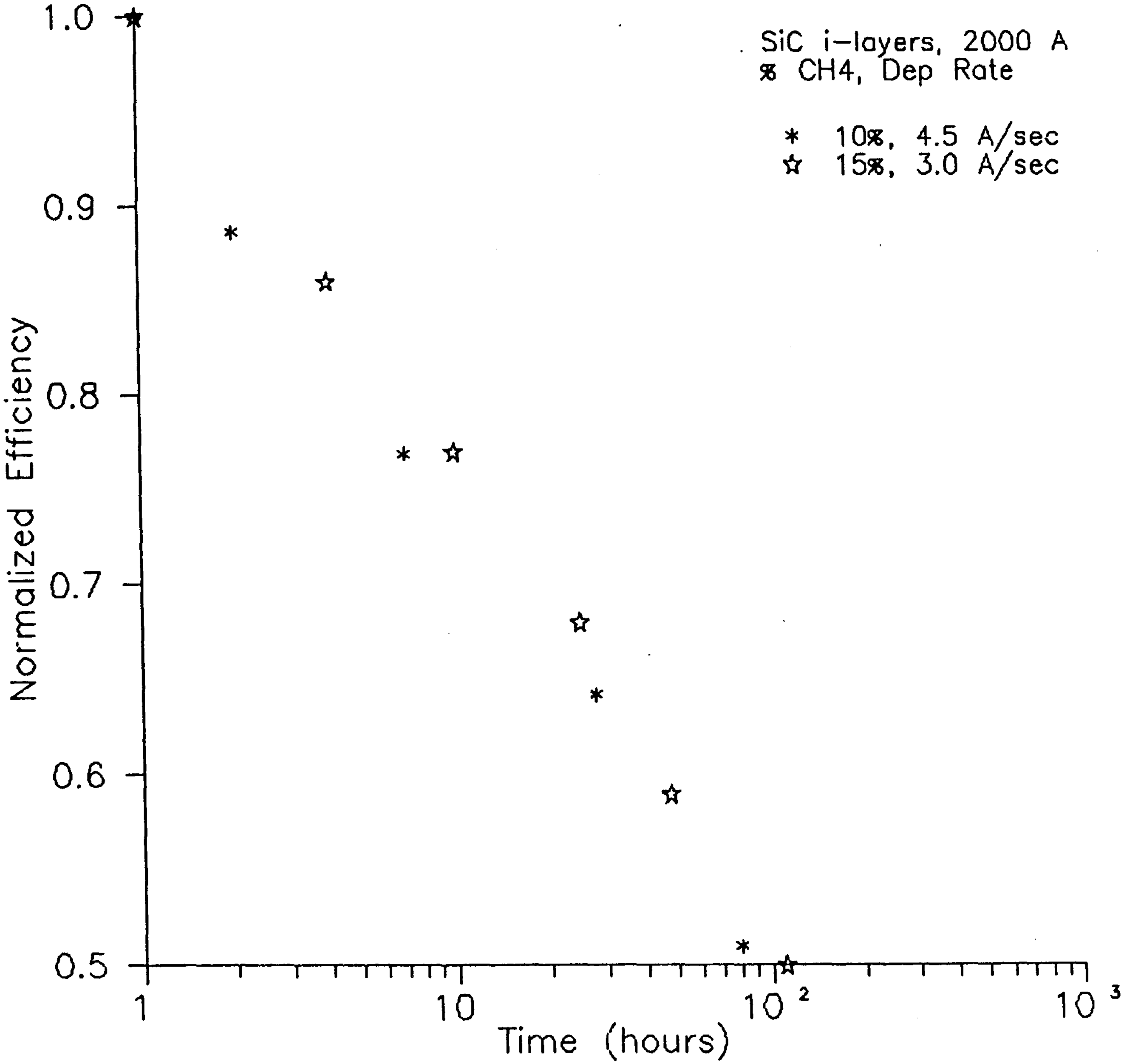

TABLE 2-13

INITIAL PV PARAMETERS FOR a-SiC CELLS GROWN UNDER DIFFERENT CONDITIONS

Growth Rate (A/sec)	CH_4 Fraction	V_{oc} (V)	FF	J_{sc} (mA/cm^2)	Efficiency
4.5	.10	.915	.679	9.0	5.59
3.0	.15	.920	.652	9.3	5.58

They can be seen to degrade at similar rates. This phenomenom seems to be generally true; that is, cells having given initial characteristics can be made in various ways; however, all cells having the same initial characteristics degrade at the same rate.

Preliminary investigations on the usefulness of disilylmethane as a feedstock are being carried out.

2.6.6 Single-Junction SiGe Cells

Cells made by incorporating SiGe have generally had a structure such as that shown in Figure 2-53. The analysis of these results is complicated by the use of these structures, however without a layer of either Si or SiC at the p/i interface, the open-circuit voltage is unacceptably low. In spite of these difficulties in analysis, it is clear that so far the SiGe i-layer cells we have made are less stable than Si i-layer cells. As an example, Figure 2-54 shows the results of light soaking cells having the structure of Figure 2-53 but without the SiC layer. A comparison of cells made with various structures of Figure 2-53 is shown in Figure 2-55 where the total i-layer thickness is in each case 2000Å.

2.6.7 Multi-Junction Cells

A number of investigations of tandem cells are now complete. The most stable devices made so far have been thin tandem cells. These are Si/Si stacks with front and back i-layer thicknesses of 450 and 2250Å and an initial efficiency of 7.8% under AM1.5 (Figure 2-56). Their projected efficiency after 1000 hours exposure is about 7.3%. They were degraded at V_{oc}, under 100mW/cm^2 illumination, at about 45°C.

Several interesting aspects of the changes in performance of stacked cells after prolonged illumination have been discovered. It has been found that current balance or imbalance affects initial efficiency but not stability. This is

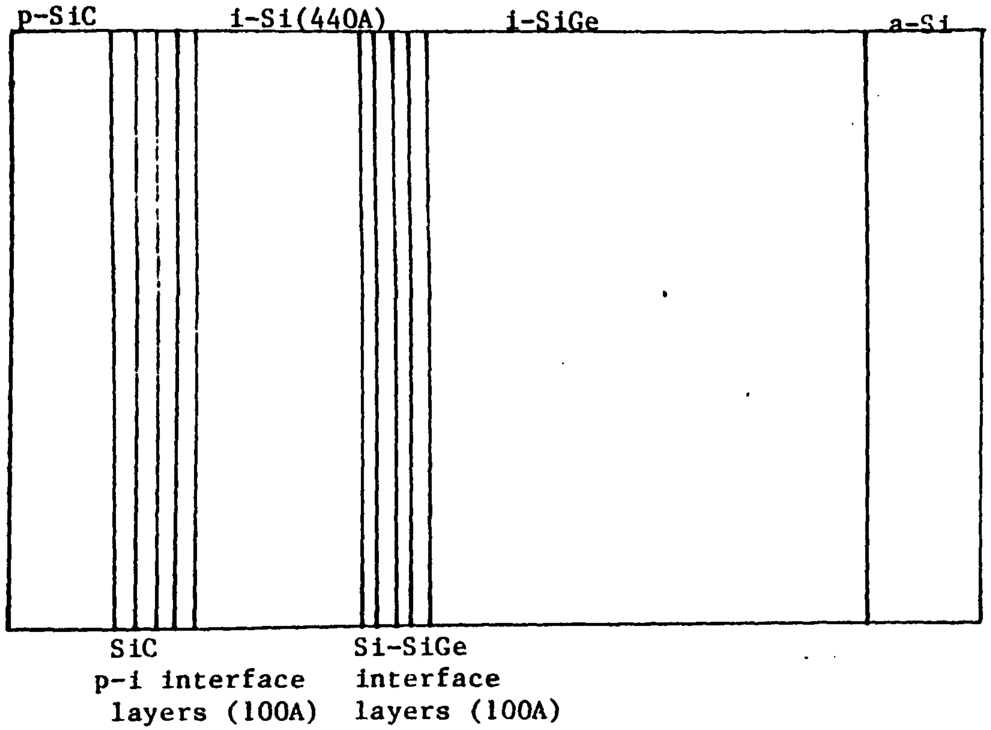

FIGURE 2-53. STRUCTURE FOR SINGLE-JUNCTION SiGe CELLS.

FIGURE 2-54. NORMALIZED EFFICIENCY OF p-i-n CELLS WITH SiGe i-LAYERS DEPOSITED IN DISCHARGE ATMOSPHERES HAVING VARIOUS GERMANE FRACTIONS.

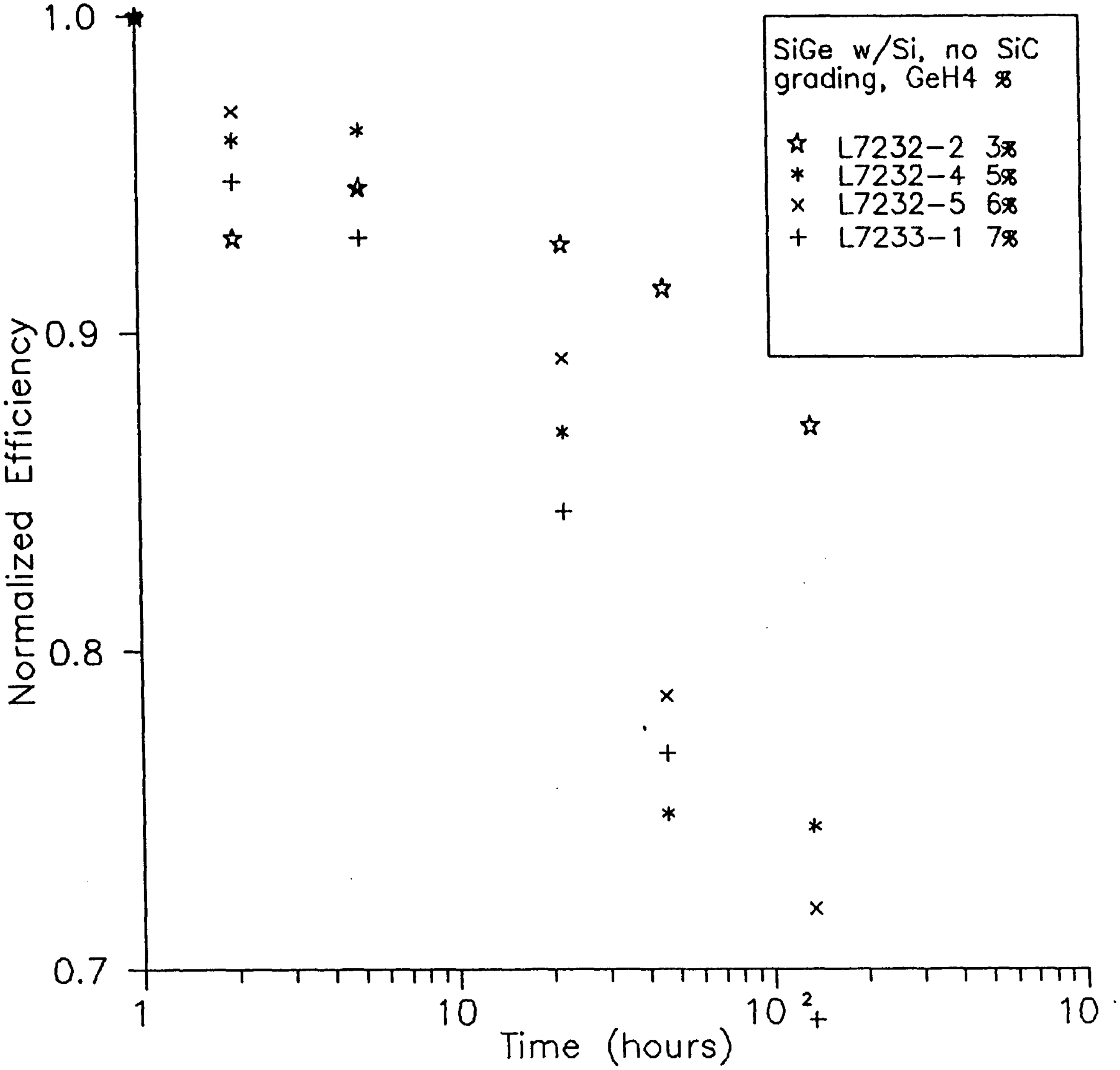

FIGURE 2-55. A COMPARISON OF THE RATE OF CHANGE OF NORMALIZED EFFICIENCY OF p-i-n CELLS WITH SiGe i-LAYERS BUT WITH DIFFERENT STRUCTURES AT THE p/i INTERFACE.

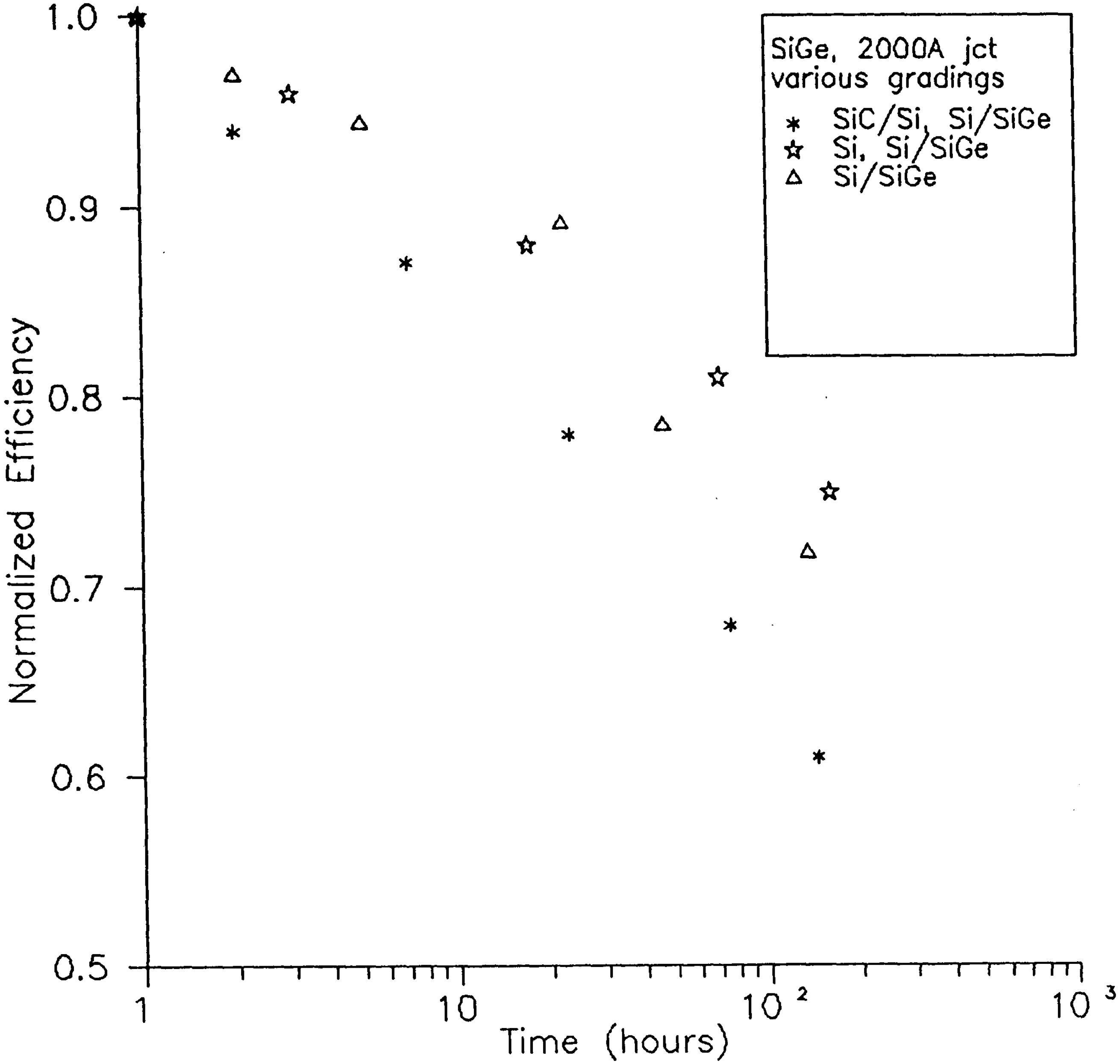

FIGURE 2-56. EFFICIENCY OF THIN TANDEM CELLS AS A FUNCTION OF ILLUMINATION TIME.

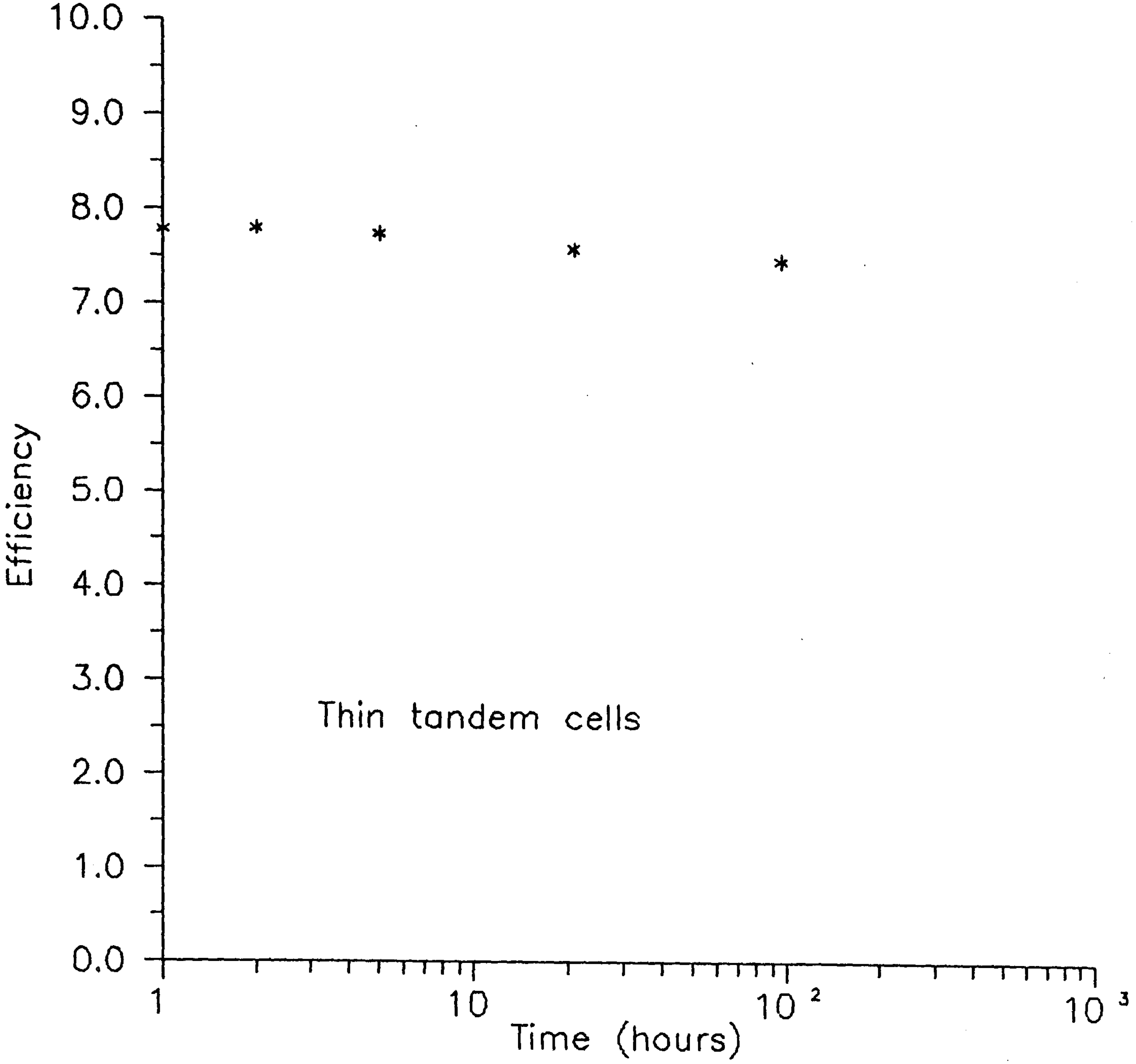

shown in Figure 2-57 where the tandems have a 7200Å thick back i-layer and a front i-layer which varies from 675Å to 1350Å. The currents calculated using quantum efficiency measurements are given in Table 2-14.

In each case the efficiency loss is about 32% in 700 hours. This experiment has been carried out several times on cells with various thicknesses with, in each case, the same qualitative result.

For a given total i-layer thickness, a tandem cell is much more stable than the corresponding single-junction cell. This improved stability is more than can be accounted for simply as a result of the lower intensity reaching the second cell in the tandem device. Figure 2-58 compares a single junction cell with 2000Å i-layer and a tandem having a 2200Å back i-layer and a 450Å front i-layer (device of Figure 2-56). The dashed line shows the efficiency which would be expected if the lowered intensity of light on the second cell was the only source of lowered degradation.

We are trying to model these results using a simple model. I-V characteristics are generated for each of the front and back components of the tandems. At the same time, single-junction cells identical to the components of the tandem device have been made and degraded, where in the case of the back-junction cell suitable filters are used to simulate conditions in back of the tandem structure. The characteristics are calculated using the model, and then made to match the measured characteristics of the individual components of the tandem. These are then added together to try to match the total characteristics of the cell. We have begun to use this sort of procedure to try to determine why stacked cells are more stable than single-junction cells of similar thickness, why current balance has no effect, etc.

It appears that the enhanced stability of the tandem is due to a to a combination of factors. The thin and stable front junction seems to act as a stabilizer for the device as a whole. That front- and back-limited junctions appear to degrade at the same rate can probably be explained by careful

FIGURE 2-57. NORMALIZED EFFICIENCY OF THICK TANDEM CELLS HAVING THE SAME BACK i-LAYER THICKNESS (6500Å) IN EACH CASE BUT VARYING FRONT i-LAYER THICKNESS.

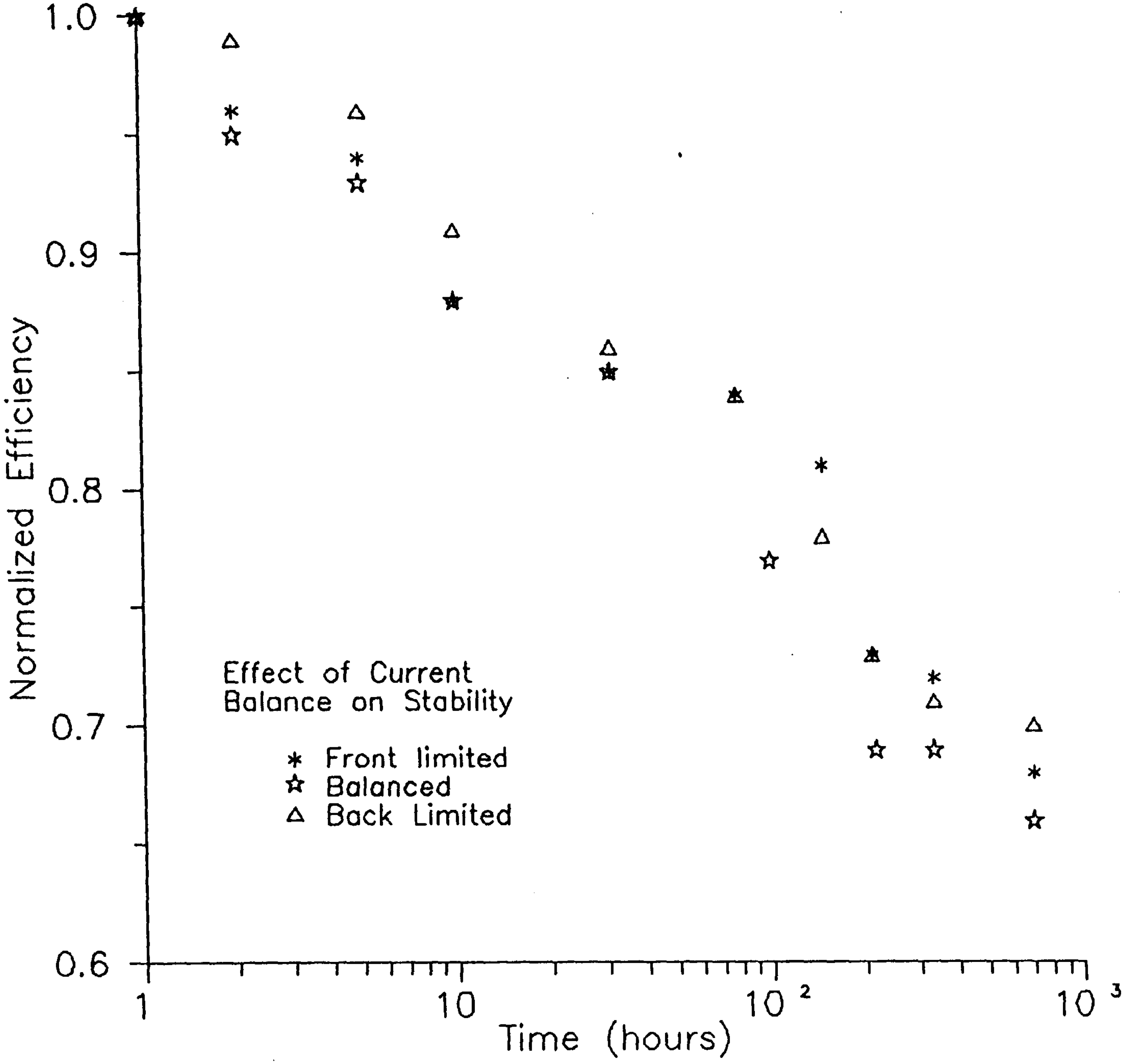

TABLE 2-14

CALCULATED CURRENT DENSITIES

Front Cell Thickness (A)	Front Cell J_{sc} (mA/cm^2)	Back Cell J_{sc} (mA/cm^2)
675	5.6	7.2
900	6.7	7.0
1350	7.0	4.9

FIGURE 2-58. COMPARISON OF THE NORMALIZED EFFICIENCY OF TANDEM CELL WITH BACK i-LAYER THICKNESS OF 2200Å WITH THAT OF A 2000A SINGLE JUNCTION CELL AS A FUNCTION OF ILLUMINATION TIME.

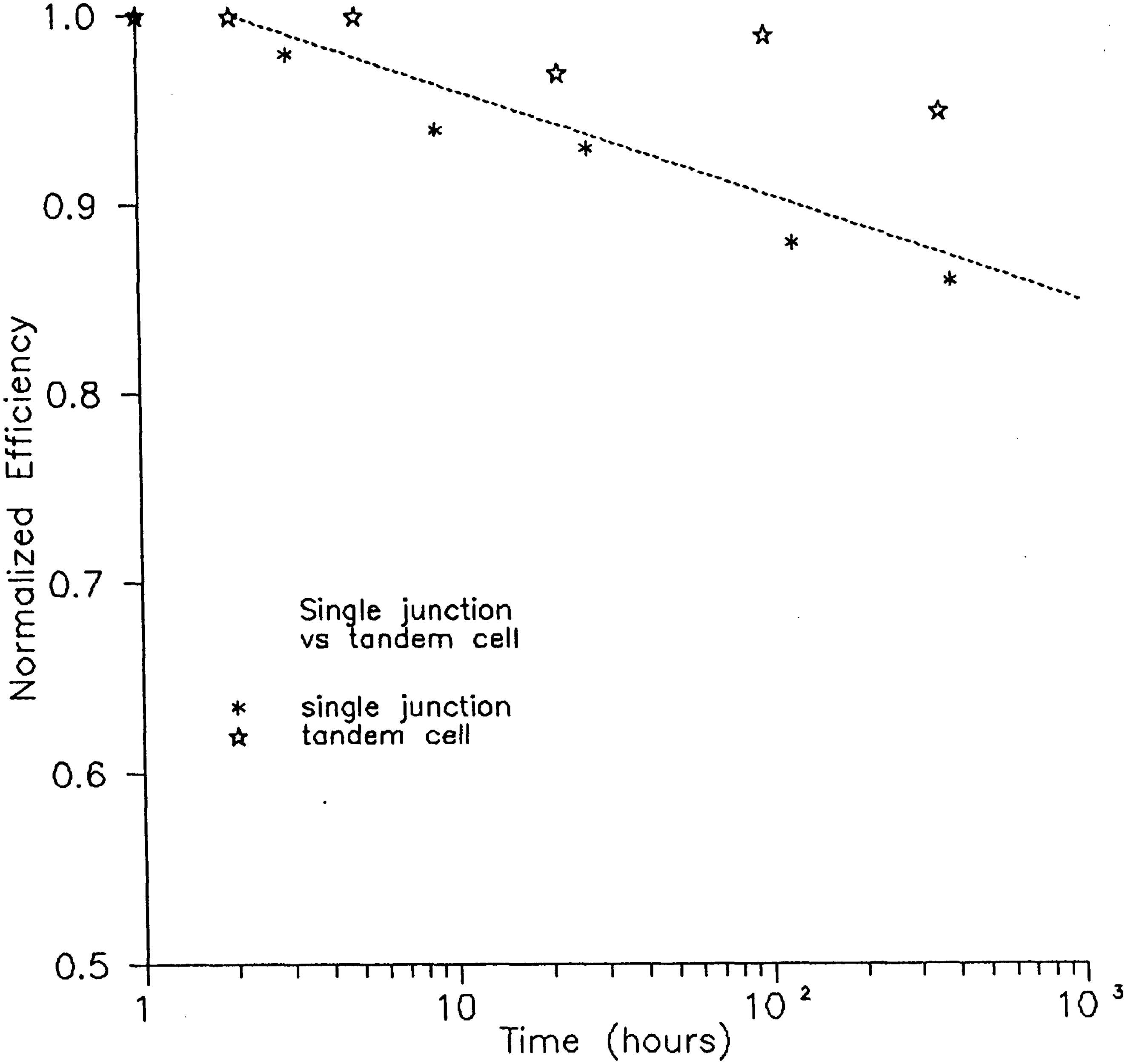

consideration of the complicated interaction between front and back cell. It must be kept in mind that the fill factor and the efficiency of the tandem device is determined not by the relative values of current at short circuit but by the relative currents at the maximum power point.

2.6.8 Test Facilities

Construction is complete on the first phase of a new outdoor test facility. We now have the capability to monitor up to 450 modules (12"x13"). There is limited meteorological data gathering capability. When completed next year there will be complete weather monitoring capability as well as capacity for about 900 12"x13" modules.

Our indoor accelerated test facilities now include 20 450W Na vapor lamps. These all have reflectors which have been coated with a diffusely reflecting paint so that intensities are about $100 \mathrm{mW/cm^2}$ ±5% over an area about 12" in diameter and about 20-30% lower over the next 3-4" ring. At present one of these lamps is timed to conform with the SERI time and temperature requirements for degradation testing.

A few experiments have been carried out to try to determine whether the indoor and outdoor degradation results can be correlated. Figure 2-59 shows results obtained from small area ($.25 \mathrm{cm^2}$) diodes degraded indoors and 1 watt modules degraded outdoors, where both were originally part of the same 12"x13" module. These can be divided into two groups. The 4000Å thick diodes and modules degrade about 30% in 100 hours, the thin diodes and modules (1800° - 2400Å) degrade about 15-20% in 100 hours. All have SiC interface layers. Within each group the small area diodes and modules degrade at about the same rate. Correspondence between the two sets of results was established by assuming that 1 day outdoors is equivalent to 5 hours indoors.

FIGURE 2-59. NORMALIZED CONVERSION EFFICIENCY OF SMALL AREA DIODES (ILLUMINATED INDOORS) AND 1W$_p$ MODULES (ILLUMINATED OUTDOORS) AS A FUNCTION OF ILLUMINATION TIME.

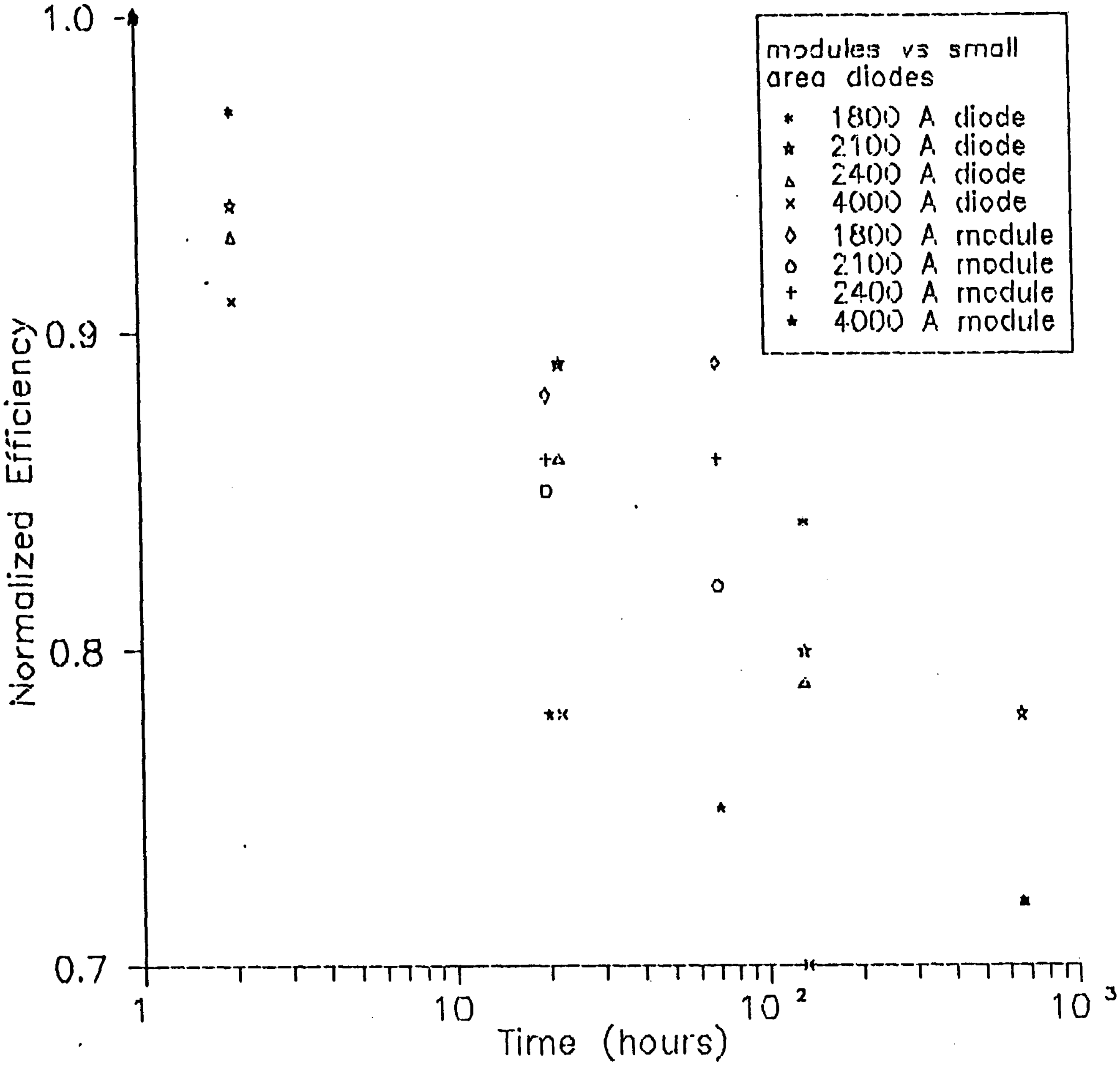

2.6.9 Photothermal Deflection Spectroscopy

When films are light-soaked at 100mW/cm^2 light (632.8nm), the subgap absorption increases. The absorption coefficient at 1.2eV increases linearly with the log of time, in a parallel fashion to the linear decay of fill factor in a solar cell with the log of exposure time (Figure 2-60a). We have also measured the change in the absorption at 1.2eV as photo-degraded films are annealed and have data on the changes in one film which was degraded at 35°C and annealed back at 130°C. Figure 2-60 shows the change in the absorption at 1.2eV and the change in fill factor for a) degradation and b) annealing of cells and the film under the same conditions. The behavior seems to be parallel.

We have measured the change in absorption coefficient with light soaking for a series of SiC films where the methane fraction of the deposition gas varied from 5% to 50%. An example of the results is shown in Figure 2-61 for the film made from a gas mixture containing 40% methane. As can be seen from this figure and from Figure 2-62 which shows the absorption normalized to the initial curve, the greatest change in absorption coefficient occurs at about 1.6eV as compared to 1.2eV for the case of a-Si. Figure 2-63 shows the energy at which the greatest change in absorption occurs vs. the energy at which the absorption coefficient is $1 \times 10^4 cm^{-1}$. The energy of greatest change is more or less constant with respect to the absorption edge. Another point of interest in comparing the case of Si to that of SiC is that although for SiC the initial absorption is greater, the fractional change in absorption coefficient is about the same.

2.7 TRANSPORT PROPERTIES OF AMORPHOUS SILICON ALLOYS

2.7.1 Measurements

The principle tool that we will use to explore the transport properties of alloy materials is the SWQE (short wavelength quantum efficiency) that was first presented in reference 1. Some aspects of the theory and development will be repeated here for the purpose of clarity. A paper on this topic is to be submitted to the Journal of Applied Physics Letters in January 1988 [9].

FIGURE 2-60. VARIATION IN FILL FACTOR AND OPTICAL ABSORPTION AT 1.2eV AS A FUNCTION OF a) ILLUMINATION TIME AND b) ANNEALING TIME AT 130°C.

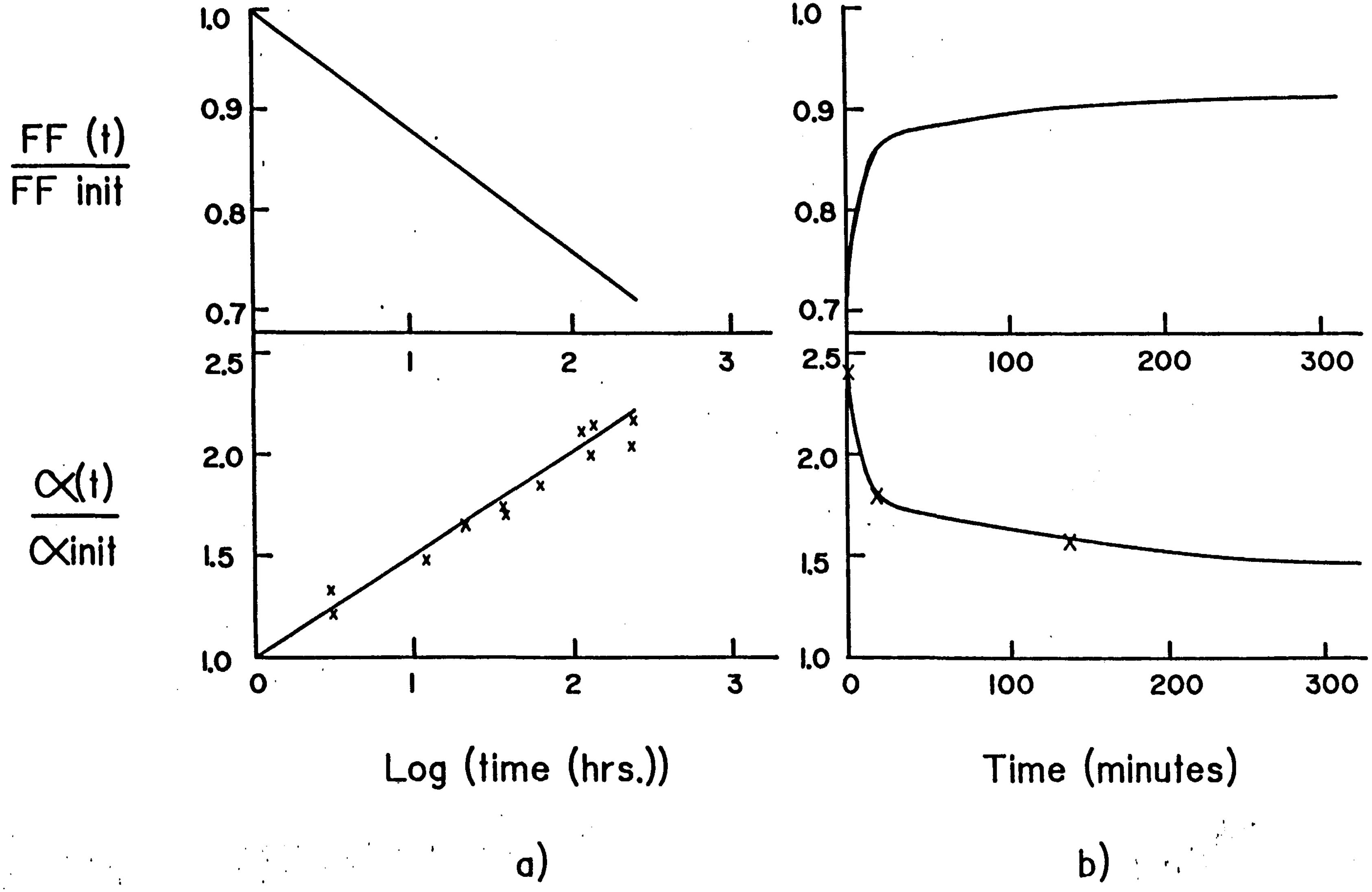

FIGURE 2-61. ABSORPTION COEFFICIENT AS A FUNCTION OF ENERGY OF A FILM GROWN IN A DISCHARGE ATMOSPHERE CONTAINING 40% CH_4 AS A FUNCTION OF ILLUMINATION TIME.

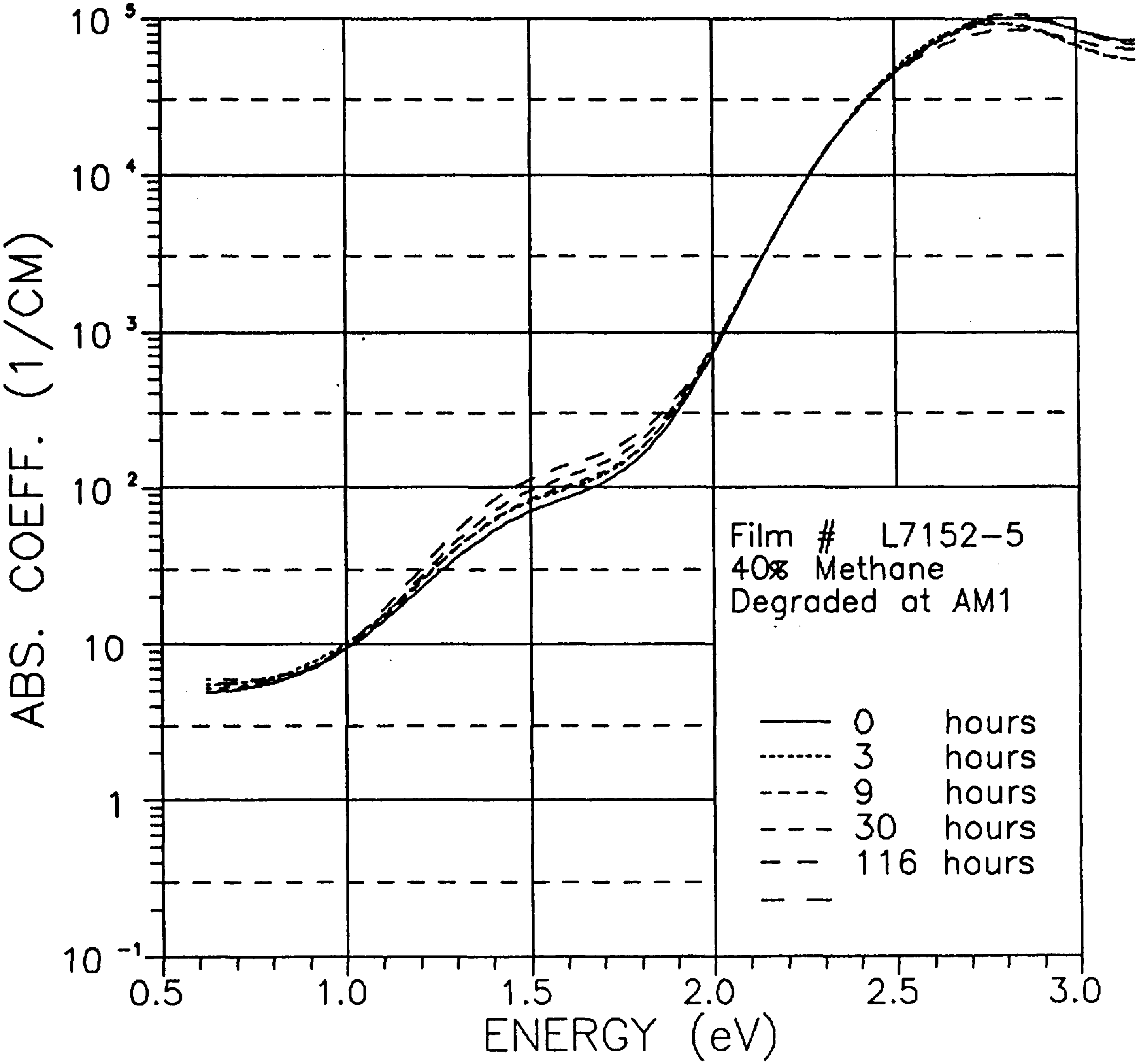

FIGURE 2-62. NORMALIZED ABSORPTION COEFFICIENT AS A FUNCTION OF ENERGY OF A FILM GROWN IN A DISCHARGE ATMOSPHERE CONTAINING 40% CH_4 AS A FUNCTION OF ILLUMINATION TIME.

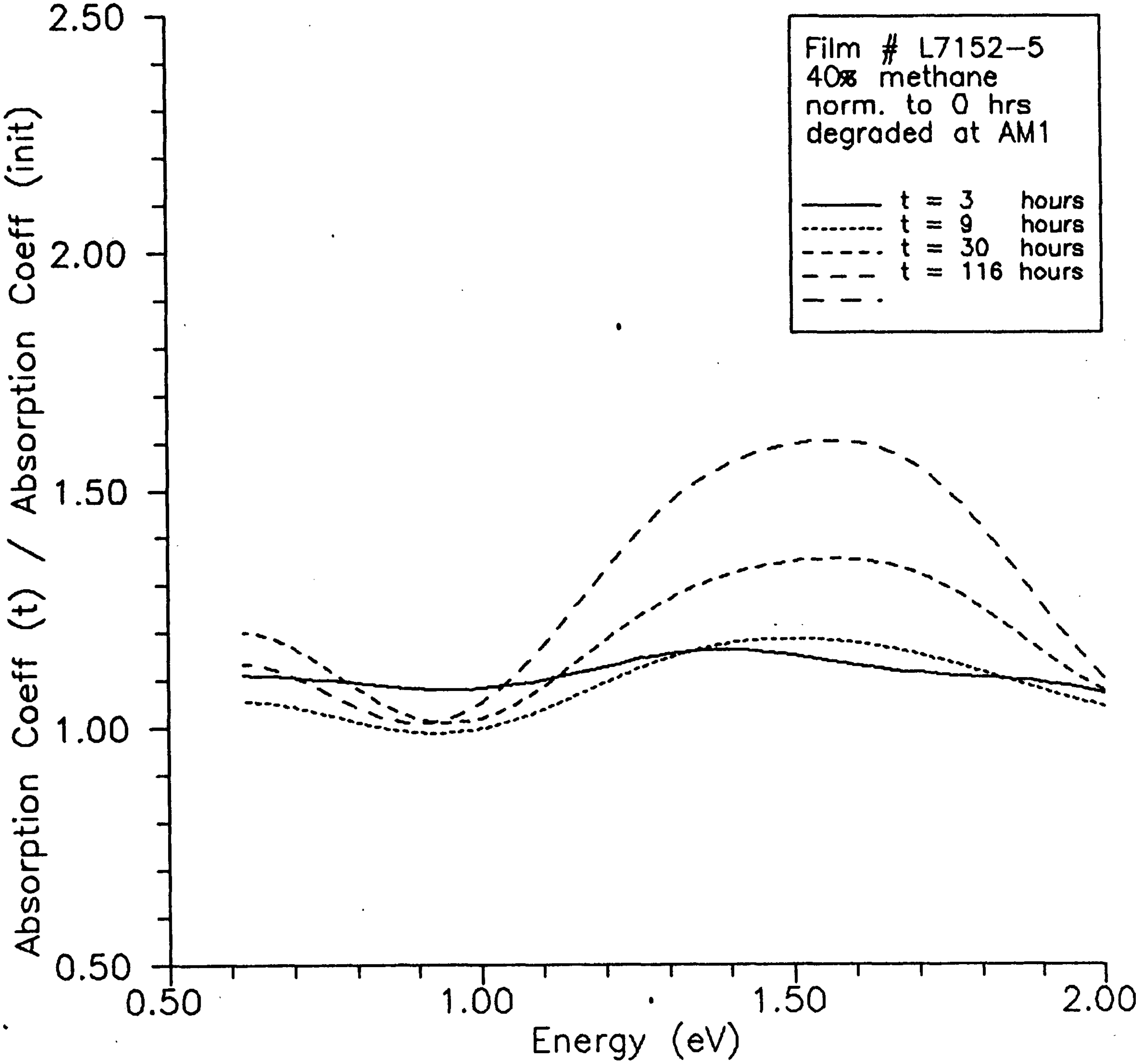

FIGURE 2-63. ENERGY OF THE PEAK IN THE NORMALIZED ABSORPTION COEFFICIENT CURVES AS A FUNCTION OF THE ENERGY AT WHICH THE ABSORPTION COEFFICIENT IS 10,000cm^{-1}.

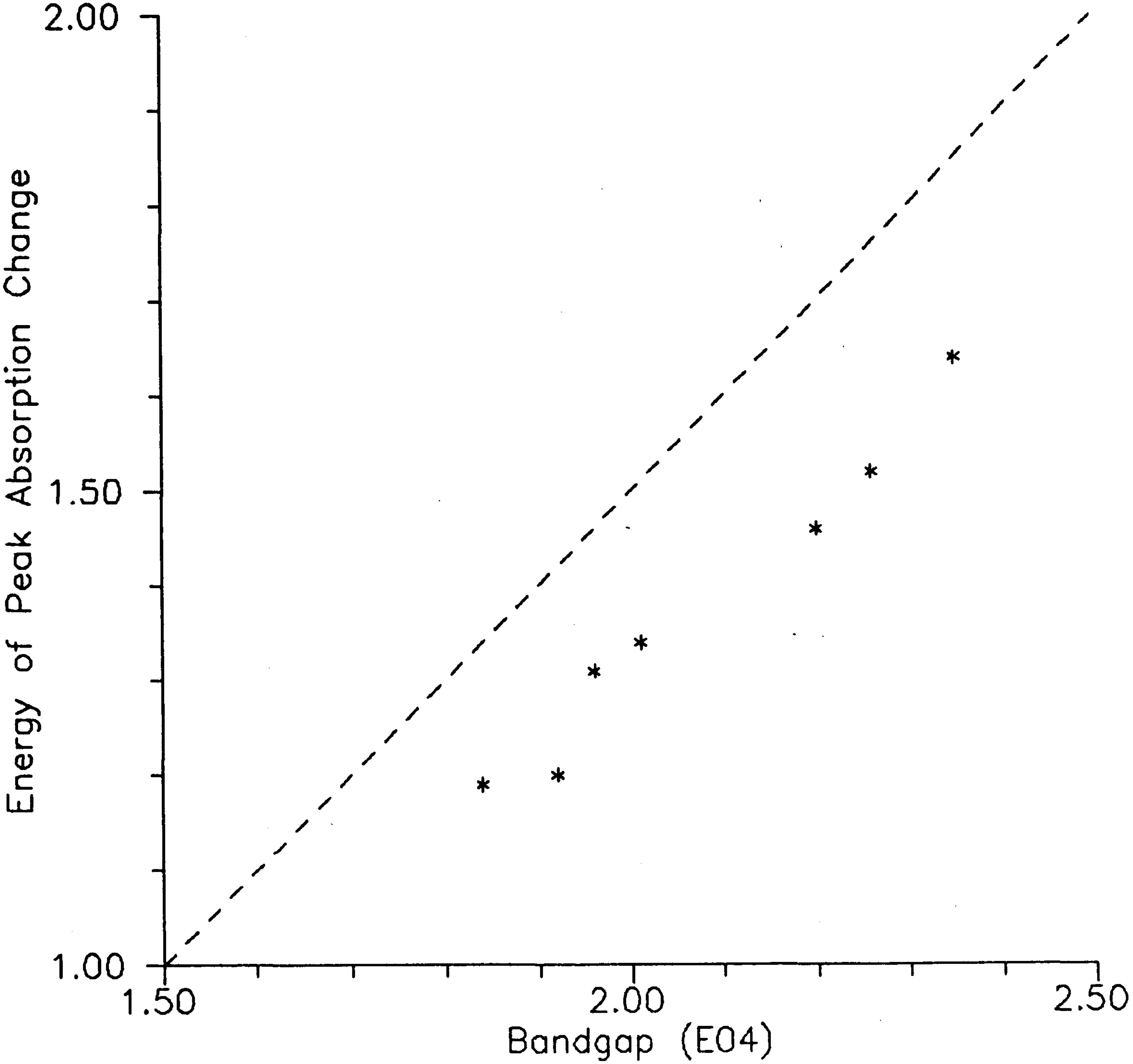

It is important to distinguish between device and material stability characterization. Device (for example solar cell) stability characterization includes the degradation of device parameters such as fill factor, efficiency, and short-circuit current. Device stability data are of considerable engineering importance, but should not be taken as a material property as it depends on device parameters (for example, cell thickness); as well as material parameters (such as the density of recombination centers). Numerical modelling has the potential to uncouple device and material parameters, but in practice the multitude of adjustable inputs leads to a somewhat ambiguous relation between material and device parameters. Our approach is to design device measurements that allow an accurate analytical description of the material properties (density of recombination centers in this case) from device measurements.

The SWQE can be expressed as:

$$\mathrm{SWQE} = (J_{flux} - J_{opt} - J_l - J_r)/J_{flux} \qquad (2\text{-}1)$$

Where J_{flux} is the current that would be measured if the quantum efficiency was 100%. J_{opt} is the current loss due to light absorption and reflection in the CTO, doped layers, and the glass substrate. J_l is the current lost at the p/i interface and J_r is the current loss due to recombination in the low field regions of the i-layer. A simple analytical treatment is possible because only J_r is dependent on i-layer thickness, red light bias (volume absorbed light) and voltage bias (J_l may be weakly bias dependent).

The essential result of this method is that the change in short wavelength quantum efficiency due to light soaking (no external light bias during measurement) is linearly related to the density of recombination centers.

$$J_r = {}_x\!\int U dx \qquad (2\text{-}2)$$

$$J_r = q p_o (D_o - 2W_d)/\tau_{po} \text{ (dark)} \qquad (2\text{-}3)$$

$$= \quad qn_o(D_o-2W_d)/\tau_{no} \text{ (light)} \qquad (2\text{-}4)$$

$$\tau_{po} = 1/(\tau_p N_r V_{th}), \; \tau_{no} = 1/(\sigma_n N_r V_{th}) \qquad (2\text{-}5)$$

$$J_r \text{ (dark)} = A_1 N_r \qquad (2\text{-}6)$$

$$\text{SWQE} = A_2 \; N_r \qquad (2\text{-}7)$$

Where U is the Schockley-Read recombination rate, D_o is the width of the i-layer, W_d is the width of the depletion regions at the p/i and n/i interfaces (assumed to be the same for simplicity), τ_{no} and τ_{po} are the effective electron and hole lifetimes, N_r is the density of light induced recombination centers, σ_n and σ_p are the electron and hole capture cross sections, and A_1 and A_2 are constants.

Figure 2-64 shows the SWQE ratio (ratio of that without light bias to that with light bias) as function of cell thickness and light soaking time. We use the SWQE (dark to light) ratio for analysis since the light-biased SWQE is not a function of light soaking time and therefore can be used as a reference (thus, eliminating calibration errors). The change in SWQE are consistent with a reduction in the hole lifetime (τ_{po}). After 100 hours of light soaking the lifetime is reduced by approximately a factor of two. Note that because the light-biased SWQE is not a function of light-soaking time, that the light-generated defects do not reduce the effective electron lifetime as indicated in Equation (2-5). A comparison between SWQE ratios, and device parameters as a function of light-soaking time is shown in Figure 2-65.

2.7.2 Defects in Amorphous Alloys

2.7.2.1 Defects in Light-Soaked a-SiGe:H

A series of solar cells with a-Si_xGe_{1-x}:H ($x \sim 0.8$) i-layers were prepared with i-layer thickness ranging from 0.25 to 7.0 microns. These cells employed a narrow (less than 300Å thick) a-Si:H buffer layer at the p/i interface to

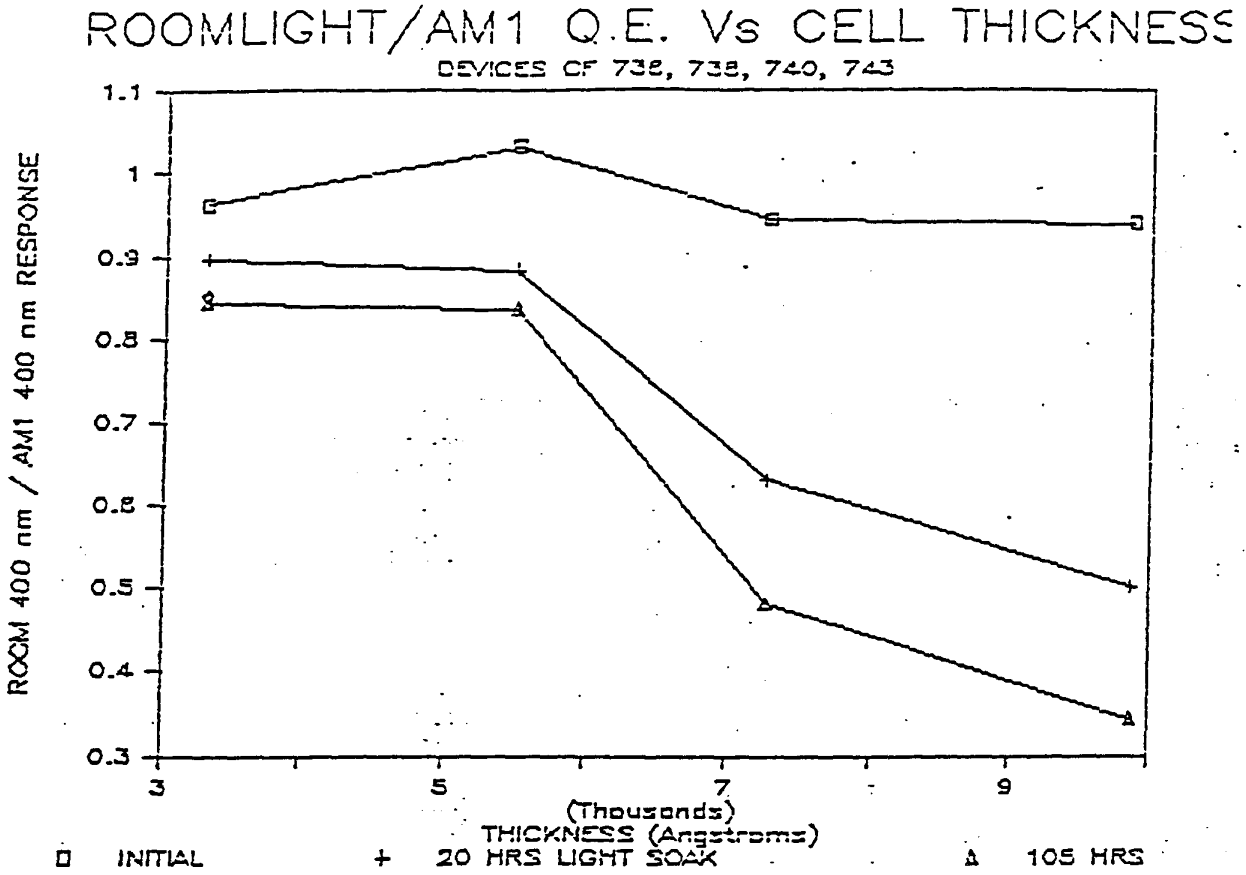

FIGURE 2-64. THE SWQE RATIO OF a-Si:H (STANDARD GROWTH RATES AND TEMPERATURE) AS A FUNCTION OF LIGHT SOAKING TIME AND i-LAYER THICKNESS.

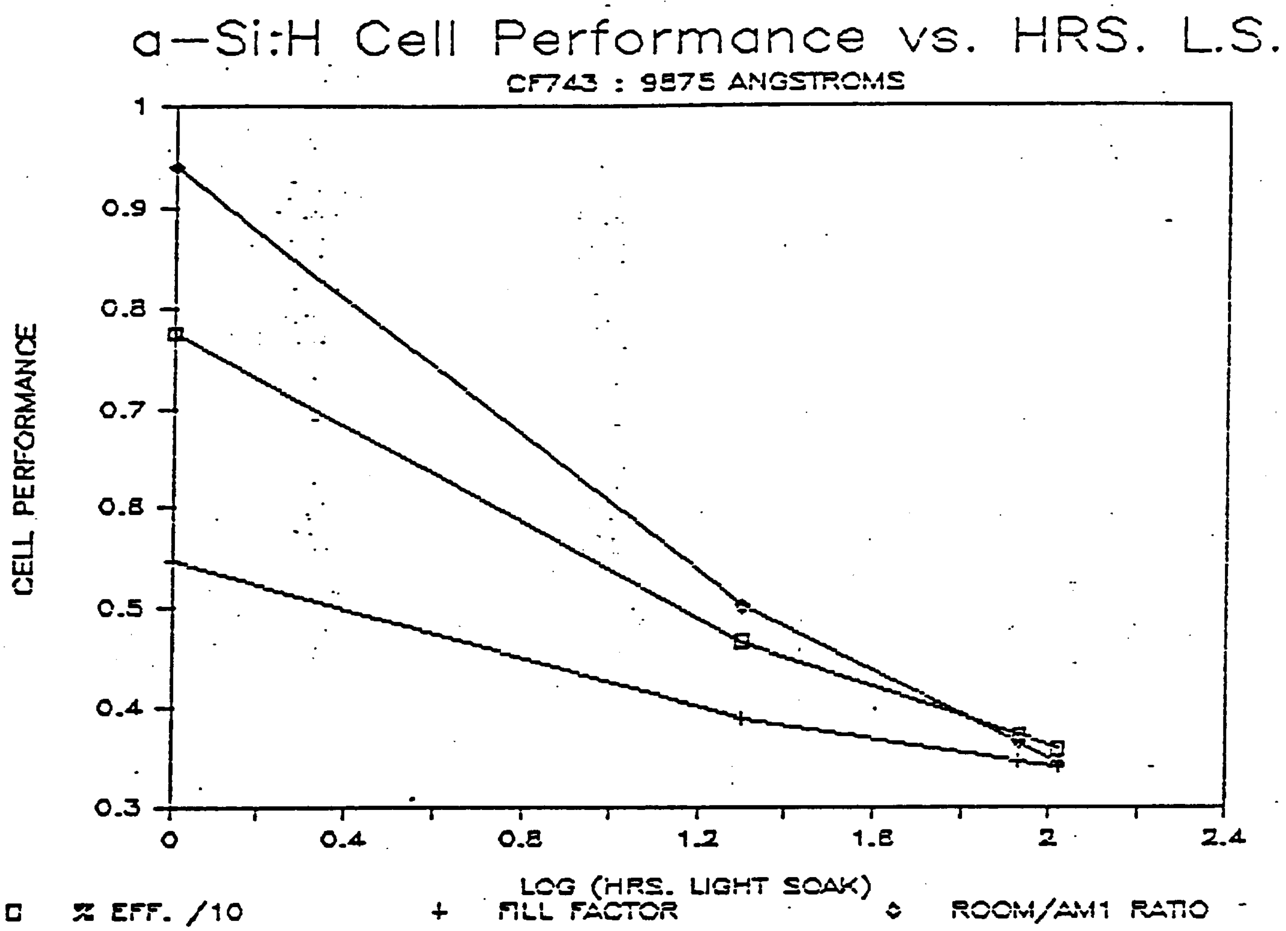

FIGURE 2-65. COMPARISON OF FILL FACTOR, EFFICIENCY AND SWQE RATIO AS A FUNCTION OF LIGHT SOAKING TIME FOR CELLS 8,500Å THICK.

enhance the SWQE . The cells were light soaked for 100 hours at V_{oc}. The change in the SWQE ratio (Figure 2-66) is remarkably similar to that of the a-Si:H cells (Figure 2-64). Like the a-Si:H cells these changes are consistent with a hole lifetime reduction by about a factor of two after 100 hours of light soaking.

2.7.2.2 Defects in Annealed a-SiGe:H

The reduction in a-Si_xGe_{1-x}:H cell performance (device parameters) that occurs with increasing germane content (decreasing x) are not accompanied by a change in the SWQE (in most cases). The fill factor of a-SiGe:H solar cells as a function of Ge content ($GeH_4/SiH_4 + GeH_4$) is shown in Figure 2-67. It is therefore likely that the defect that results from increasing Ge content is not the same as the defect caused by light soaking (dangling bonds). It is our hypothesis that the defect in annealed a-SiGe:H is a germanium cluster. To test this hypothesis we initiated a study of multi-layer structures to determine if a narrow bandgap material in a larger band gap matrix would result in transport problems analogous to those of high Ge content a-SiGe:H.

Germanium clusters are expected to occur due to either favored Ge-Ge bonding or completely random mixing in high content alloys. To determine if a Ge cluster would be an effective trap or recombination centers we prepared solar cells with a-Si:H (1000Å)/a-Ge:H (∿4Å) multi-layer i-layers (a SIMS profile of a similar layer deposited onto a silicon substrate is shown in Figure 2-68). The incorporation of five (∿4Å thick) a-Ge:H layers in an a-Si:H i-layer resulted in a significant loss in solar cell performance (fill factors less than 0.4). A comparison of cell parameters for multi-layer i-layer, high Ge content i-layer, and standard a-Si:H i-layers is shown in Table 2-15. Similar cells prepared with an interruption of growth, an interruption of growth and GeH_4 flow but no deposition (no glow discharge), or the deposition of thin (∿4Å thick) a-SiC:H layers did not cause a reduction in cell performance. FTIR (Fourier Transform Infrared) absorption spectroscopy of multi-layers deposited onto crystalline Si substates did not show a significant change in dihydride content over our standard a-Si:H. It is reasonable to conclude that the Ge layer in the

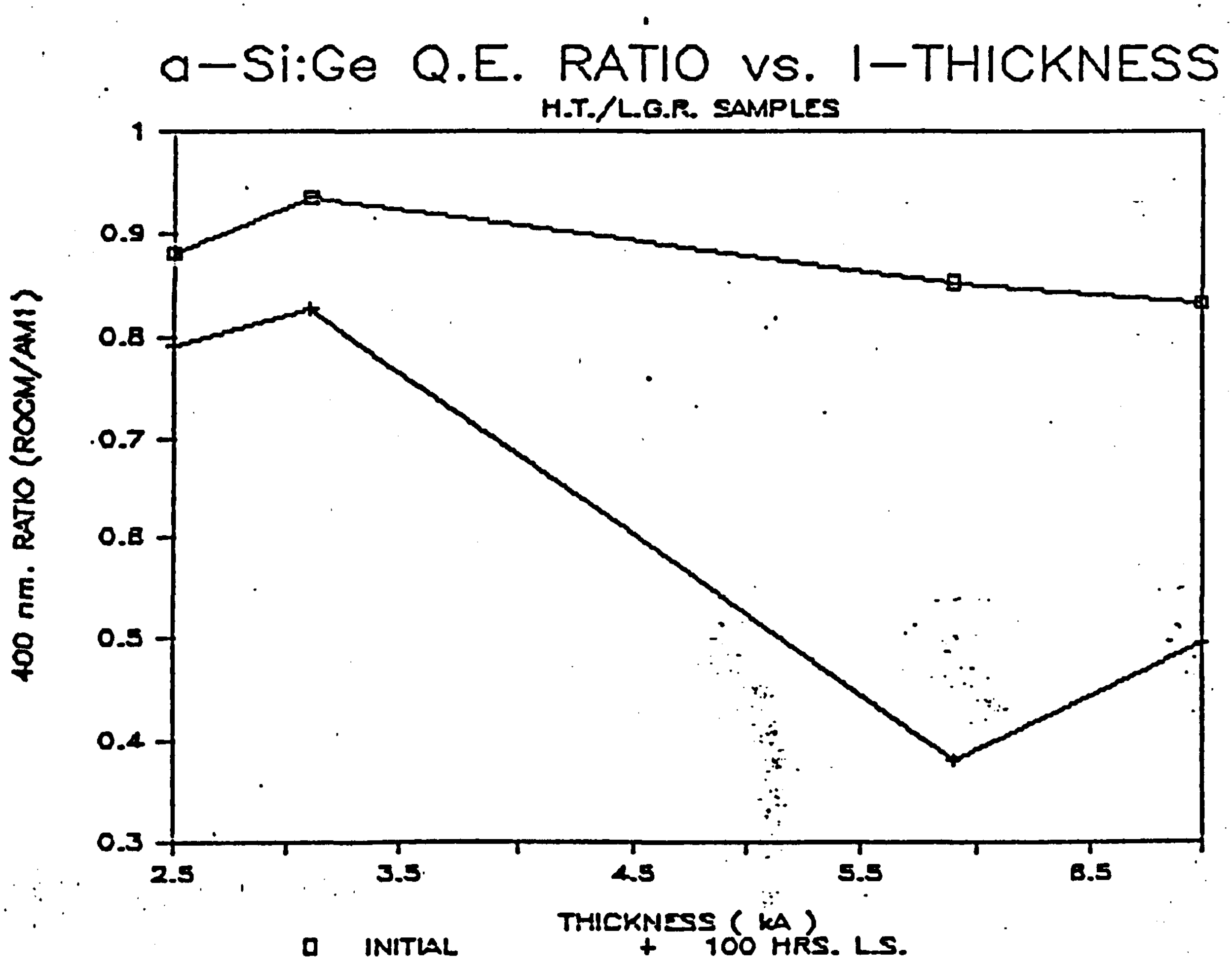

FIGURE 2-66. THE SWQE RATIO OF A SERIES OF a-Si$_x$Ge$_{1-x}$ (x = 0.8) OF ANNEALED AND LIGHT SOAKED CELLS.

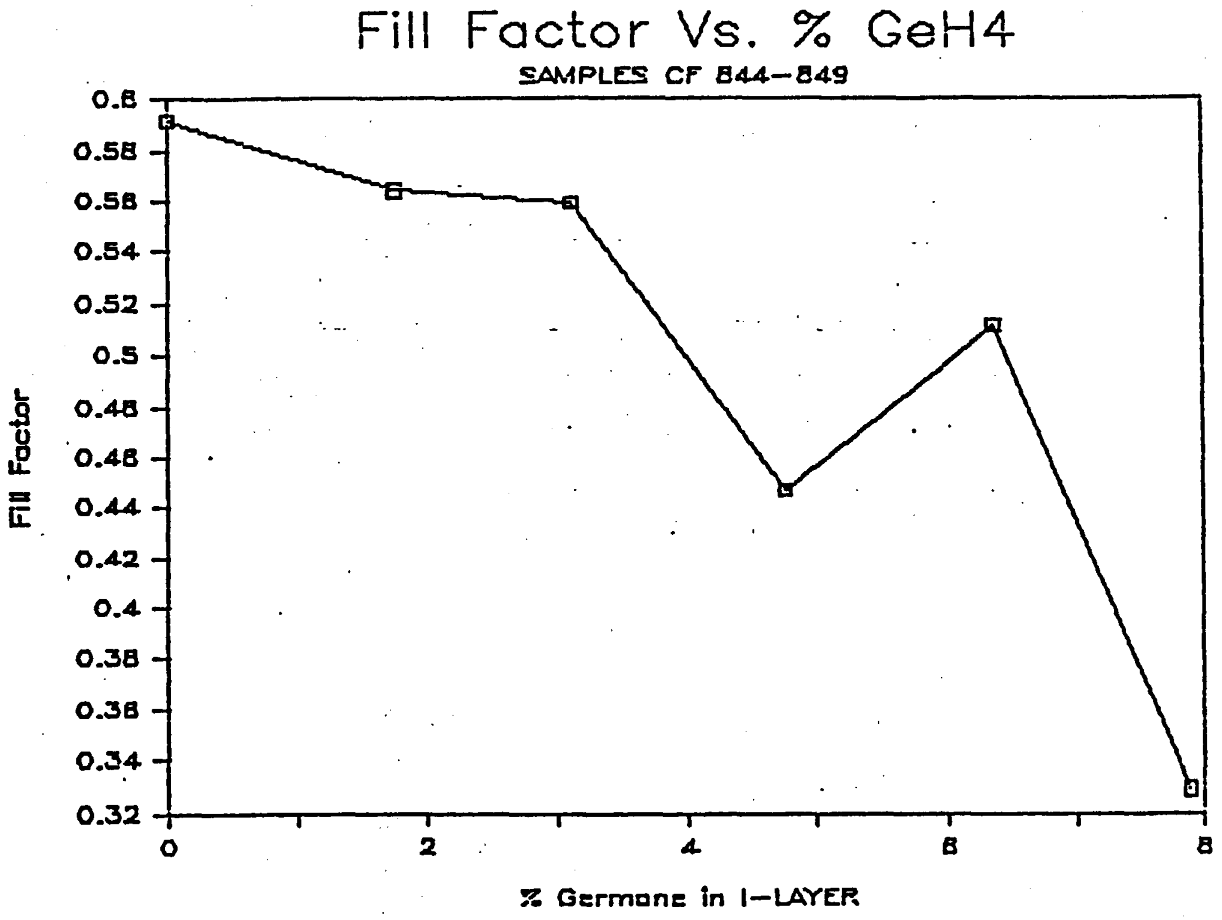

FIGURE 2-67. FILL FACTOR AS A FUNCTION OF $GeH_4/GeH_4 + SiH_4$ USED TO PREPARE THE i-LAYERS.

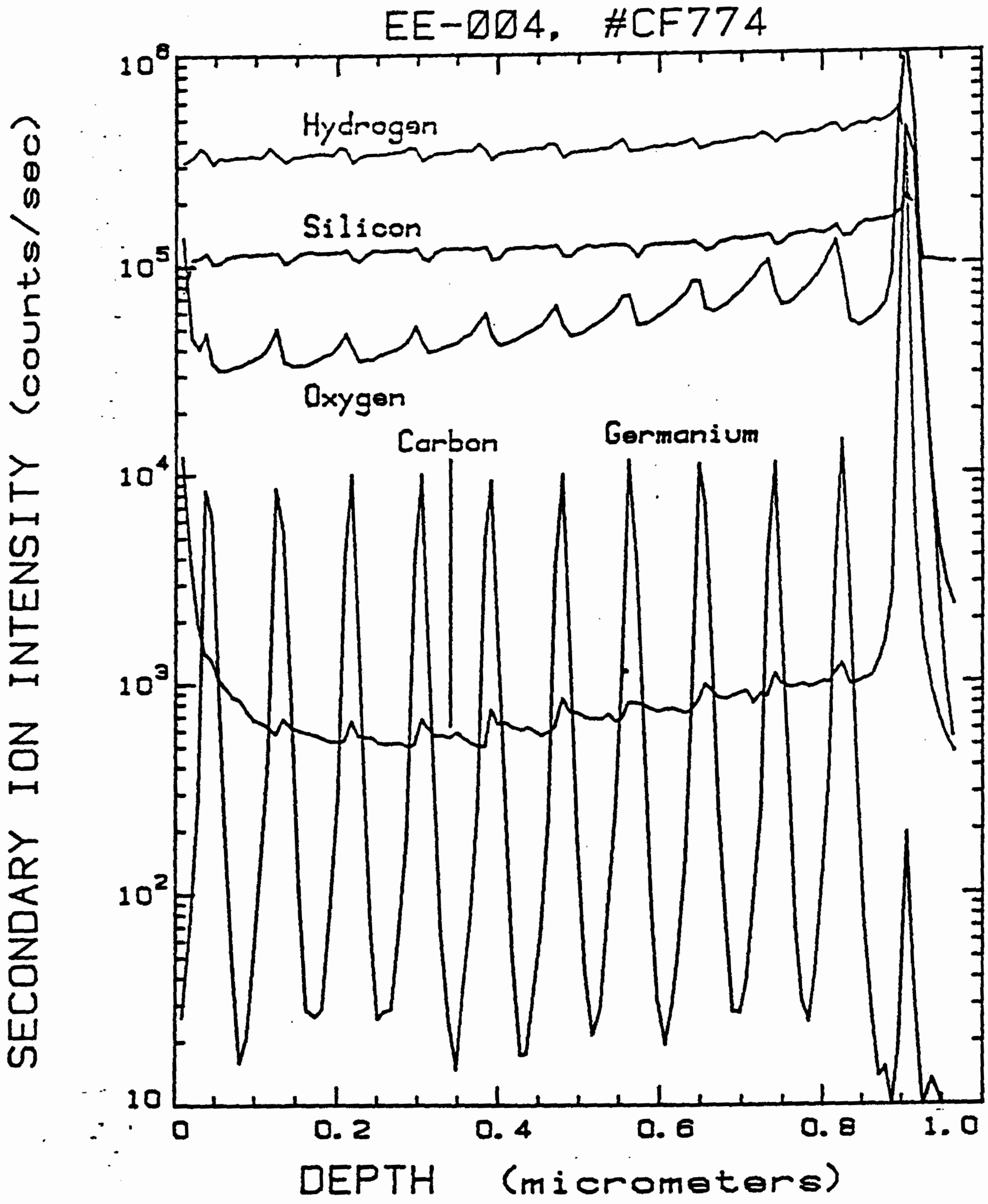

FIGURE 2-68. SIMS PROFILE OF a-Si:H/a-Ge:H MULTI-LAYER DEPOSITED ONTO A SINGLE CRYSTAL SILICON SUBSTRATE.

TABLE 2-15

COMPARISON OF a-Si:H, a-SiGe:H, and a-Si:H/a-Ge:H CELL DATA

Property	Std. Cell	a-SiGe:H	a-Si:H/a-Ge:H
Cell #		781	776
V_{oc}	0.83	0.758	0.793
FF	0.62	0.49	0.355
J_{sc}	16.0	17.4	15.9
SWQE ratio	0.93	0.87	0.92
LWQE (0/-3V) (AM1 bias illumination)	0.92	0.76	0.80

multi-layer i-layer is an effective recombination center (or trap). Details of this work have been accepted for presentation at the spring MRS conference [10]. We are presently conducting a Raman study of a-Si_xGe_{1-x}:H as a function of germanium content (x) to gain more direct evidence of Ge clustering.

2.7.3 Silicon-Carbon Alloy Buffer Layers

Silicon-carbon alloys are of interest as they can be used as either i-layers (for a high voltage top cell in stacked-cell applications) or as buffer layers for V_{oc} enhancement in single-junction or second (and third) cells in stacked cell configurations. The silicon-carbon alloys are not easily examined by the SWQE method described above due to the difficulty in preparing thick cells with sufficiently good performance. Our current approach to the study of these materials is to develop an analysis of the silicon-carbon alloy as a buffer layer. Here the transport of holes across the buffer layer is studied through examination of the long wavelength quantum efficiency as a function of applied blue bias illumination. In this way the photoconductive properties of a-SiC:H can be revealed. It should be noted, that unless special precautions are taken (for example, p-i-p, test configurations) a standard photoconductivity measurement does not address hole transport due to the small hole mobility relative to that of the electron.

In this study we used slowly deposited a-SiC:H buffer layers (∿300Å thick) of various carbon contents (from 0 to 20% C). The cells studied included those with a-Si:H and a-SiGe:H i-layers. Figure 2-69 shows the degradation of cell parameters as a function of $CH_4/(CH_4 + SiH_4)$ used in the buffer layer of cells with a-Si:H i-layers (5,500Å thick). In general the stability decreases with increasing C content. Figure 2-70 shows the decrease in cell performance as a function of $GeH_4/(SiH_4 + GeH_4)$ used for the i-layer preparation when the buffer layers were prepared with $CH_4/(CH_4 + SiH_4) = 6\%$.

The ratio of long wavelength response without blue light bias to that with blue light bias is an indication of the photoconductivity of the buffer layer (holes are the majority carrier in the buffer layer). Figure 2-71 shows the quantum

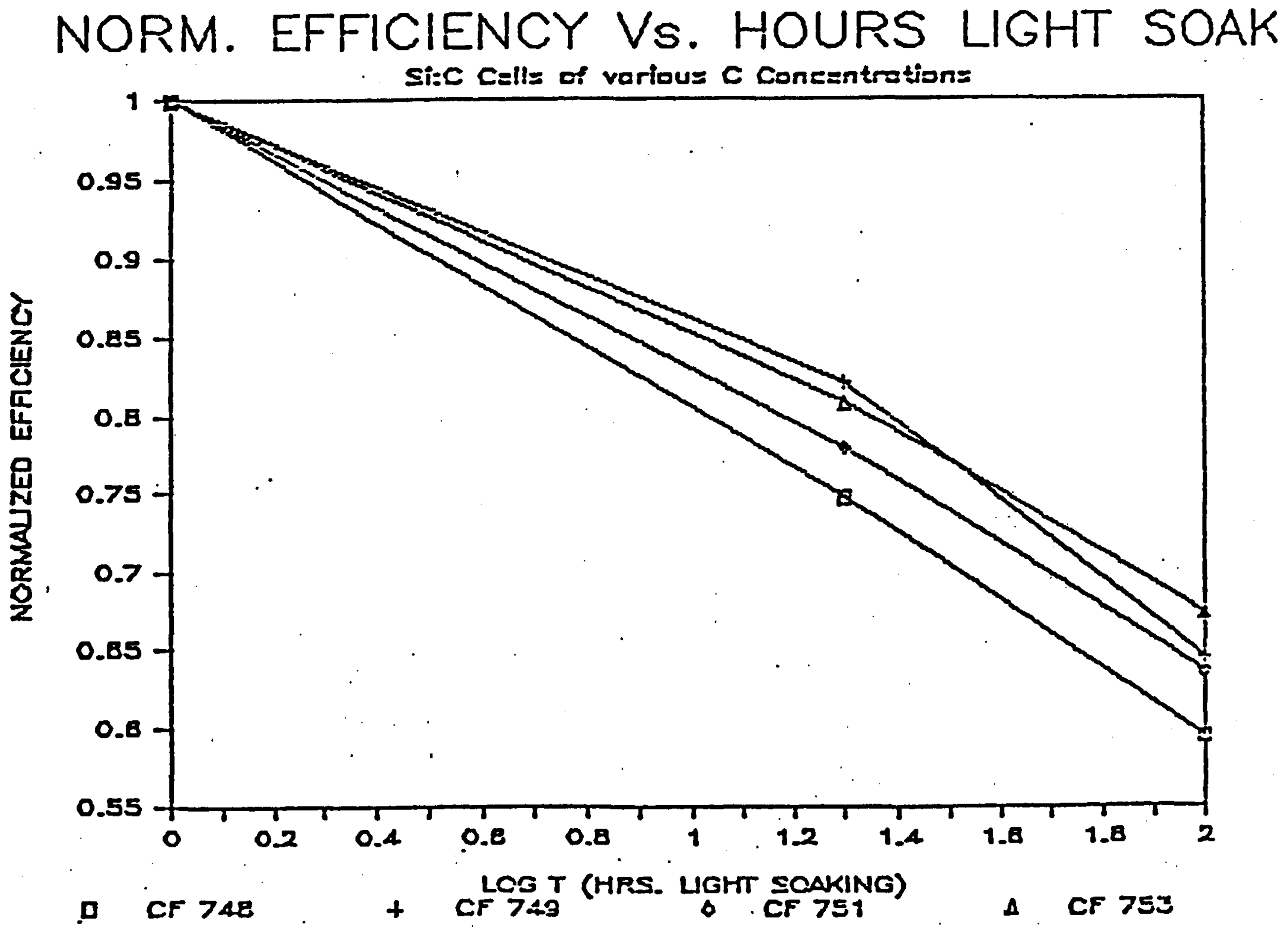

FIGURE 2-69. NORMALIZED EFFICIENCY AS A FUNCTION OF LIGHT SOAKING TIME AND CH_4 RATIO USED FOR THE BUFFER LAYER DEPOSITION. THE CH_4 RATIOS ARE 50% FOR CELL 748, 42% FOR CELL 749, 30% FOR CELL 751 AND 18% FOR CELL 753.

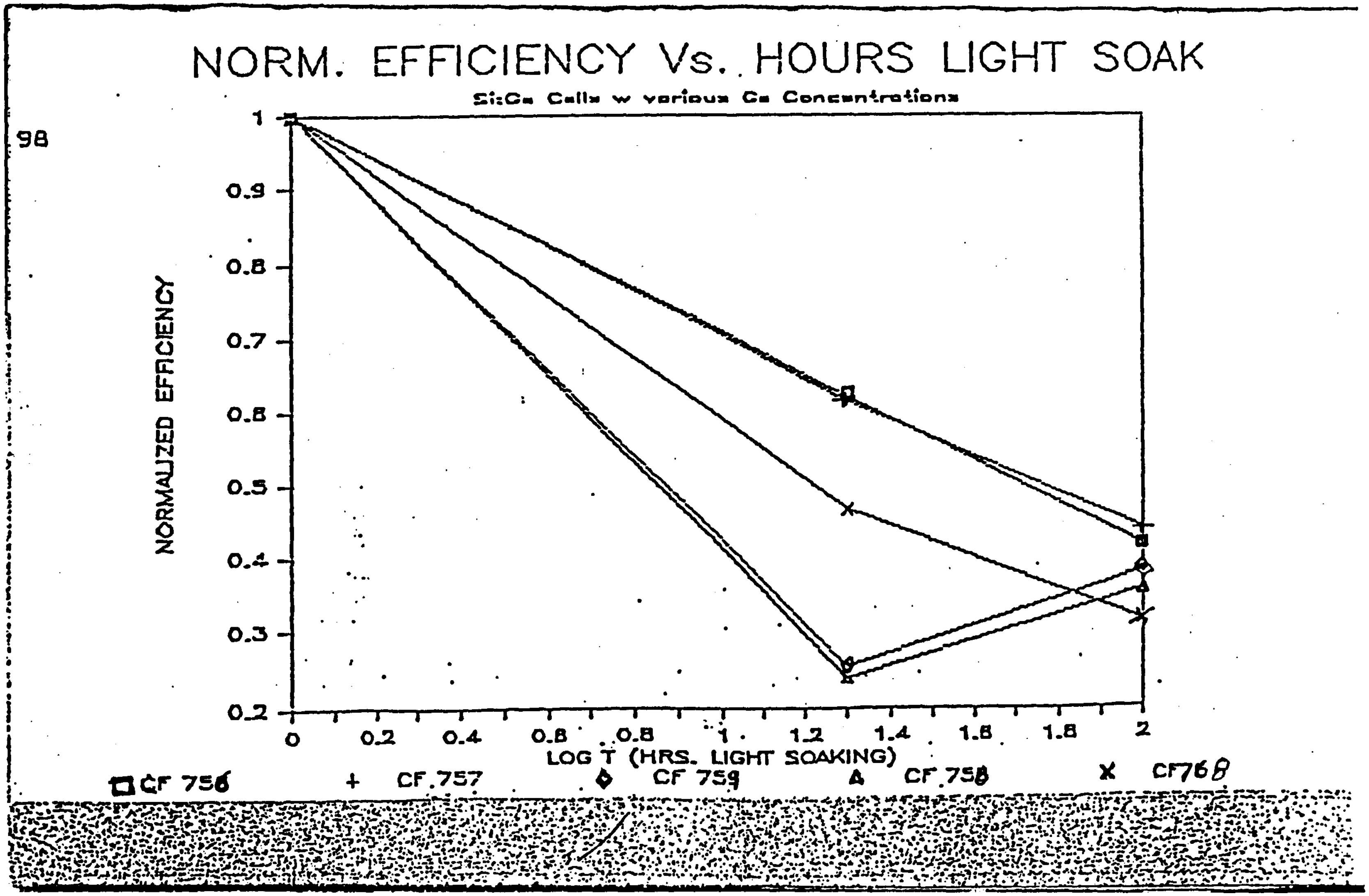

FIGURE 2-70. THE NORMALIZED EFFICIENCY AS A FUNCTION OF GeH_4 RATIO USED IN THE i-LAYER DEPOSITION (BUFFER LAYERS USED A 6% CH_4 RATIO). THE GeH_4 RATIOS WERE 2.4% FOR CELL 756, 3.1% FOR CELL 757, 3.8% FOR CELL 758 AND CELL 759, AND 4.4% FOR CELL 768.

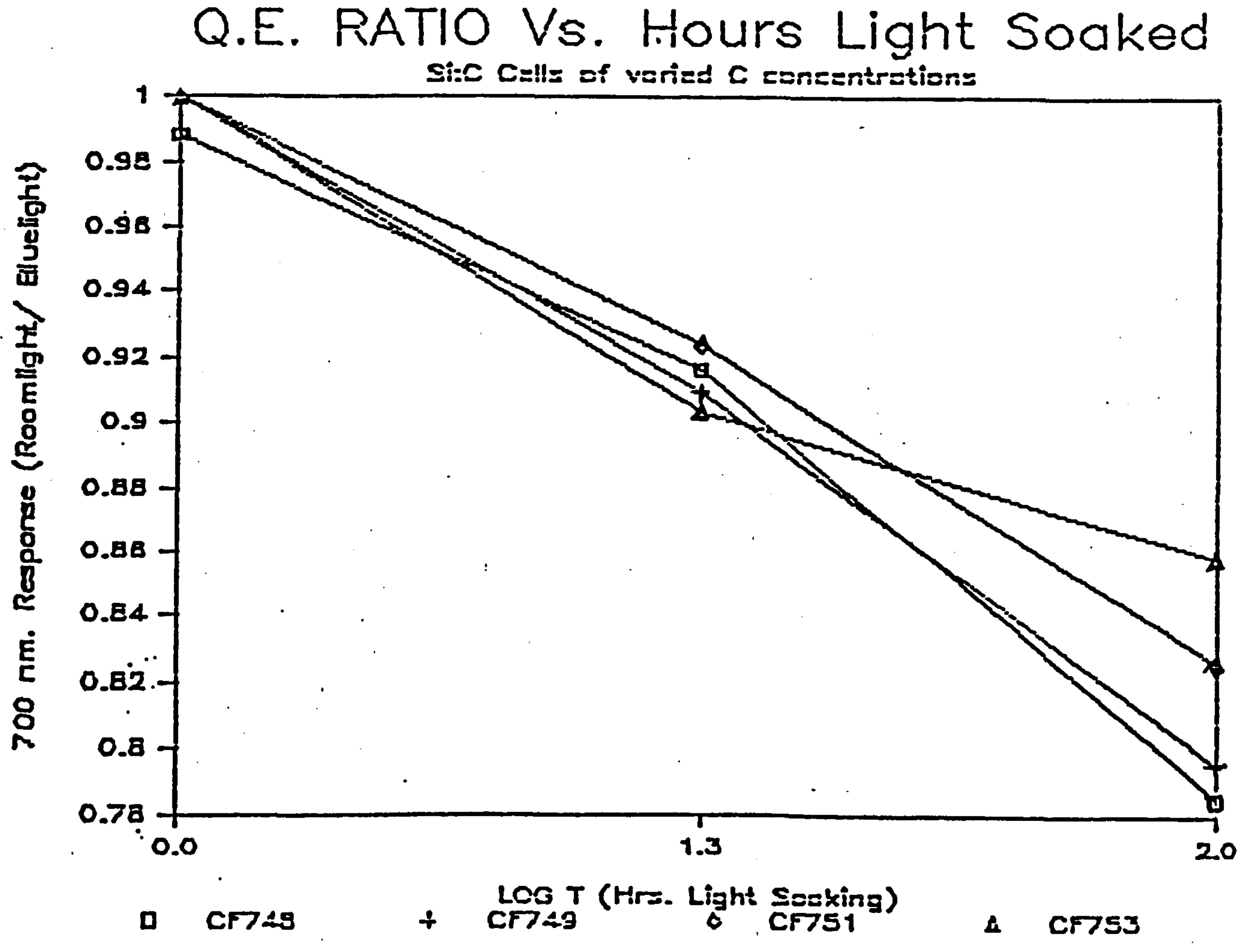

FIGURE 2-71. THE QE AT 700NM RATIO (NO BIAS/BLUE BIAS ILLUMINATION) AS A FUNCTION OF LIGHT SOAKING TIME AND CH_4 FRACTION USED FOR THE BUFFER DEPOSITION. THE CH_4 RATIOS ARE 50% FOR CELL 748, 42% FOR CELL 749, 30% FOR CELL 751 AND 18% FOR CELL 753.

efficiency ratio (dark bias to blue light bias) at 700nm as a function of CH_4 content in the cells with standard a-Si:H i-layers.

The results of this investigation are consistent with an increasing light-induced degradtion with increasing C content in the buffer layer. The reduced stability observed could either be due to a poor mobility in C buffer layers that is made worse by light soaking, or the initial poor mobility of these layers causes the hole concentration in the bulk of the i-layer to increase when cell is under illumination, and the hole lifetime reduction that occurs in the bulk due to light soaking extracts a larger current loss due to the larger hole concentrations. These considerations are currently under review.

2.7.4 a-SiGe:H Solar Cells

A series of p-i-n (p-a-SiC:H/i-a-SiGe:H/n-a-SiGe:H/n-a-Si:H) solar cells were prepared with i-layers ranging from 2,500 to 7,000Å thick (the same cells used in the characterization of light-induced defects in a-SiGe:H in Section 2.7.2.1). The deposition temperature of these cells was ∿330°C compared to a standard growth temperature of ∿275°C. Higher growth temperatures were chosen for two reasons: first, higher temperatures can lead to a smaller bandgap due to less hydrogen for a given amount of germanium content (the Ge content is suspected of being correlated to the defect in annealed a-SiGe:H as described in Section 2.7.2.2); and second, increasing growth temperatures are found to reduce the poly-hydride content in the amorphous materials (poly-hydrides are thought to be related to the light-induced defects). The stability (efficiency measurement) of these solar cells was similar to standard a-Si:H cells of similar thickness.

The best long wavelength performance we found for a-SiGe:H during the last half of 1987 was a cell grown at these higher temperatures. Cell #813 had a quantum efficiency of ∿32% at 800nm which increased to ∿42% at -3V bias (see Figure 2-72). Other cell parameters include a V_{oc} of 0.60V, J_{sc} of 18.4mA/cm^2 and fill

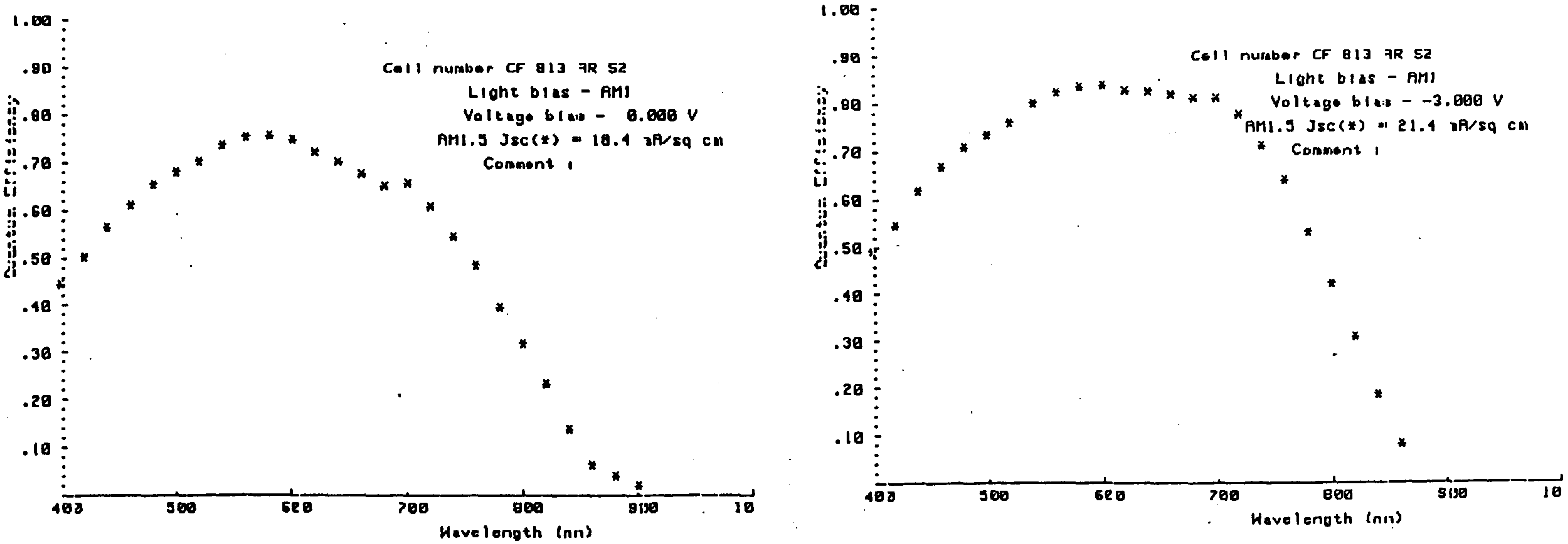

FIGURE 2-72. THE QUANTUM EFFICIENCY OF CELL #813 GROWN AT 330°C AT 0V BIAS (LEFT) AND -3V BIAS (RIGHT).

factor of 0.493. Further material investigations of materials grown at higher temperatures is planned for early 1988.

2.7.5 The Charge Dependency of the Staebler-Wronski Effect

2.7.5.1 Investigation

The possibility that the root of the Staebler-Wronski effect is an equilibrium between charged carriers, or charged centers, and metastable sites was investigated. This hypothesis was tested through a detailed examination of the reverse bias heat treatment (RBHT) often given to cells to improve their performance. Here the voltage and i-layer thickness dependency were studied (shown in Figure 2-73), establishing that the effect is related to i-layer quality. The temperature and the current density dependence of forward bias current injection degradation was also examined. The study of forward bias revealed a degree of saturated degradation that is not strongly temperature dependent (Figure 2-74). Saturation occurs at temperatures greater than 150°C where it occurs within one hour. The PDS absorption of i-layers light soaked at temperatures ranging from 150 to 250°C also showed an absorption increase that was also not temperature dependent (although the PDS technique is not very reliable for measurements not done in situ). The degree of degradation is however forward current density dependent (Figure 2-75). Recently we employed the SWQE technique on cells degraded at high temperature as a function of forward bias current to gain greater insight into the quantitative relationship between charge density and defect density (see Figure 2-76 and Table 2-16).

These experiments can be used to provide some insight into the proposed equilibrium:1) the equilibrium constant must be approximately unity (with the energy difference between the initial and final states being less than 0.1eV); 2) the equilibrium is proportional to recombination currents in forward bias; 3) the saturation (temp. $\sim$ 150°C) happens at a lower degree of degradation than that found in room temperature light soaking studies. The last consideration may indicate that the room temperature effects involve departures from equilibrium due to a large activation barrier between the initial and final

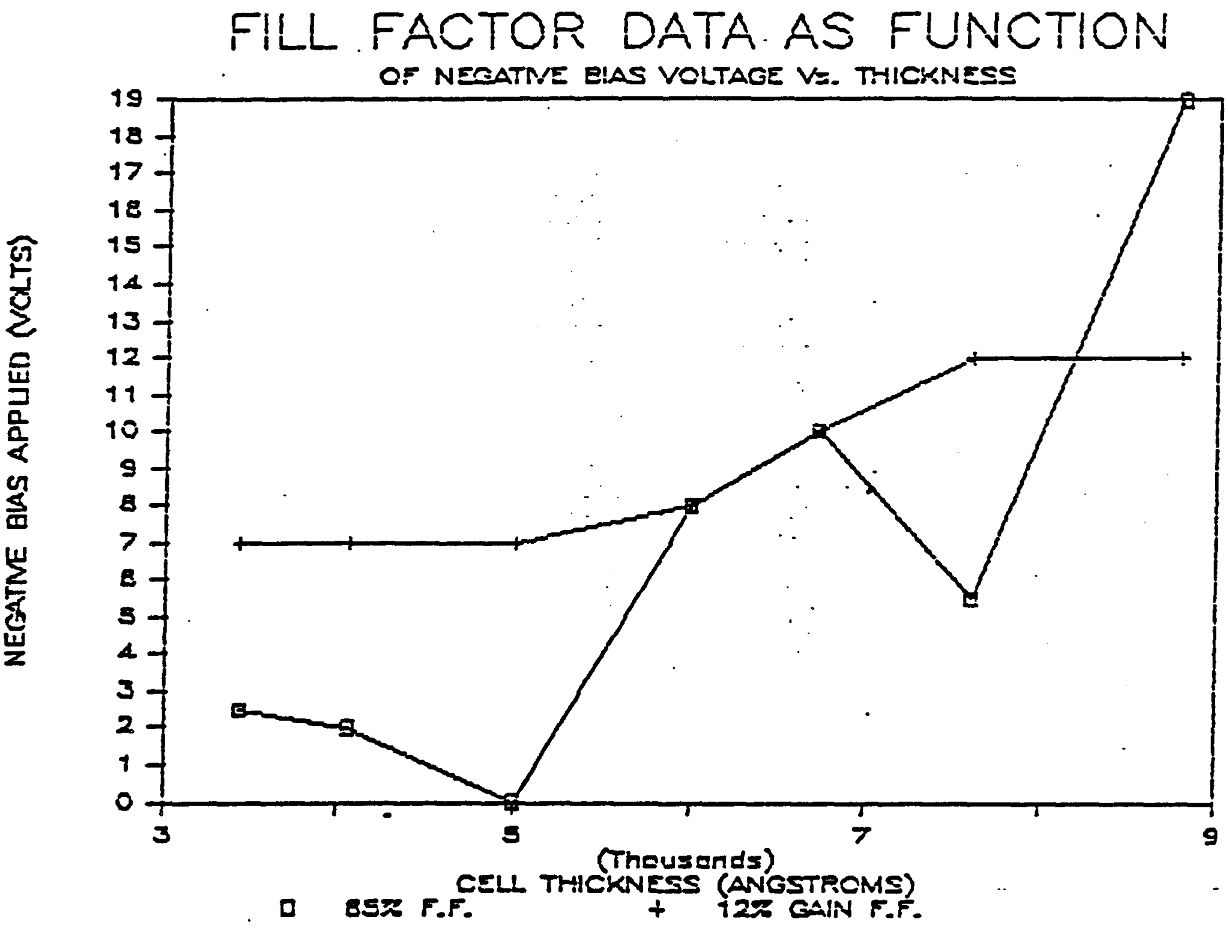

FIGURE 2-73. REVERSE BIAS TREATMENT VOLTAGES REQUIRED FOR A 12% FILL FACTOR GAIN AND A 65% FILL FACTOR AS A FUNCTION OF i-LAYER THICKNESS.

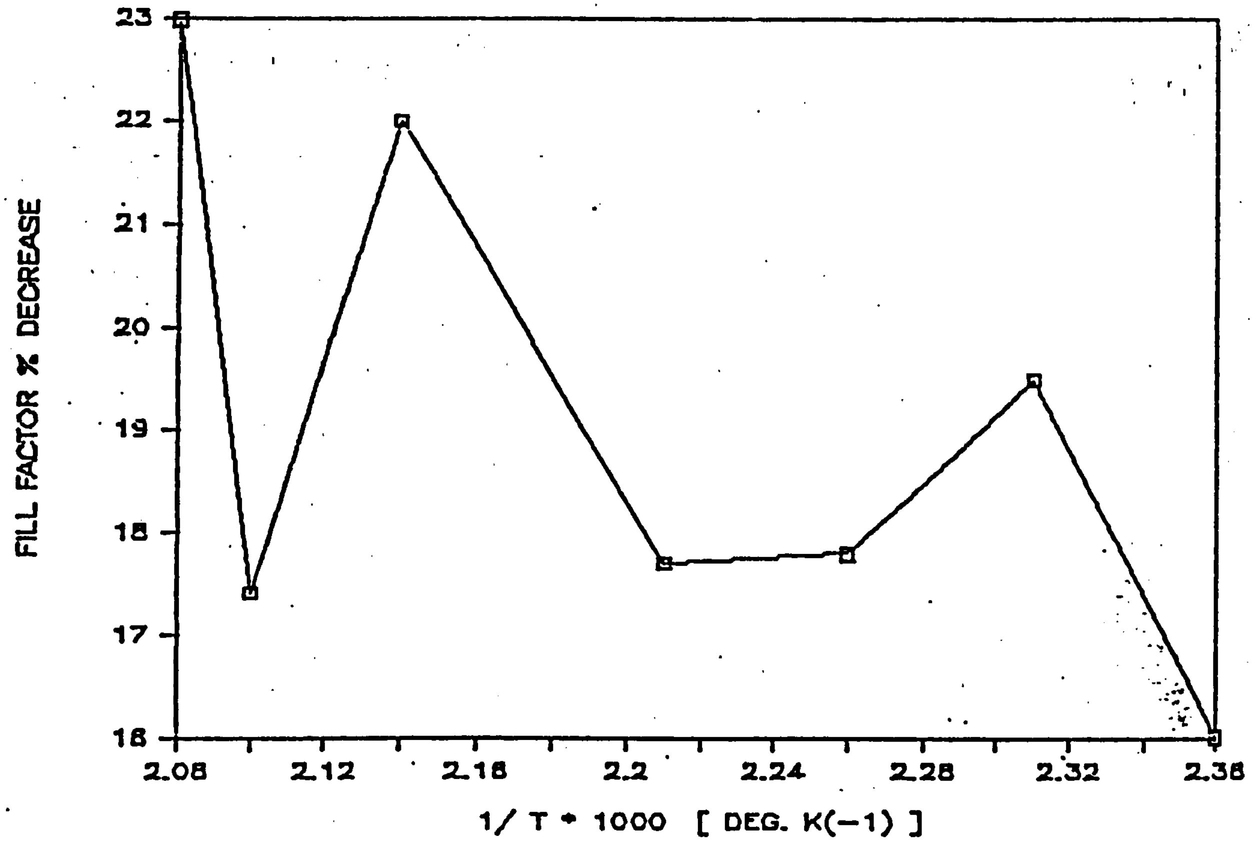

FIGURE 2-74. THE FILL FACTOR LOSS DUE TO FBHT (FORWARD BIAS HEAT TREATMENT) AT ∼150mA/cm^2 AS A FUNCTION OF TEMPERATURE.

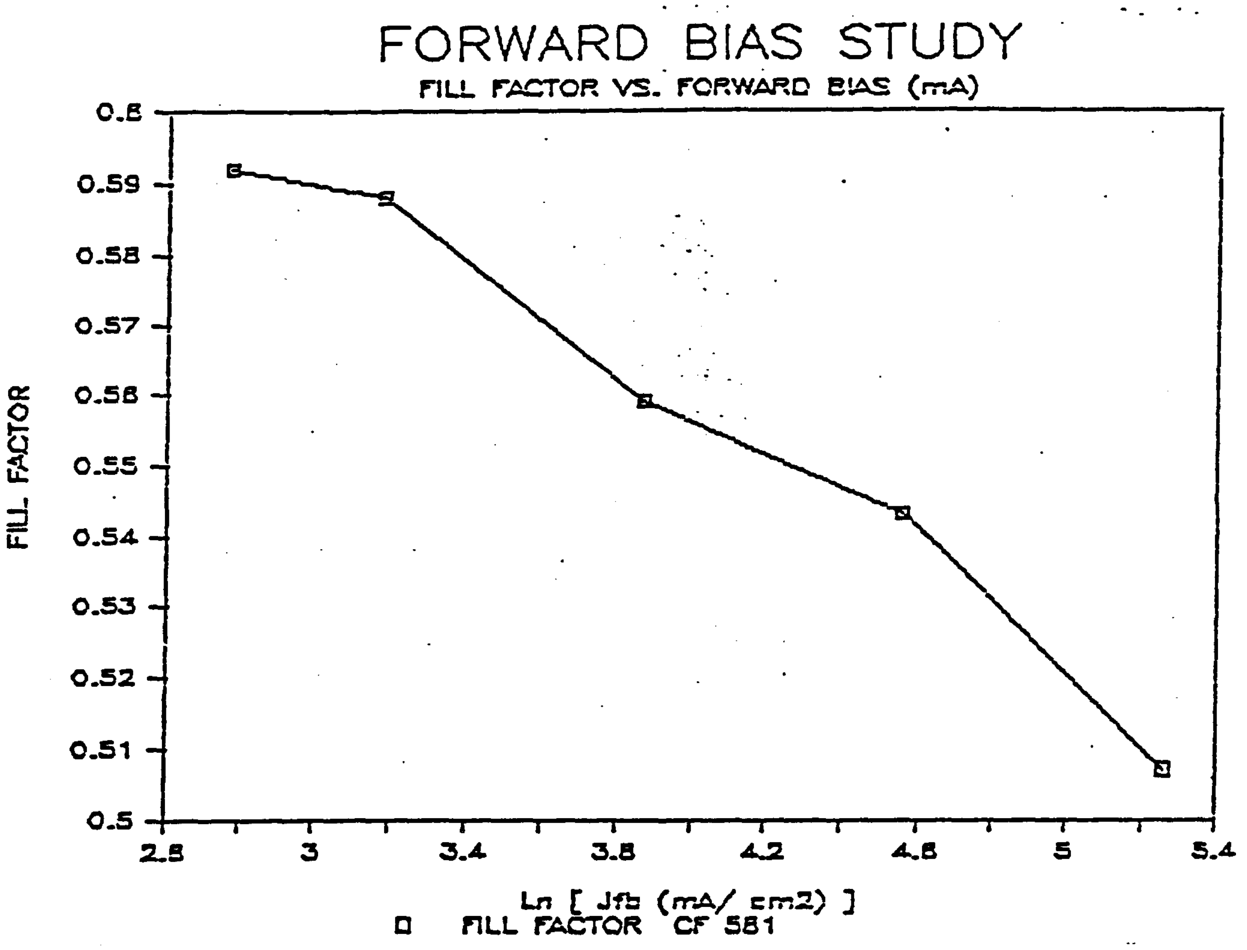

FIGURE 2-75. FILL FACTOR AND EFFICIENCY LOST DUE TO FBHT AS A FUNCTION OF FORWARD BIAS CURRENT DENSITY AT 175°C.

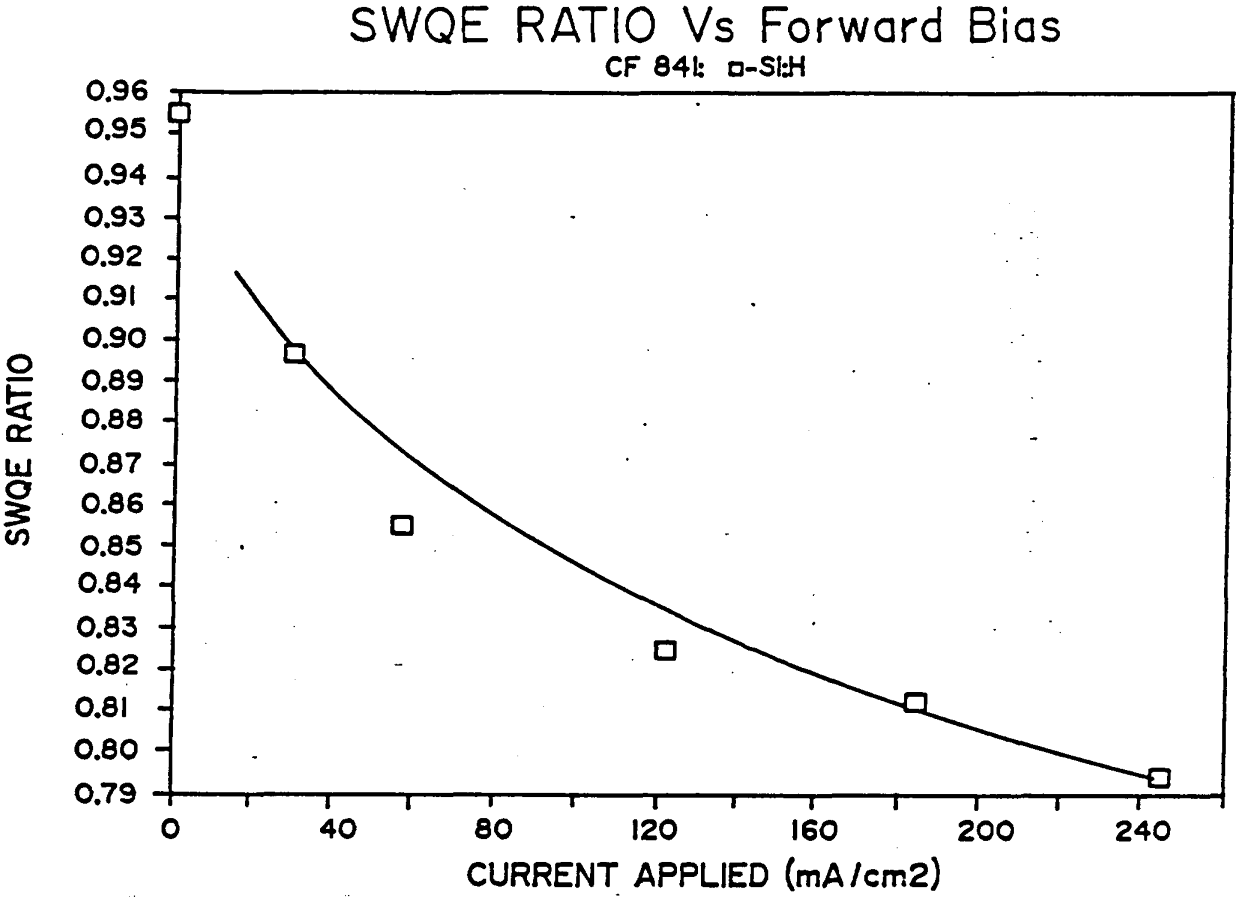

FIGURE 2-76. THE SWQE AS A FUNCTION OF FORWARD BIAS CURRENT (USED FOR DEGRADATION) AT 175°C (INDICATED BY □). ALSO SHOWN ARE MODELED DEGRADATIONS USING THE ANALYSIS OF SECTION 2.7.1 AND EQUATION (2-11).

TABLE 2-16

THE SWQE AS A FUNCTION OF FORWARD CURRENT AT T = 175°C

J_{app}	SWQE Ratio	Eq. 9	Eq. 11
0	0.955	need to know n_o and p_o at T	
31	0.897	0.897	0.897
58	0.855	0.846	0.875
123	0.824	0.725	0.839
185	0.812	0.609	0.813
246	0.794	0.495	0.791

states. Experiments to determine if room temperature saturation can take place are currently being carried out. It is probable that all studies of degradation at temperatures less than ∿150°C are in fact characterizations of the activation barrier between initial and degraded states. From this point onward we will limit our attention to the higher temperature effects where equilibrium descriptions apply. The first two considerations can be used to develop an equilibrium description of the SWE. Some possible reactions are shown below:

$$n + p + N_s = 2N_m \quad E < .1eV \tag{2-8}$$

$$N_m^2/[N_s * p * n] = K \sim 1 \tag{2-9}$$

$$N_s^- + p \text{ (or n)} = 2N_m \quad E < 0.1eV \tag{2-10}$$

$$N_m^2/[n * N_s] = K \sim 1 \tag{2-11}$$

Where n is the electron concentration, p is that of holes, N_s is the density of lattice sites that are susceptible to transition to the metastable center (concentrations of at least $10^{16} cm^{-3}$ are required), K is the equilibrium constant (∿1), N_m is the density of metastable centers (∿$10^{16} cm^{-3}$ after 20 hours of light soaking). Equations (2-8) and (2-9) are the chemical equilibrium expressions that correspond to recombination equilibrium degradation considerations (it requires both a hole and an electron). In the cases illustrated here the metastable sites are produced two at a time as would be the case if this defect was a dangling bond. Substitution of these values into Equation (2-9) yields ridiculously small hole and electron concentrations. The problem with densities can be circumvented through the use of a single charge carrier being involved with the equilibrium (for an example a trapped hole on a weak bond). Charge conservation requires that either the weak bond site is initially charged (opposite to the carrier charge) or that one of the danging bonds is charged (the same as the initiating carrier). Illustrative reactions with charged precursors are given by Equations (2-10) and (2-11). These equations do not have trouble with unphysical densities, but they do not define the charge of the initiating charge carrier. The experiments performed here suggest that light-induced degradation, forward-bias degradation and RBHT are in fact different facets of the same process - e.g., an equilibrium between charged centers, charged carriers, and metastable centers (perhaps these are dangling bonds). Under conditions where saturation occurs (RBHT and higher temp. FBHT) the processes are best described by ordinary equilibrium thermodynamics. Equilibrium is also consistent with balanced transition rates between metastable sites susceptible to transition to the metastable center. While it remains valid that the transition rates are balanced, the activation barrier no longer controls the rate or extent of degradation. Details of the above considerations have been accepted for presentation at the spring MRS meeting [11].

2.7.5.2 Applications to Device Design and Measurements

The identification of an expression that describes the equilibrium of the SWE carries with it a thermodynamic context (the phase rule) for measurements and device design considerations. Deviations from equilibrium (for example room temperature degradations) require the specification of even more variables for complete definition. An experiment that reports the increase in dangling bond densities as function of light-soaking time but does not specify the charge density or some measure of weak bond density is an undefined experiment in the context described in Section 2.7.5.1. Again, measurements require a detailed analysis to elucidate a dangling bond density. It is our belief that the polymeric $(SiH_2)_n$ absorption modes seen in the IR absorption [12,13] are related to the weak bond densities. During the first quarter of 1988 we plan a detailed analysis of the relation between poly-hydride content and stability using the measurement techniques described in Section 2.7.1 as well as an investigation of room temperature saturation effects in p-i-n solar cells (it is possible to design a solar cell to have a charge density similar to that required to cause saturation in the high temperature forward bias experiments).

SECTION 3.0

SUBTASK B2: NON-SEMICONDUCTOR MATERIALS RESEARCH

3.1 REFLECTING REAR CONTACTS FOR a-Si SOLAR CELLS

In a previous report [1] we demonstrated that superior long wavelength spectral response is obtained when an indium-tin-oxide (ITO) layer is inserted between the a-Si:H n-layer and the metal reflector. The effect of the ITO layer is to increase the metal reflectivity by changing the optical media in which the metal is immersed.

In Figure 3-1, we present representative quantum efficiency measurements for devices formed on the same tin-oxide/a-Si:H substrate using four rear contacts. The quantum efficiencies vs. wavelength shown were measured under AM1 illumination and at a -3 volt bias to ensure that all carriers generated are collected. These devices were grown on moderately textured tin oxide using a standard p-i-n cell incorporating a 5000Å thick i-layer.

The quantum efficiency of a device at long wavelengths (>600nm) is the result of multiple passes through the i-layer of the weakly absorbed radiation. The measured total photogenerated current consists of two contributions: the current generated upon absorption on the first pass, i.e., prior to reflection off the rear reflector, and the current generated upon absorption of all subsequent passes, i.e., after at least one reflection off the rear contact. That is:

$$QE(\lambda_o) = QE(\lambda_o)_{\text{first pass}} + QE(\lambda_o)_{\text{subsequent passes}} \tag{3-1}$$

The contribution to the total photogenerated current due to the first pass is determined by the amount of light entering the i-layer and the absorption coefficient of the layer. For a given amount of light entering the i-layer:

$$QE(\lambda_o)_{\text{first pass}} = 1-e^{-\alpha(\lambda_o)d} \tag{3-2}$$

FIGURE 3-1. SPECTRAL RESPONSE CURVES FOR a-Si p-i-n CELLS WITH VARIOUS REAR CONTACTS.

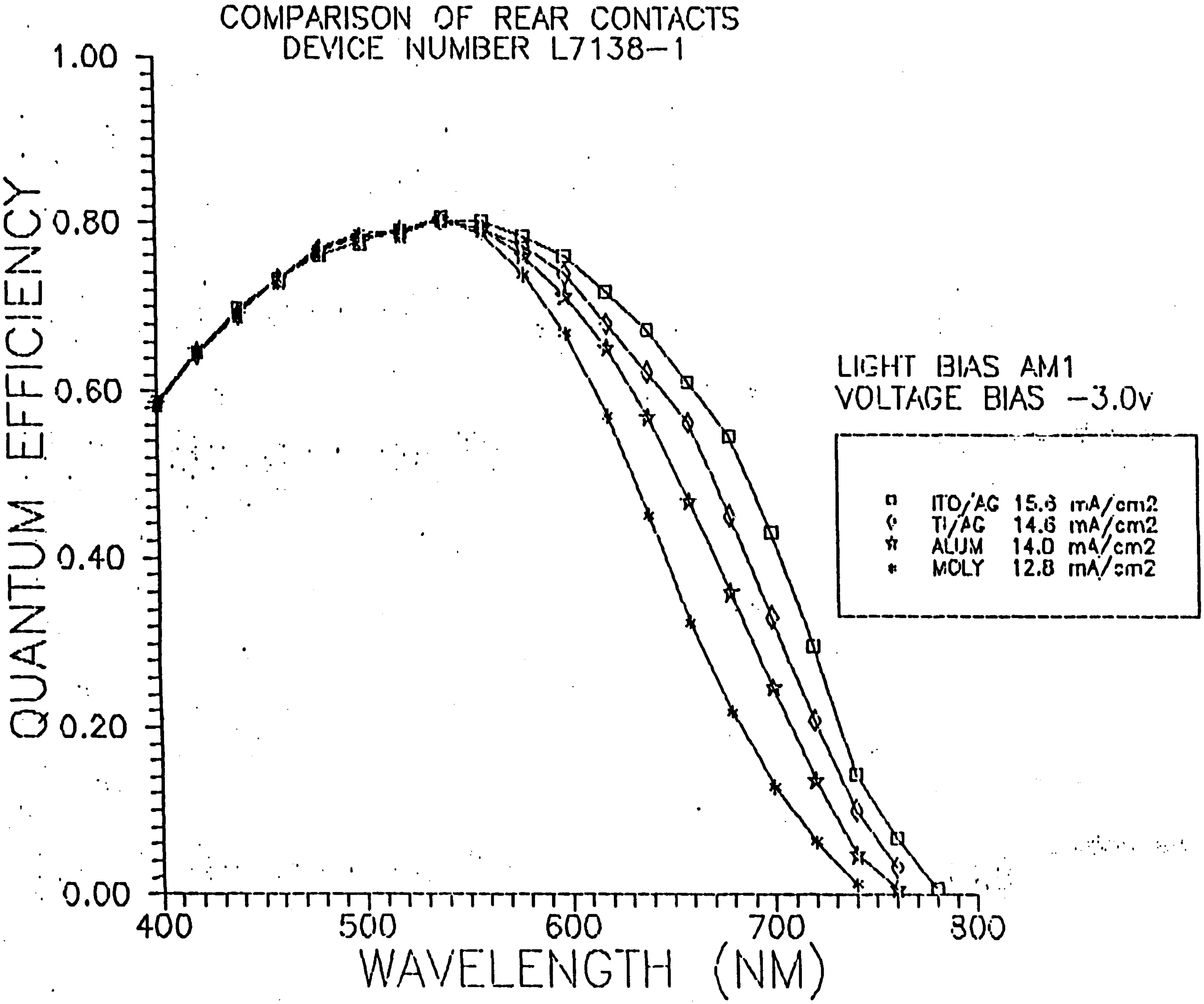

where $\alpha(\lambda_o)$ is the absorption coefficient of the i-layer at wavelength λ_o and d is the thickness of the layer.

The contribution to the photogenerated current due to all subsequent passes is modified by the reflectivity of the rear contact. We assume:

$$QE(\lambda_o)_a \quad \alpha R(\lambda_o)_a \qquad (3\text{-}3)$$

where $R(\lambda_o)_a$ is the reflectivity of the rear contact at wavelength λ_o, and the subscript a denotes contact metal a.

Combining expressions (3-1), (3-2), and (3-3) we obtain a relation between the ratio of the rear contact reflectivities, $(R(\lambda_o)_a/R(\lambda_o)_b)$, to the total photogenerated current obtained from rear contact metal a, $QE(\lambda_o)_a$ and b, $QE(\lambda_o)_b$.

$$QE\ (\lambda_o)_a = \frac{R(\lambda_o)_a}{R(\lambda_o)_b} QE(\lambda_o)_b + 1 - \frac{R(\lambda_o)_a}{R(\lambda_o)_b} \quad 1 - e^{-\alpha(\lambda_o)d} \qquad (3\text{-}4)$$

To obtain an estimate of the ratio $R(\lambda_o)_a/R(\lambda_o)_b$ the structure glass/tin oxide/500Å a-Si:H was formed on three substrates. These substrates were then over coated with one of the contact systems: aluminum; titanium-silver, and ITO-silver. The total reflection as a function of wavelength was measured with the light incident upon the glass for each of the contact systems. The results are shown in Figure 3-2.

The interference extrema were "averaged" from 600nm to 800nm by drawing the lines shown in Figure 3-2. The contributions to the measured total reflectance due to all interfaces other than the a-Si:H/reflector interface are ignored.

Values for the ratio $R(\lambda_o)_a/R(\lambda_o)_b$ were obtained from Figure 3-2. Values for the absorption coefficient $\alpha(\lambda_o)$ were obtained from photothermal deflection spectroscopy (PDS) done on i-layer material.

FIGURE 3-2. TOTAL REFLECTION FROM GLASS/TIN OXIDE/a-Si/REAR CONTACT STRUCTURES WITH VARIOUS REAR CONTACTS.

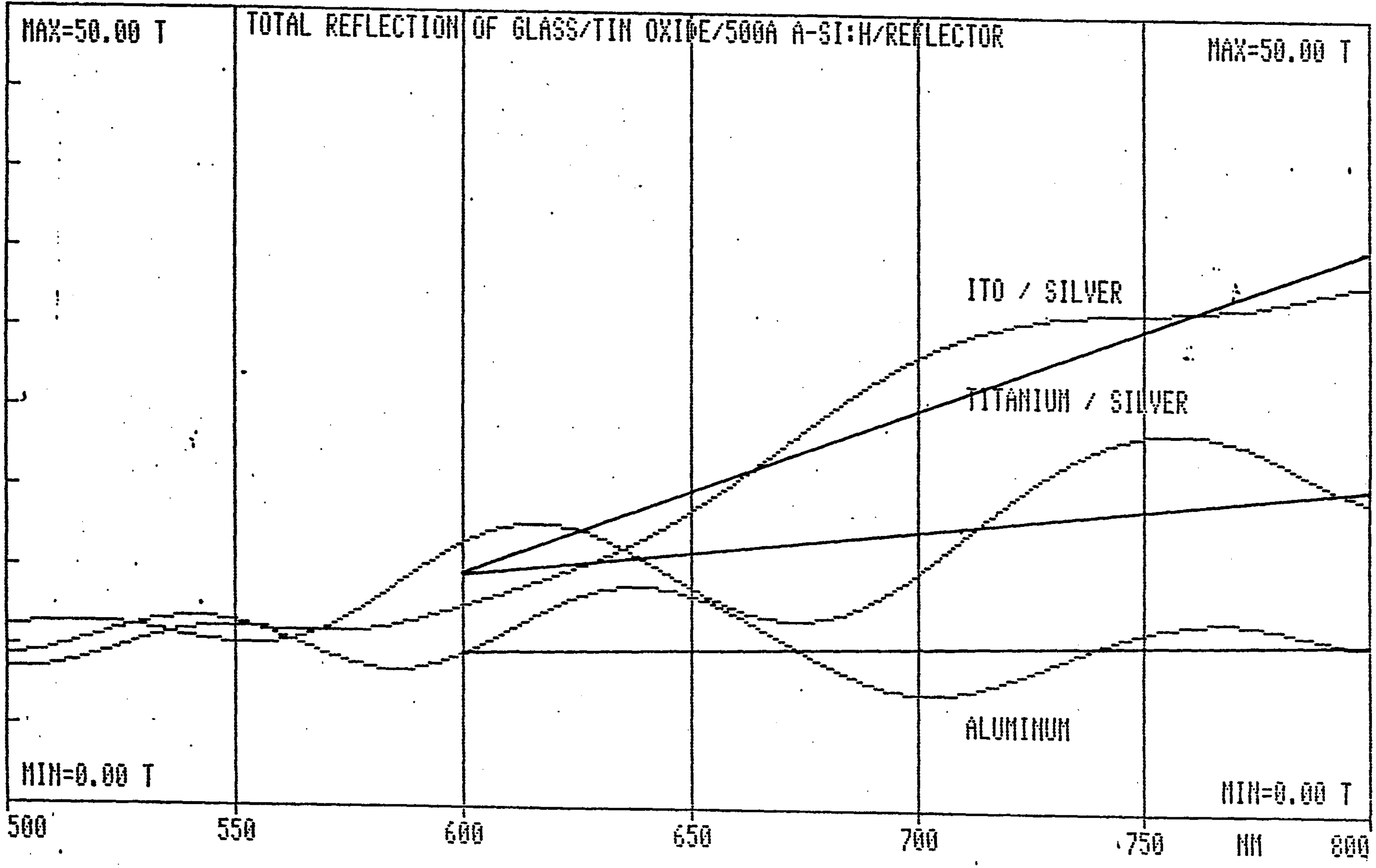

Application of Equation (3-4) to the measured photogenerated current of the device with ITO-silver rear contact shown in Figure 3-1 allows one to predict the corresponding photogenerated currents for this same device with different rear contacts. The the results for the titanium-silver and aluminum contacts at four wavelengths is given in Table 3-1. Table 3-1 also contains the actual values measured and the % discrepancies. This analysis has been applied to a number of substrates with similar results. Work toward a comprehensive optical analysis of the a-Si:H p-i-n solar cell device is ongoing.

3.2 SPRAY APPLIED COATING ENCAPSULANTS

There are 2 methods currently in use at the Solarex Thin Film Division to encapsulate a-Si submodules for outdoor environmental protection. Large submodules ($20W_p$) are encapsulated with Tedlar and EVA material in a lamination process. All other submodules for outdoor use are encapsulated with an acrylic film in a roll-on process. The film process was chosen over lamination on smaller submodules because of lower cost while maintaining and improving the environmental protection of the submodule.

We recently began the evaluation of encapsulant coatings which can be sprayed on the submodule. The process would be less costly than either the lamination or film process, and the coating should maintain or improve environmental protection.

Over 30 coatings were procured for evaluation. The coatings were polyurethanes, epoxies, silicons, powder coatings, etc. The coatings were applied to 12"x13" submodules. The submodules were immersed in water as a preliminary accelerated environmental test. Survival of the submodule for 10 or more days in the bath with little or no corrosion effects would mean the coating passed this particular test. Of the 30 coatings evaluated, 5 passed the test. These coatings will be evaluated further in temperature-humidity cycling and outdoor exposure tests.

TABLE 3-1

CALCULATED QUANTUM EFFICIENCIES

Sample Number L7138-1

Titanium Silver

Wavelength	Predicted QE	Actual QE	% Discrepancy
660 nm	.558	.563	-.9
680	.448	.451	-.7
700	.321	.333	-3.6
720	.210	.211	+.5

Aluminum

Wavelength	Predicted QE	Actual QE	% Discrepancy
660	.498	.470	+6
680	.362	.358	+1
700	.240	.249	-3.6
720	.143	.136	+5.1

In addition to environmental protection, the coatings should also electrically insulate the submodule at high voltages to eliminate leakage currents. UL leakage tests are also being conducted on submodules coated with the 5 coatings which survived immersion.

The chosen candidate will be applied with an automatic spray process.

SECTION 4.0

SUBTASK B3: SUBMODULE RESEARCH

4.1 MULTI-JUNCTION a-Si:H ALLOY BASED SUBMODULE

We have fabricated of multi-junction submodules with the device configuration of a-SiC:H/a-SiGe:H and a-SiC:H/a-Si:H where the bandgap of the silicon-carbon i-layer is about 1.8eV and that of the silicon-germanium i-layer is about 1.55eV. These submodules are deposited on 12"x13" CTO coated substrates and have aluminum rear contacts. The total active area of these submodules is 908cm^2. The submodules consist of 15 series-connected segments where the area of each segment is 60.6cm^2. The best a-SiC:H/a-SiGe:H module fabricated had a conversion efficiency of 7.03% with the following parameters: $V_{oc} = 25.3\text{V}$ (1.686V per segment), $I_{sc} = 0.367\text{A}$ ($J_{sc} = 6.05\text{mA/cm}^2$), and fillfactor = 0.68. Figure 4-1 shows the J-V characteristics of this submodule. Figure 4-2 shows the J-V characteristics of a submodule with the device configuration of a-SiC:H/a-Si:H which had a conversion efficiency of 6.24%.

FIGURE 4-1. CURRENT-VOLTAGE CHARACTERISTICS OF a-SiC/a-SiGe SUBMODULE UNDER AM1.5 ILLUMINATION.

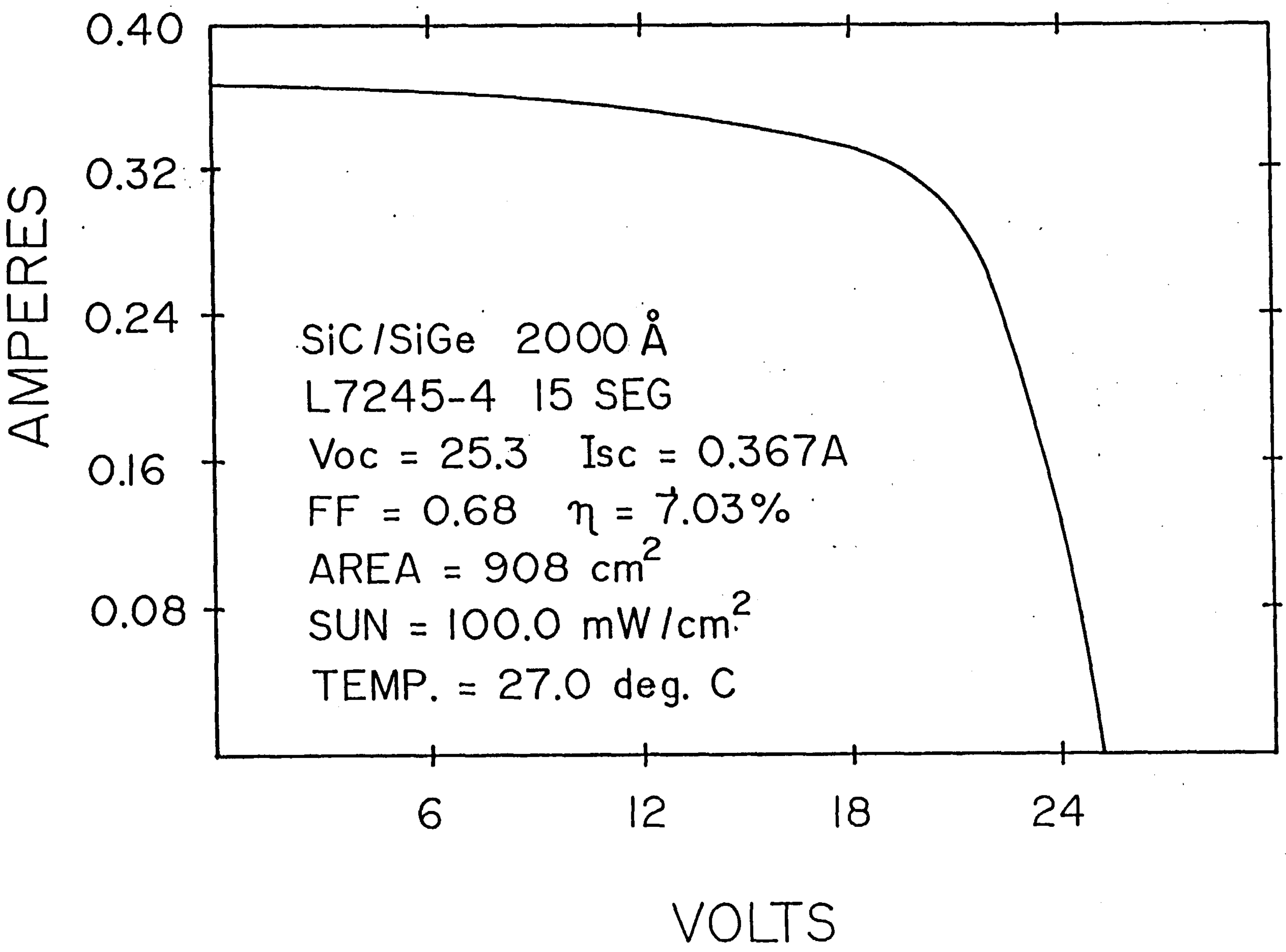

SiC/Si MODULE
Serial # L7210-2
Date 8/7/87
Sun = 100.0 mW/cm
Temp. = 28 deg. C
Voc = 24.943 Volts
Isc = .399 Amps
Vld = 17.5 Volts

Ild = .324 Amps
Plod = 5.663 Watts
Vmp = 17.38 Volts
Imp = .326 Amps
Pm = 5.67 Watts
Eff = 6.24%
F.F. = .57
Rs = 17.95 ohms

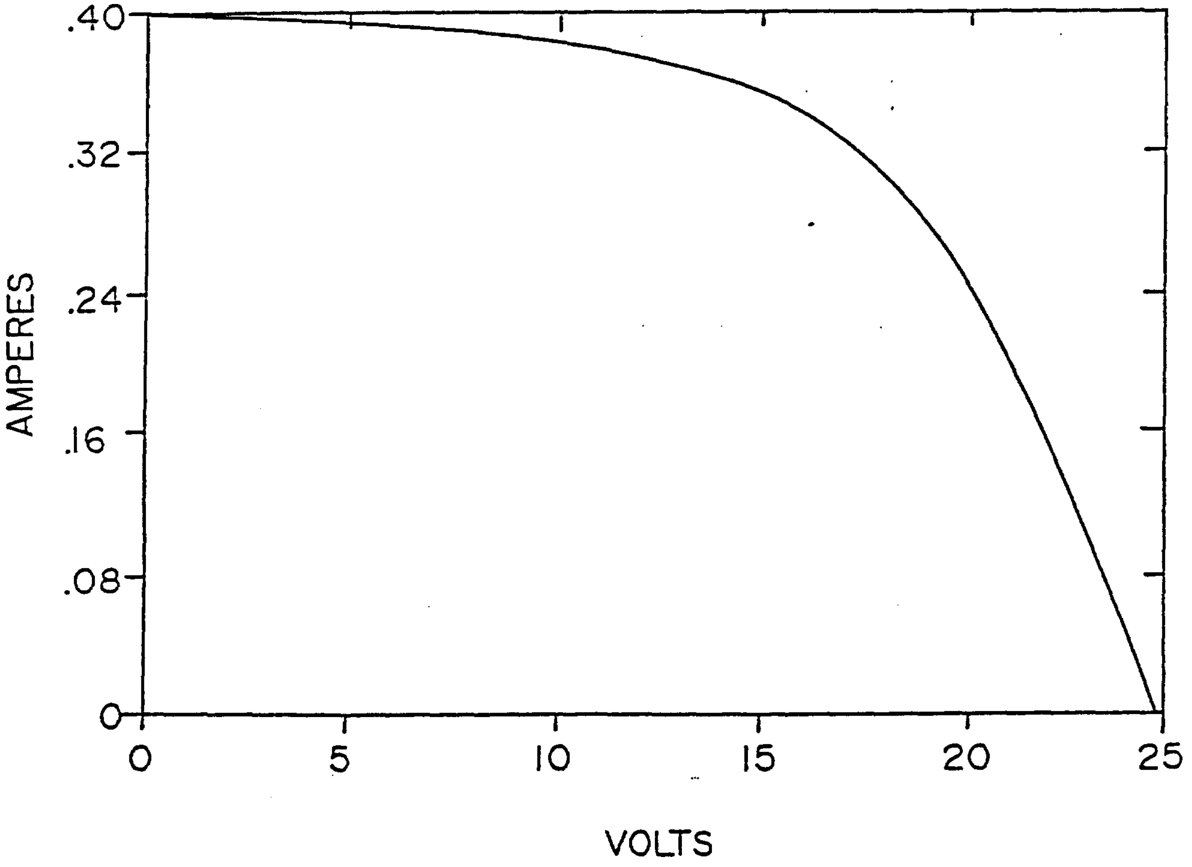

FIGURE 4-2. CURRENT-VOLTAGE CHARACTERISTICS OF a-SiC/a-Si SUBMODULE UNDER AM1.5 ILLUMINATION.

SECTION 5.0
REFERENCES

1. D.E. Carlson, R.R. Arya, M.S. Bennett, A. Catalano, R.V. D'Aiello, C.R. Dickson, C.M. Fortmann, B. Goldstein, J. Morris, J.L. Newton, D. Rogers and S. Wiedeman, Semi-Annual Technical Progress Report, SERI Subcontract No. ZB-7-06003-2, September 1987.

2. R.R. Arya, A. Catalano and R.S. Oswald, Appl.Phys. Lett. 49 [17] 1089 (1986).

3. R.R. Arya, M.S. Bennett, A. Catalano and K. Rajan, 3rd Int'l. Photovoltaic Science and Engineering Conf., Nov. 3-6, 1987, Tokyo, Japan.

4. A. Catalano, R.R. Arya, C. Fortmann, J. Morris, J. Newton and J.G. O'Dowd, Conf. Record of 19th IEEE Photovoltaic Specialists Conf. (IEEE, NY) 1987, p. 1506.

5. B. Goldstein, C.R. Dickson and D. Carlson, private communication.

6. J. Morris and J. O'Dowd, private communication.

7. Y. Hattori, D. Kruangam, K. Katoh, Y. Nitta, A. Okamoto and Y. Hamakawa, Conf. Record of 19th IEEE Photovoltaic Specialists Conf. (IEEE, NY) 1987, p. 689.

8. D. Morel, AIP Conf. Proc. No. 157, eds. B.L. Stafford and E. Sabisky, (AIP, NY) 1987, p. 302.

9. C.M. Fortmann, S. Lange, M. Hicks, C. Wronski to be submitted to JPL on January 1988.

10. C.M. Fortmann and S. Lange to be presented at the Spring Materials Research Society meeting to be held in Reno, NV, April 1988.

11. C.M. Fortmann and S. Lange to be presented at the Spring Materials Research Society meeting to be held in Reno, NV, April 1988.

12. C.M. Fortmann, M. Farley and S. Lange, presented at the 19th IEEE PVSC, (May, 1987), New Orleans, LA.

13. C.M. Fortmann, J. O'Dowd, J. Newton and J. Fischer in the AIP Conference Proceedings #157 (1987) B.L. Stafford and E. Sabisky, eds.

Document Control Page

1. SERI Report No.
SERI/STR-211-3582

2. NTIS Accession No.
DE89009495

3. Recipient's Accession No.

4. Title and Subtitle
Research on High-Efficiency, Single-Junction, Monolithic Thin-Film Amorphous Silicon Solar Cells, Phase I
Annual Subcontract Report

5. Publication Date
October 1989

6.

7. Author(s)
A.W. Catalano et al

8. Performing Organization Rept. No.

9. Performing Organization Name and Address
Solarex Thin Film Division
826 Newtown-Yardley Road
Newtown, Pennsylvania 18940

10. Project/Task/Work Unit No.

11. Contract (C) or Grant (G) No.
(C) ZB-7-06003-2
(G)

12. Sponsoring Organization Name and Address
Solar Energy Research Institute
1617 Cole Boulevard
Golden, Colorado 80401-3393

13. Type of Report & Period Covered
Technical Report

14.
1 Feb 1987 - 31 Jan 1988

15. Supplementary Notes
SERI Technical Monitor: Byron Stafford, (303) 231-7126

16. Abstract (Limit: 200 words)

This document describes the progress made in obtaining stable, a-Si-based submodules that have a large area and high efficiency. Conversion efficiencies of up to 11.95% were obtained in small-area, single-junction a-Si solar cells using textured TiO_2, superlattice p-layers, graded carbon concentrations near the p/i interface, and highly reflective ITO/silver back contacts. Single-junction a-SiC and a-SiGe p-i-n cells were also fabricated that had conversion efficiencies of 9%-11%, and some recently fabricated stacked-junction cells had conversion efficiencies of about 10%. In materials research boron-doped microcrystalline SiC films were recently developed containing up to 6 at.% carbon with conductivities of $3 \times 10^{-3}/\Omega$-cm at room temperature and activation energies of 0.11 eV. Microcrystalline film growth was shown to be strongly influenced by the nature of the substrate, with nucleation occurring more readily on a-Si substrates than on TiO_2. Stability studies show that light-induced degradation is usually enhanced by the presence of carbon grading near the p/i interface. In general, adding either germanium (from GeH_4) or carbon (from CH_4) to the i-layer of a p-i-n cell leads to enhanced light-induced degradation.

17. Document Analysis
a. Descriptors Efficiency ; degradation ; thin films ; microcrystalline films

b. Identifiers/Open-Ended Terms

c. UC Categories 271

18. Availability Statement
National Technical Information Service
U.S. Department of Commerce
5285 Port Royal Road
Springfield, Virginia 22161

19. No. of Pages
161

20. Price
A08

Form No. 0069 (3-25-82)